POLITECNICO DI MILANO

School of Industrial and Information Engineering

Master of Science in Electrical Engineering

FLEXIBLE ELECTRICAL POWER SYSTEM FOR INTERPLANETARY AND LUNAR CUBESATS

Supervisor: Prof. Morris Brenna
Co-supervisors: Eng. Karthik Venkatesh Mani
Prof. Francesco Topputo

Author: Jose Enrique Ruiz Sarrió
Matricola: 87609

Academic year 2017/2018

Acknowledgements

I would like to thank Prof. Morris Brenna and Prof. Francesco Topputo for their time, advice and for giving me the opportunity of working in such an interesting topic. I would like to thank in a special way Eng. Karthik Venkatesh Mani who proposed me for the thesis and always believed in the project. I will never forget the lessons you taught me and the encouragement for addressing my life towards the research field.

I couldn't have done this job without my life partner Paula Soler. Everyday life is just beautiful when I wake up next to such an amazing person.

I would like to thank my mother Eva María Sarrió and my father Enrique Ruiz who have always supported me in every decision I made. Without you all of this could not be possible, I love you.

I want to special mention my grandparents: Juan Ruiz, Rosario Ramirez and Antonia Perez. I miss you so much.

Murió el poeta lejos del hogar.
Le cubre el polvo de un país vecino.
Al alejarse le vieron llorar.
"Caminante no hay camino,
se hace camino al andar..."

Antonio Machado - Caminante no hay camino

Politecnico di Milano
July 5, 2018

Jose Enrique Ruiz Sarrió

Abstract

Lunar and interplanetary CubeSat missions pose several challenges for power generation and management. Flexibility is an inherent concept for this kind of missions due to the broad range of conditions the system is facing in its lifetime. This work is aimed to design an Electrical Power System which shall enable lunar and interplanetary missions by analysing two different case studies which frame the design.

The procedure is mainly focused on shaping the main electrical interface & architecture and the dimensioning of the main elements of the system such as dc-dc converters, batteries, etc. MARIO and LUMIO missions are the starting points for the design. They are analysed, obtaining the main boundary conditions for EPS operation. The main architecture comprises the maximum power point tracking converter feeding a battery voltage bus. It is achieved by using an inverting Buck-Boost converter facing the PV power source and different voltage levels are defined for load feeding based on their particular requirements. Energy storage systems and PV arrays are imposed conditions by the case study analysis which are already sized in the previous stages of the projects. Dc-dc converters are shaped to provide good power-quality conditions by reducing current and voltage ripples and harmonic content. The control architecture and logic is also designed to ensure system stability and desired performance.

In order to prove the proper performance of the system, Matlab Simulink simulations are carried out taking into account the existing mission designs. Several scenarios are defined including the most critical conditions in both CubeSat life cycles, defining temperature and irradiation profiles as well as power duty cycles for each scenario. Transient behaviour of the generation current and voltages as well as the state of charge of the battery and the proper performance of the implemented control methods is demonstrated under the defined scenarios. It is found that the system is stable under every defined condition by providing proper load feeding and satisfying the maximum allowable depth of discharge requirement of the battery for each case study. The collection of simulation results and the design procedure provide a guideline for future design stages, where the system will be prototyped and tested under more realistic conditions.

Sommario

Le missioni Lunari ed Interplanetarie posano diverse sfide al riguardo di produzione e gestione dell'energia. La flessibilità è un concetto inherente per questo tipo di missioni a causa dell'ampia variazione delle diverse condizioni che questi sistemi devono affrontare al lungo della sua vita utile. Questo lavoro ha come obbietivo la proggetazione di un sistema elettrico di potenza per abilitare missioni lunari ed interplanetarie. Questo obbietvo è raggiunto tramite l'analisi di due casi di studio.

Il progetto è principalmente focalizzato nella modellazione delle parti principali della interfaccia elettrica e il dimensionamento degli elementi principalli del sistema come convertitori, batterie, paneli solari, etc. MARIO e LUMIO sono le due missioni che definiscono i punti di partenza dello studio. Questi forniscono le condizioni di contorno del progetto. L'architettura principale del sistema include la traccia del punto di massima potenza tramite un convertitore alimentando un bus col voltaggio della batteria. Questo è raggiunto tramite un convertitore Buck-Boost con i terminali invertiti, interfacciando il sistema photovoltaico di potenza. Diversi punti di carico sono stati definiti a secondo delle specificazioni dei subsistemi alimentati. Il sistema di accumulo di energia è una condizione imposta dai casi di studio analizzati, essendo questa definita in fasi precedenti. I convertitori dc-dc sono dimensionati per produrre una energia di alta qualità, regolando la increspatura ed il contenuto armonico nella corrente e nel voltaggio. La logica di controllo è anche progettata per raggiungere le condizioni desiderate e la stabilità del sistema.

Al fine di dimostrare le corrette prestazioni del sistema, simulazioni Matlab Simulink sono eseguite avendo in conto le condizioni delle missioni sotto studio. Diversi scenari sono definiti includendo le condizioni più critiche per i due CubeSat analizzati, fornendo i profili di temperatura, irradiazione e potenza per ogni scenario. I transitori nella corrente e nel voltaggio del sistema di generazione, lo stato del carico della batteria, ed il corretto funzionamento del controlo progettato sono stati provati sotto le condizioni previamente definite. è stato trovato che il sistema è stabile sotto tutte le condizioni, fornendo una alimentazzione del carico ottima e soddisfaccendo la proffondità di scarico per le batterie per ogni scenario. La collezione dei risultati delle simulazioni e la procedura di progetazzione, forniscono le linee guida per i progetti futuri in cui il sistema sarà prototipato e testato sotto condizioni più reali.

Contents

List of Figures

List of Tables

Glossary

List of Acronyms

EPS	Electrical Power System
LUMIO	Lunar Meteoroid Impacts Observer
MARIO	Mars Atmospheric Radiation Imaging Orbiter
LEO	Low Earth Orbit
COTS	Commercial Off-The-Shelf
TRL	Technology Readiness level
AU	Astronomical Unit
PV	Photovoltaic
SADA	Solar Array Drive Actuator
BOL	Beginning of Life
EOL	End of Life
ESS	Energy Storage System
SoC	State of Charge
OBC	On-Board Computer
DSP	Digital Signal Processing
PMAD	Power Management and Distribution
PPT	Peak-Power Tracker
DET	Direct Energy Transfer
BCDR	Battery Charge/Discharge Regulator

GTO	Geostationary Transfer Orbit
GEO	Geostationary Earth Orbit
MPPT	Maximum Power Point Tracking
MPP	Maximum Power Point
PCB	Printed Circuit Board
IC	Integrated Circuit
POL	Point of Load
MPS	Modular Power System
SABR	Solar Array Battery Regulator
FBCM	Flexible Battery Charging Module
FDPOL	Flexible Digital Point of Load
LEOP	Launch and Early Operation
SOC	System on a Chip
CCM	Continuous Conduction Mode
DoD	Depth of Discharge
HGA	High Gain Antenna
LGA	Low Gain Antenna
ADCS	Altitude Determination and Control
AOCS	Altitude and Orbit Control System
SMIM	Stable Manifold Injection Manoeuvre
HIM	Halo Injection Manoeuvre
SK	Station-Keeping
IODP	Impacts Observation and Data Processing
ODNAV	Orbit Determination, Navigation and Acquisition
PROC	Processing
ESR	Equivalent Series Resistance

Chapter 1

Introduction

1-1 CubeSat Technology. What is it?

A CubeSat is a small spacecraft consisting of single or multiple cubic units, each with dimensions $10 \times 10 \times 10$ cm^3. According to the standard developed at California Polytechnic State University and Stanford University [14], along with the said dimensions, each unit should weigh 1.33 kg. However, further research, development and building of new CubeSats has contributed to the relaxation of mass requirements per unit. Thus we have different CubeSat configurations depending how these 1U units are connected together. Figure 1-1 shows how these units are assembled.

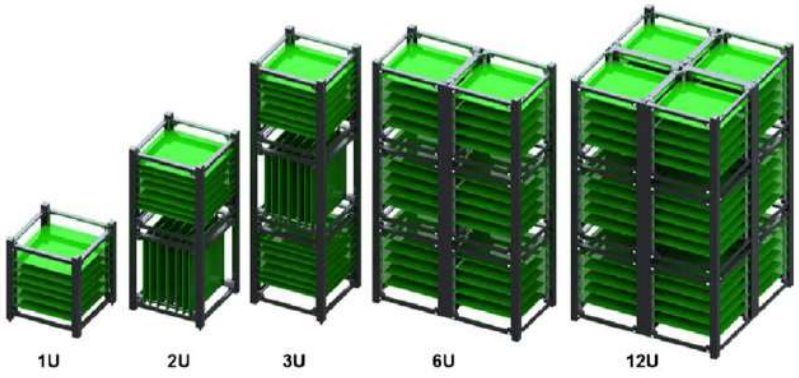

Figure 1-1: Multi-U CubeSat sizes [5]

Since their conception, CubeSats have been used to perform scientific research and technology demonstrations in Low Earth Orbit (LEO). The first CubeSats were launched on a Russian Eurockot in June 2003. The organizations responsible for them were some research institutions and universities such as Stanford University (QuakeSat, for earthquake detection) or the Tokyo Institute of Technology (CUTE-I, for amateur radio). Since then, almost 250 CubeSats have been launched mainly at LEO [15].

CubeSats usually use Commercial Off-The-Shelf (COTS) products related to electronics, materials, small propulsion units, satellite bus etc. Most of these equipment are not space-tested and have a medium/medium-high Technology Readiness level (TRL). Despite this fact, some missions use custom designs for some of the subsystems.

It is possible to identify several subsystems inside one single CubeSat independently of its size. Figure 1-2 shows the main subsystems included in a standard CubeSat.

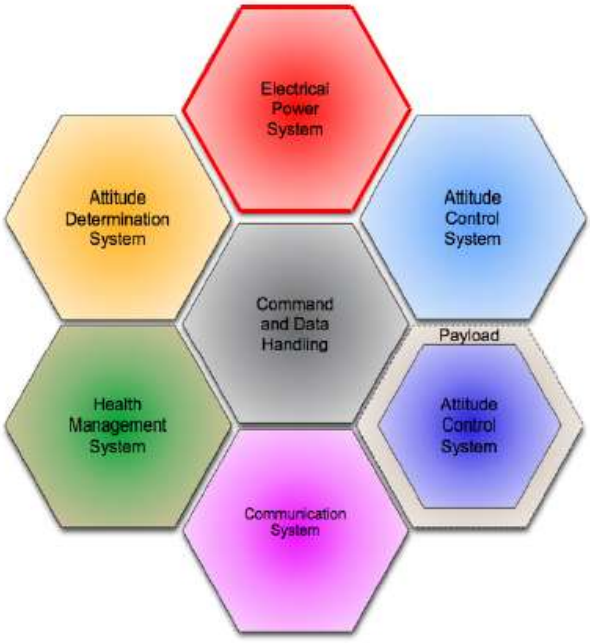

Figure 1-2: CubeSat subsystems [1]

The present work is mainly focused on the Electrical Power System (EPS) subsystem and its interaction with other subsystems in different mission stages. The interactions among the rest of subsystems have been discarded.

1-2 EPS subsystem features

The EPS manages electrical power generation, storage and management. Figure 1-3 shows the main block diagram of an EPS.

Some of the main elements of the EPS subsystem are:

- **Power Source:** The majority of small spacecraft missions exploit the photoelectric effect to generate electrical current during their mission. Photovoltaic cells, or solar cells, are made out of thin wafers of semiconductors that produce electric current when exposed to light. Solar irradiation varies as the inverse square of the distance from the Sun and the projected surface area of the panels exposed to the Sun varies as a cosine of the angle between the panel's normal axis.

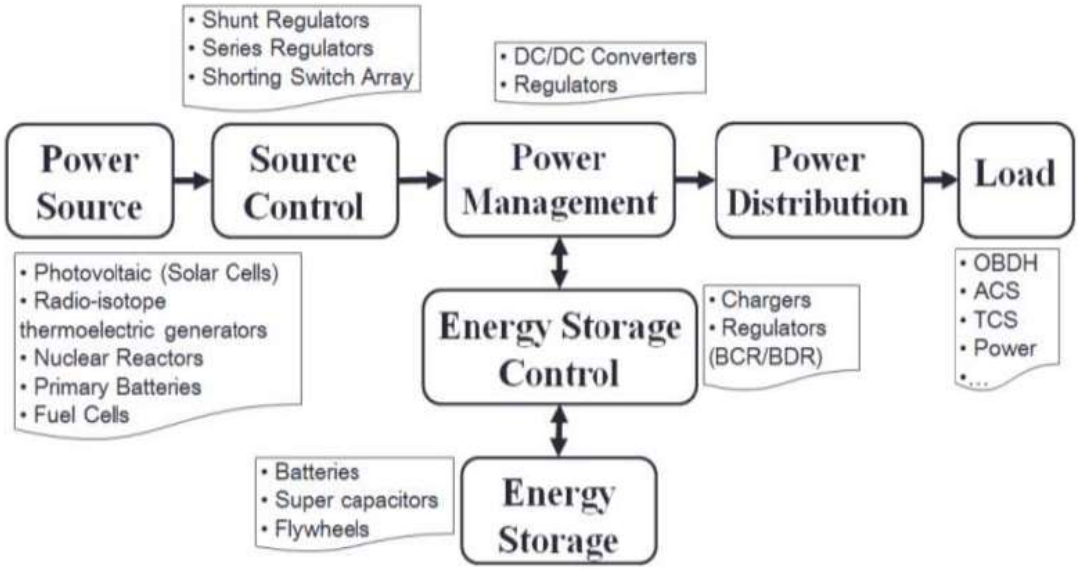

Figure 1-3: EPS subsystem block diagram [2]

- **Energy Storage:** Solar power generation is not always available for spaceflight operations. Orbit, mission duration, distance from the Sun or required peak instrument power may need stored on-board energy. Batteries can be divided in two types regarding their function:
  - *Primary batteries:* Primary type batteries are not rechargeable, they are used only for real short mission durations (around 1 day, up to 1 week).
  - *Secondary batteries:* Secondary type batteries are rechargeable and they are typically used. In particular Li-ion batteries have been used extensively in the past on small spacecraft.
- **Power Management and Distribution:** Power management and distribution systems control the flow of power to spacecraft subsystems and instruments. This part includes converters, auxiliary equipment, buses, etc. Present work is mainly focused on this part of the EPS and it will be studied in deep.

Figure 1-4 show examples of Power Management and Distribution module (practically called EPS) and Batteries developed by ClydeSpace[a] for CubeSat applications.

1-3 Motivation and objective

To expand the horizons, interplanetary CubeSats development will be a necessary step for increasing the solar system exploration efforts at high science-to-investment ratio.

[a] www.clyde.space/products

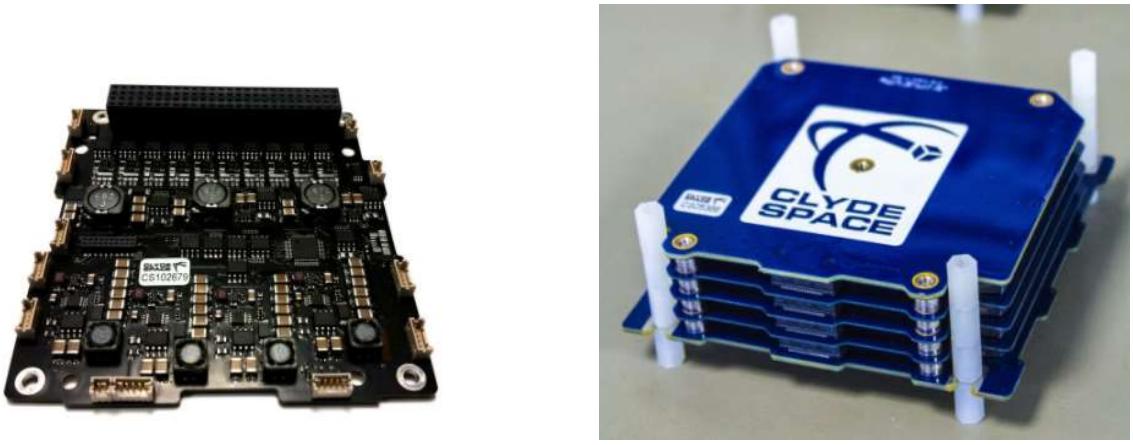

(a) EPS by ClydeSpace **(b)** Battery module by ClySpace

Figure 1-4: COTS equipment for CubeSat application

Interplanetary CubeSats design and development shall push the frontiers of engineering and technology by the means of miniaturising and simultaneously increasing the functionality of critical space systems.

Interplanetary CubeSats require several improvements over the existing LEO CubeSat design. Some of the main challenges related to the EPS subsystem are listed:

- **Solar power collection is low at >1 Astronomical Unit (AU)**[b] **:** The irradiation incident on the satellite solar panels is reduced following the Inverse Square Law, sunlight decreases in intensity over distance by a factor of $1/r^2$, where r is the distance from the Sun. Figure 1-5 shows the solar energy flux variation with the distance from the sun. Acquisition, storage, and distribution of power is very critical for the operational capability of CubeSats.

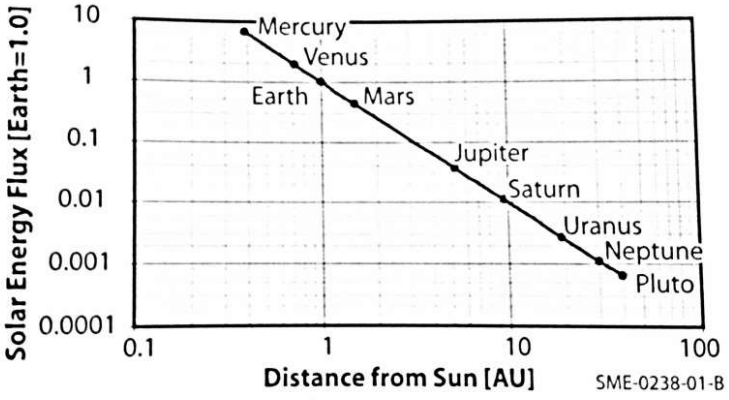

Figure 1-5: Solar Energy vs Distance from the Sun [3]

[b] AU: 1 AU is equal to the distance from the earth to the sun, equal to 149.598.000 kilometres

- **High power requirements:** In this class of missions the employed CubeSats are usually bigger and could use systems for On-Board propulsion (not transported by a bigger spacecraft). Also signal transmission systems need higher dimensions and higher power to transmit the science data and the telemetry.
- **Durable electronics and subsystems:** There are enviromental conditions that may vary from a LEO zone to an interplanetary one. Electronics and other equipment have to endure the harsh environment in the interplanetary space, especially radiation endurance.

Until now, a lot of EPS components have been developed for a wide number of CubeSat missions. Some universities and companies have focused their studies on swiftly building their own CubeSat by using COTS equipment. It is possible to find scalable EPS systems on the market developed by some of the most important space equipment manufacturers. These apparatus are used mainly for low-power CubeSats. Flexible system handling a wide range of parameters in CubeSats are still under development.

The motivation of the present work is also enabled by the factor of **Flexibility**. It is necessary to deal with more complex missions (beyond LEO) that require standard equipment to be able to deal with stringent constraints and drastic variations in power demand. Flexibility characteristic in the EPS design solves some key points in mission power adaptability. Normally, each subsystem has different converters inside them which reduces efficiency due to double conversion. Some subsystem can run more efficiently at lower voltages or at specified voltages. There are different types of payloads that would require different power supply.

Thus, motivation and the subsequently objectives behind this work are:

1. **Design a flexible EPS for 12U to 16U CubeSat pursuing lunar and interplanetary missions.**
2. **Analyse performance and characteristics of flexible EPS during different mission scenarios.**
3. **Transpose the knowledge of the design characteristics and performance to the system designers in order to enable technologies for affordable interplanetary missions.**

EPS design in a flexible environment obtain its relevance from Lunar Meteoroid Impacts Observer (LUMIO) and Mars Atmospheric Radiation Imaging Orbiter (MARIO) missions. In the following sections, both missions are described in order to provide a basic picture about the context on study.

1-4 Lunar Meteoroid Impact Observer (LUMIO) mission

LUMIO is a CubeSat mission that shall observe, quantify, and characterise meteoroid impacts on the Lunar farside by detecting their impact flashes, to provide global information on the Lunar Meteoroid Environment [4].

The mission is launched into a highly eccentric parking orbit around the Moon. It then executes a manifold injection manoeuvre to be transferred from the lunar parking orbit to a quasi-halo orbit around Earth-Moon L2. The mission implements a novel orbit design and latest CubeSat technologies to serve as a pioneer in demonstrating how CubeSats can become a viable tool for deep space science and exploration [4].

Figure 1-6 describes the whole life-cycle for LUMIO mission in a simple and visual way, showing the different phases in the mission and main characteristics.

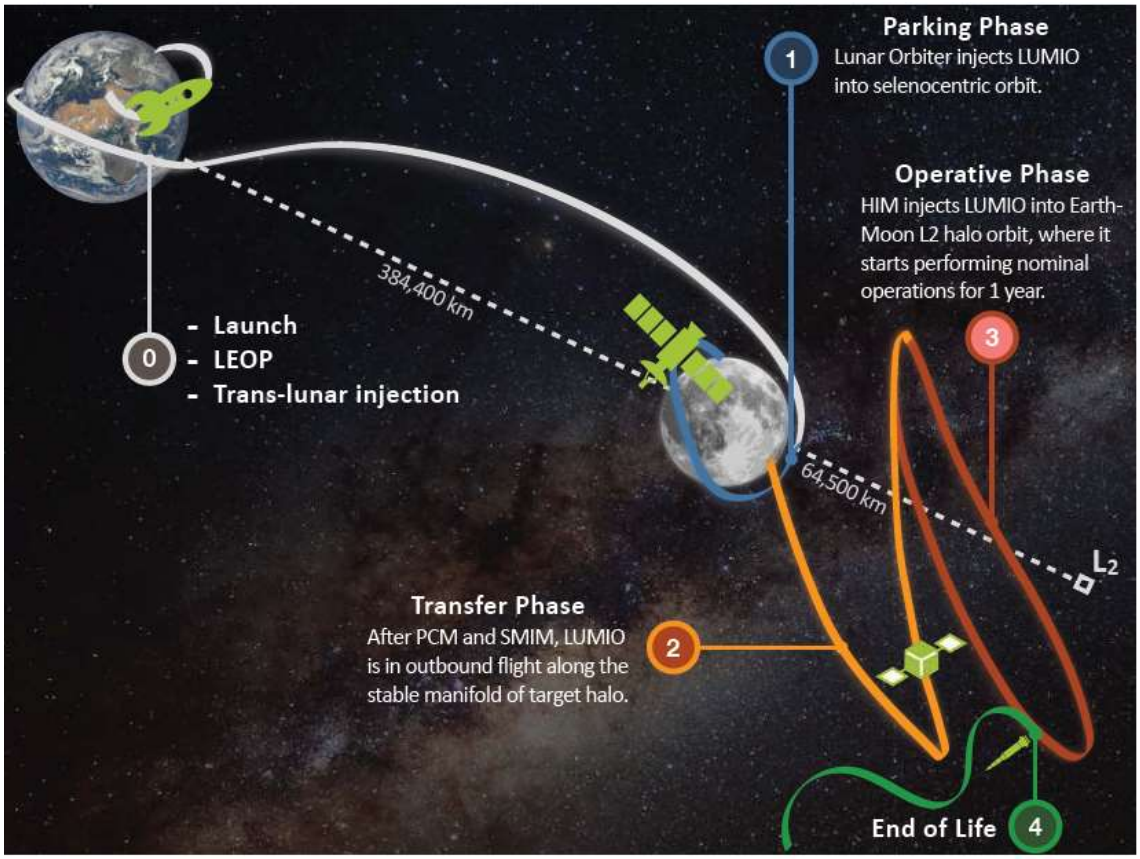

Figure 1-6: LUMIO mission overview [4]

1-5 Mars Atmospheric Radiation Imaging Orbiter (MARIO) mission

MARIO mission statement is provided by Mani et al [6]:

"The Mars Atmospheric Radiation Imaging Orbiter (MARIO) is a stand-alone CubeSat exploration mission to Mars that shall demonstrate the capabilities of CubeSats to escape Earth, perform autonomous deep-space cruise, achieve ballistic capture, and be emplaced on an areosynchronous orbit at Mars. It shall utilise dual chemical-electric propulsion, concomitant with hybrid high-thrust low-thrust trajectories and autonomous

Guidance, Navigation and Control. The MARIO mission shall conduct radiation imaging to characterise the thermal environment in the Mars upper atmosphere. The mission shall serve as a pioneer for Interplanetary CubeSat missions with high launch flexibility and cost efficiency".

The mission encounters vastly different environments from the beginning of life to the end of life. The solar irradiation, power generation, operations and the thermal environment, have strong variations throughout the mission.

The main engineering challenge for MARIO CubeSat is the interplanetary transfer phase, which will employ a special thruster to achieve the required thrust in order to reach the Mars orbit. Figure 1-7 depicts MARIO CubeSat operating in Earth and Mars conditions.

(a) Earth operation **(b)** Mars operation

Figure 1-7: MARIO CubeSat different operation stages [5, 6]

1-6 Research questions

This section highlights the main research questions of this study:

1. In the context of beyond LEO missions, how the EPS deals with such a broad range of power?
    - Hypothesis: High variations in irradiation incidence will represent a power generation variation inside a range which can be very broad. The EPS shall be able to deal with this power range and manage the power production, storage and delivery in a controlled and stable way by also assuring power quality in the different parts of the EPS.
2. How does the electrical interface design look like in such an spacecraft?
    - Hypothesis: The EPS must be able to face the power source, energy storage system and the loads. For load facing, different voltage levels are usually

required depending on subsystem manufacturer specifications. For generation and battery, it will be necessary to use a device able to manage the battery characteristics and generation parameters. Interface between the EPS and the different loads is established depending on a maximum allowable current value per bus.

3. How is the system behaviour under the most critical working conditions in considered case studies?

   - Hypothesis: Transient behaviour in voltage and current in different parts of the EPS must be studied. Generation evolution under different working conditions will vary depending on load requirement and battery status. The system shall mitigate and protect the system from extreme variations of the different parameters. The battery shall not achieve high values of DoD in order to assure the energy availability during the whole mission lifetime.

1-7 Document structure

The document is organised as follows:

- State of the art and theoretical background: The main technologies and existing systems are analysed.
- EPS basic design: The main boundary conditions and requirements of the EPS are set. The different characteristics of the system are also defined in this chapter.
- EPS model development: All the simulation models employed for the system and the main element design and working principles are described.
- EPS basic control: It explains the different control architectures and algorithms.
- Converter parameters and design: It describes the dimensioning of the components inside the different EPS parts.
- Case study simulations: The simulations for MARIO and LUMIO case studies are described and illustrated.
- Closure: Final summary and conclusions.

Chapter 2

State of the art and theoretical background

In this chapter, available technology is analysed as well as similar projects carried out in the context of study. The main study is focused on the power distribution and management but it is also necessary to highlight the current state of the technology of the whole EPS subsystem, including power source and Energy Storage Systems (ESS). COTS equipment already employed in several CubeSat missions are also analysed. Some authors such as Notani et al [1], Clark et al [8] and Peng et al [10], have already developed flexible Electrical Power System (EPS) models dealing with lower ranges of power and they are explained.

2-1 Solar array technology

Photoelectric effect is exploited in order to produce electrical power in space missions. There exists a high amount of solar panel technologies on the market but only some of them are used in small spacecrafts. Especially in this case of applications, efficiency plays a key role since the available panel surface is limited by the size of the CubeSat.

The solar power generation of the small spacecrafts is affected by the increase in Sun-spacecraft distance and the maximum allowable solar array size due to overall mass and size contraints. Additionally the solar cells degrade over the mission lifetime due to radiation accumulation[7].

In the space industry, triple junction cells are commonly used due to their high efficiency-to-cost ratio compared to other cells. For small spacecraft applications, there exists a wide number of manufacturers that provide solar cells for this kind of missions. Figure 2-1 shows different solar cell Commercial Off-The-Shelf (COTS) models and their achievable efficiencies [7].

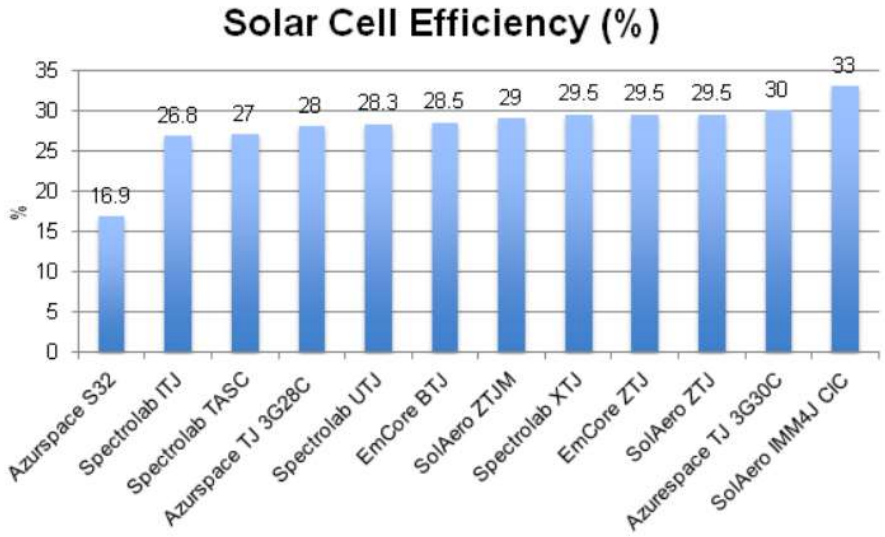

Figure 2-1: COTS solar cell efficiencies [7]

For small CubeSats, the Photovoltaic (PV) array is installed on the surface of the satellite. This means that the available power is limited by the fact that all the installed arrays cannot generate power at the same time. Solar irradiation incident on the panels depends on the cosine of the angle between the normal of the panel surface and the Sun. Thus, the surface-mounted panels are suboptimal for a continuous constant power generation. Figure 2-2 shows a typical on-body mounted solar array for a 3U CubeSat.

Higher power demands require the power source to be adapted to the mission requirements. In order to meet this feature, deployable PV arrays are used. This kind of arrangement can be controlled by means of Sun sensors and gyroscopes monitoring the solar panels and Sun position. Then, a Solar Array Drive Actuator (SADA) changes the position of the solar arrays to properly collect the solar irradiation. Usually, Interplanetary CubeSats use deployable solar arrays as shown in Figure 2-2 [a].

The normal behaviour of the PV cells can be described through their IV (Current-Voltage) curves. These curves show the performance of the power collection in terms of the terminal-measured voltage and the current supplied for each cell. There exists a degradation during the life of the solar assembly defining two different characteristics: Beginning of Life (BOL) and End of Life (EOL) curves [3]. Figure 2-3 shows the IV plot for a generic array showing the main characteristic points. Power available is the area under the curve.

Key design issues for solar arrays include spacecraft configuration, required power level (peak and average), operating temperatures, shadowing/eclipses, radiation environment, orientation, mission life, physical characteristics (mass and area), cost and risk [3]. It is necessary to identify the critical points regarding solar array performance in order to properly set the boundary conditions for the present design.

[a] Mars Cube One (MarCO) is a NASA-JPL mission planned to be launched with InSight Mars lander in Atlas-V and independently fly to Mars [16].

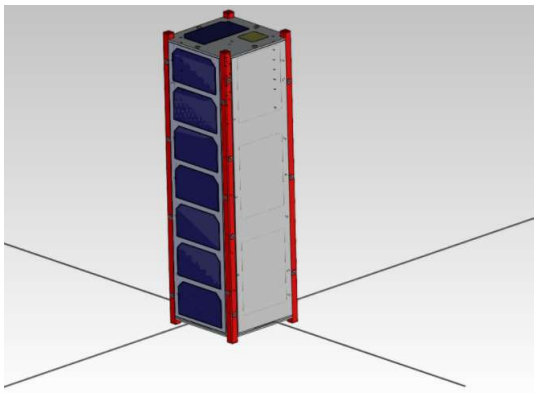

(a) 3U Cubesat for LEO operation

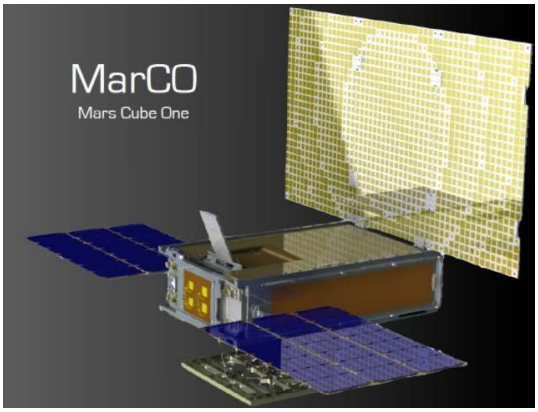

(b) 6U CubeSat MarCO mission

Figure 2-2: Solar array positioning examples [16]

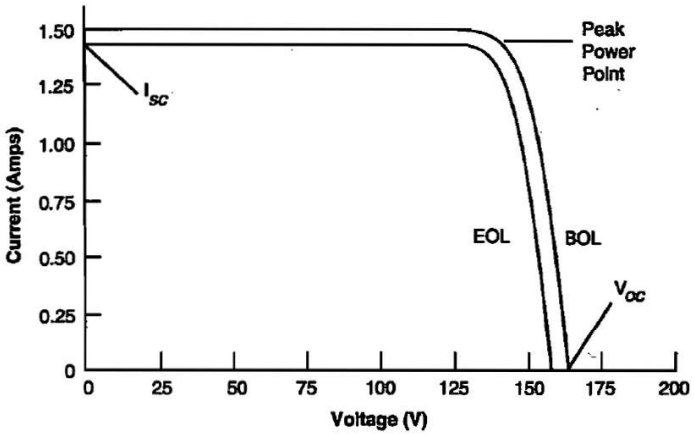

Figure 2-3: IV plot for a solar array [3]

2-2 Energy Storage System technology

There exist some stages on spacecraft life when an Energy Storage System (ESS) is required such as during eclipse or extra peak power requirements. As it was said in Chapter 1, main effort should be placed in the secondary battery type (rechargeable).

Secondary type batteries include Nickel-Cadmium (NiCd), Nickel-Hydrogen (NiH2), Lithium-ion (Li-ion) and Lithium polymer (Li-po) that are used extensively in the past on small spacecrafts. Lithium-based secondary batteries are commonly used in portable electronic devices because of their rechargeability, low weight and high energy density, thus becoming ubiquitous on spacecraft mission [7].

Batteries are a key point in small spacecraft design. Energy density is one of the most critical parameters because of the weight and space constraints. Figure 2-4 depicts the different battery technologies while Table 2-1 shows their Technology Readiness level (TRL) and some data of some COTS equipment employed for small spacecraft manufacturing [7].

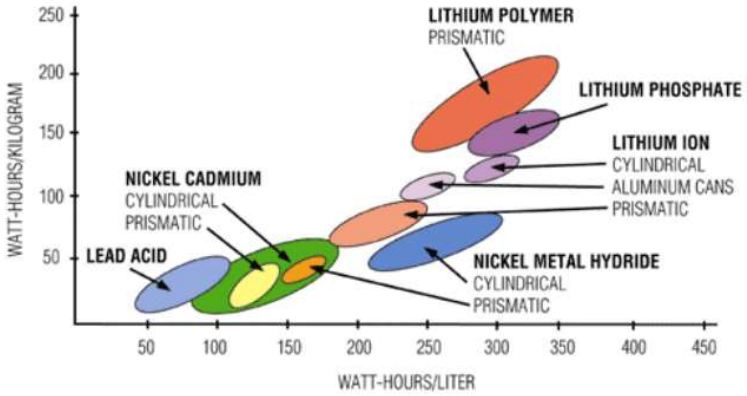

Figure 2-4: Energy densities for different battery types [7]

Table 2-1: Lithium-based battery energy densities [7]

PRODUCT	MANUFACTURER	ENERGY DENSITY [W*h/kg]	STATUS
COTS 18650 ion battery	ABSL	90	TRL 8
BP-930s	Canon	132	TRL 9
Li-Polymer 8.2V, 1.25 Ah - 20 Ah	Clyde Space	150	TRL 9
Li-Polymer, 32V, 6.25 Ah	Clyde Space	150	TRL 8
Rechargeable Space Battery (NPD-002271)	Eagle Pitcher	153.5	TRL 7
NanoPower BP4	GomSpace	160	TRL 9
NanoPower BPX	GomSpace	157	TRL 9
Li-ion Battery Block VLB-X	Vectronic	Unkn.	Unkn.

In present designs, two to five batteries are typical. It is necessary to have at least two (unless the battery uses redundant cells) because the spacecraft needs redundant operation with one unit failed.

Electrical parameters affecting ESS performance are voltage, current loading, duty cycles, storage time and limits on State of Charge (SoC). Nominal voltage of the battery usually depends upon the type of the bus in which it is connected. Profile of Charge/Discharge is also an important characteristic since imbalances may stress and degrade the batteries (Overcharging quickly degrades batteries) [7]. Figure 2-5 shows classic Charge/Discharge profile in which the ideal behaviour would be that the curve is as flat as possible. Typical limits of SoC are between 20% and 80% of total capacity.

One of the most important issues of the ESS is its integration and monitoring action carried out by the On-Board Computer (OBC) and microcontrollers. Usually, the system incorporates a Digital Signal Processing (DSP) unit in charge of acquiring different kinds of signals. In order to monitor the SoC of the battery, the DSP includes inside its memory modules equivalent circuit models of the batteries [1]. For Li-ion battery, a proposed model is presented in Notani et al[1]. Figure 2-6 shows the equivalent circuit.

By knowing its gain and phase-angle, SoC of the battery can be estimated and a proper assessment of the battery status can be performed. Figure 2-7 shows the impedance curves for a generic Li-ion battery.

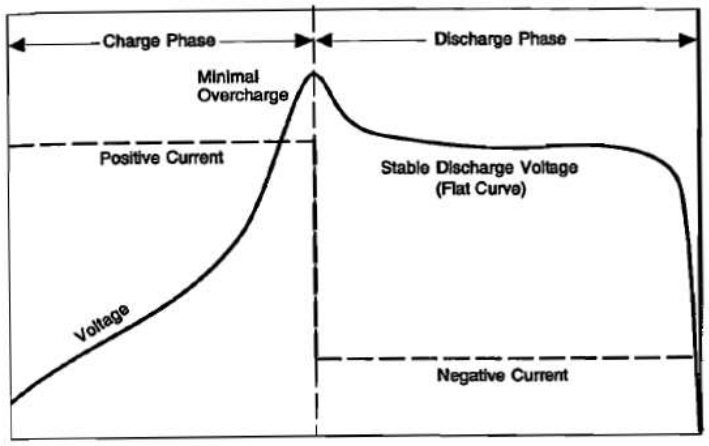

Figure 2-5: Profile of Charge/Discharge for batteries [7]

Equation 2-1 represents equivalent impedance.

$$Z_{bat}(s) = \frac{R_L L s}{R_L + Ls} + R_{ohm} + \frac{R_1}{1 + R_1 C_1 s} + \frac{R_{ct}}{1 + R_{ct} Y_2 s^{n2}} \tag{2-1}$$

Where:

$Z_{bat}(s)$ = Equivalent impedance of the battery

R_L = Parallel resistance to the inductance in the battery

R_{ohm} = Ohmic resistance of the battery

R_1= Parallel resistance to C_1

C = Capacitance of the constant element Q1

R_{ct} = Charge transfer resistance

Y_2 = Admittance of the constant element Q2

n2 = power of the admittance of constant phase element Q2

Q2 & Q1 = Constant phase elements

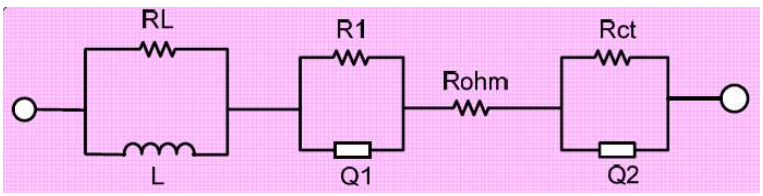

Figure 2-6: Equivalent electrical circuit for a Li-ion battery [1]

The aim of this ESS analysis is to set the main requirements for battery design and integration. ESS detailed design is out of scope of the present work and focus is on different parts of the EPS subsystem.

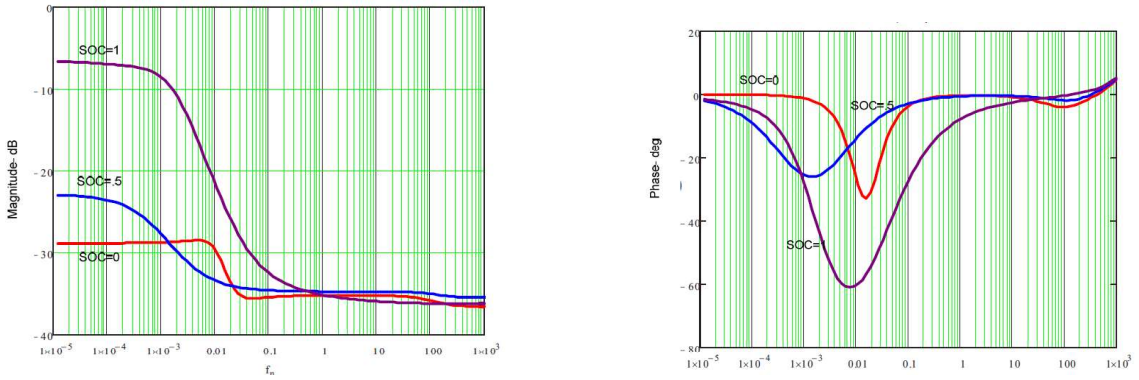

(a) Impedance Gain **(b)** Impedance Phase angle

Figure 2-7: Equivalent impedance characteristic [1]

2-3 Power Management and Distribution

It is necessary to set some terminology on the topic. Typical spacecraft EPS consists of a power generating source, storage (if necessary), Power Management and Distribution (PMAD) unit and loads [17]. This EPS is defined as the entire subsystem.

Some of the manufacturers provide integrated systems that include several functions such as protection of electronics and batteries from extreme current and voltage conditions. Commercially, these systems are known as integrated EPS. Despite this fact, there exist some companies that provide other kind of simpler systems.

PMAD systems control the flow of power to spacecraft subsystems and instruments and are often custom designed by mission engineers for specific spacecraft power requirements. There exists a wide number of manufacturers who have started to supply EPS and PMAD systems for small spacecraft integration. Next step will be to analyse COTS equipment available for small spacecraft integration and some flexible/modular EPS designs conceived for improving current COTS technology.

2-3-1 COTS EPS equipment

Several manufacturers supply EPS which typically have a main battery bus voltage of 8.2 V but can distribute a regulated 5.0 V and 3.3 V to various subsystems. As electronics vendors settle on standard voltages, EPS will become more standardized. Well-known producers of EPS systems that focus on the small spacecraft market include Pumpkin, GomSpace, Stras Space and Clyde Space. Table 2-2 shows main COTS equipment available for small spacecraft use showing their TRL (EPS, PMAD and Power Converters)[b] [7].

[b]More information about every particular system can be found in: https://www.nasa.gov/sites/default/files/atoms/files/small_spacecraft_technology_state_of_the_art_2015_tagged.pdf

Table 2-2: Power Management and Distribution Systems [7]

PRODUCT	MANUFACTURER	TECHNOLOGY TYPE	STATUS
DPCU-2100, -2200, -2300	AAC Microtec	PMAD	Unkn.
BCT CubeSat EPS	Blue Canyon Tech	EPS	Unkn.
Small Satellite PCDU	Clyde Space	PMAD	TRL 9
Nanosatellite EPS	Clyde Space	EPS	TRL 8
P1U "Vasik"	Crystalspace	EPS	TRL 7
NanoPower P31us	GomSpace	PMAD	Unkn.
Series 3699 DC-DC	Modular Services Inc.	Power Conv.	Unkn.
Drop-In Power Converter	Stras Space	Power Conv.	TRL 9
LEO PDCU	Surrey	PMAD	TRL 9
Vectronic PCDU	Vectronic	PMAD	Unkn.

2-3-2 Power Regulation and Control

Power management includes power regulation and control. The main aim of this component is to assure a correct supply for the connected loads. This includes: Voltage range, current, acceptable transient time duration, and voltage ripple.

Power regulation at the main bus is divided into three main sections:

- Control of the solar array power
- Regulation of the main bus voltage
- Charge/Discharge of the battery

Different power bus control techniques are employed in order to deal with the regulation of the system. Figure 2-8 illustrates the main strategies for power regulation.

Two main power bus control techniques are the Peak-Power Tracker (PPT) and Direct Energy Transfer (DET). Main difference between them is how they deal with the input power from the solar array. The PPT allows to decouple the PV array voltage from the battery bus while DET forces the panels to have the same voltages as the battery bus, which is determined by the battery voltage level (only reaching the maximum power point when the battery is at its highest voltage).

PPT systems use a DC-DC converter to achieve its goal.They adjust the duty cycle to bring the solar array terminal voltage to the desired maximum power point. A disadvantage is that the converters have losses and add complexity and weight to the system.

For DET systems, a shunt regulator is used in parallel to the array and shunts the array current away the subsystem when the batteries or loads do not need power. These kind of systems are extremely efficient but the cannot operate at the maximum

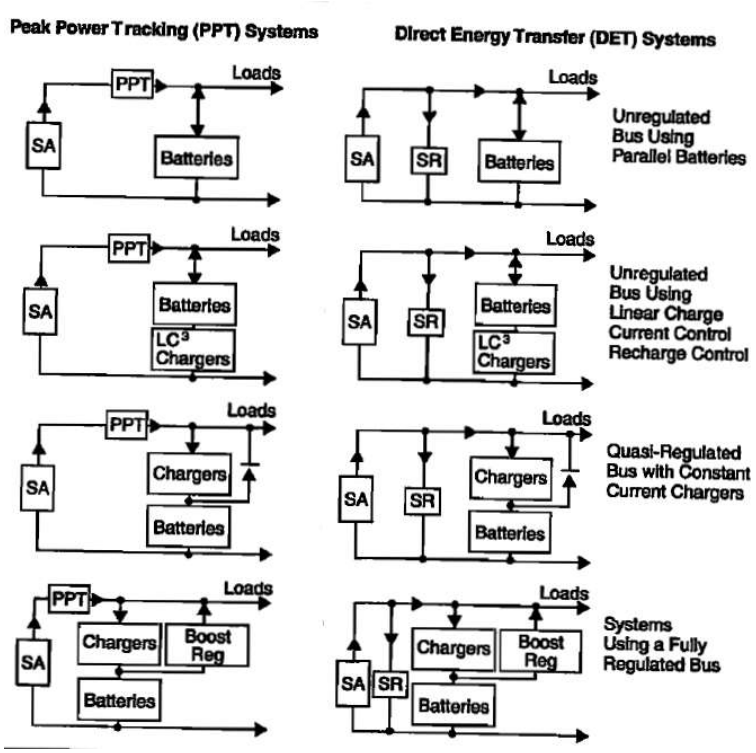

Figure 2-8: System Architectures for Power Regulation [3]

power in normal operation, so the needed array will be greater than that which uses PPT method.

The three most common power system implementation approaches found on small satellites are [8]:

- DET with Battery Bus
- DET with Regulated Bus
- PPT with Battery Bus

It is clear that Battery Bus refers to an Unregulated bus since the bus voltage is imposed by the battery. Now, it is necessary to analyse the common types .

DET with Battery Bus

It is the simplest of the power bus type of regulators. However, the DET with battery bus requires larger solar arrays. The need of much larger solar arrays results in a more expensive and heavier spacecraft. Figure 2-9 shows the schematics of this kind of system. S3R stands for switching shunt regulator.

The main drawback is that the solar array performance is at its maximum when the battery is fully charged and in these conditions, power is not needed in high amounts.

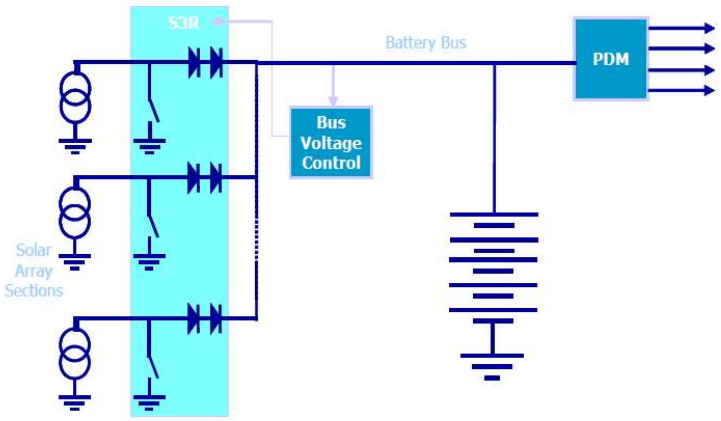

Figure 2-9: DET with battery bus architecture [8]

It is clear from this basic analysis that this kind of power system is not suitable for this study.

DET with Regulated Bus

This system is the most commonly found power system topology in European spacecrafts [8]. This topology is most suited for applications where the spacecraft experiences extended periods of sunlight. The system incorporates the shunt regulator (always used in DET systems) plus a Battery Charge/Discharge Regulator (BCDR). Figure 2-10 present the proposed architecture.

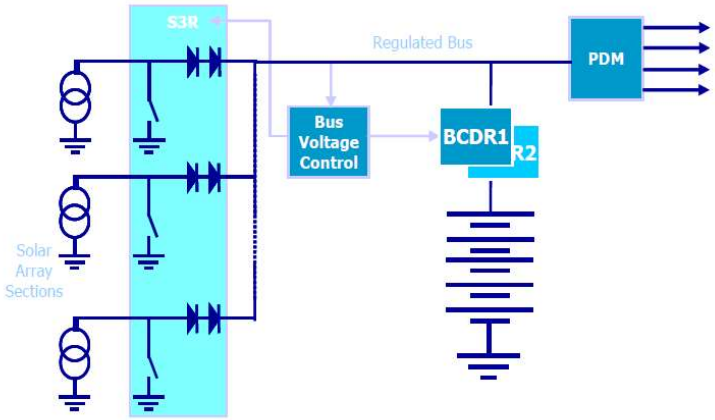

Figure 2-10: DET with regulated bus architecture [8]

During sunlight, the bus voltage is regulated by the shunt regulator and for periods of higher demand, battery power is supplied to the bus via the BCDR. Usually this type of architecture is used in satellites operating at Geostationary Transfer Orbit (GTO)

or Geostationary Earth Orbit (GEO). Eclipse periods introduce inefficiencies in the system so it cannot be used when prolonged eclipse times are experienced.

For the present design, it could be useful during interplanetary travel due to the availability of sunlight. Although, as irradiation changes with inverse squared of the distance to the Sun, the IV characteristic of the panel will vary and it will be necessary to follow the maximum point of the curve. That is the main reason why this architecture will not be feasible.

Peak Power Tracker with Battery Bus

This scheme incorporates a PPT or Maximum Power Point Tracking (MPPT). The system works on the principle of charging the battery and supplying the bus during sunlight while setting the array voltage at the maximum power point. Figure 2-11 shows the typical arrangement including the MPPT executer. In this case, BCR stands for Battery charge Regulators and PDM for Power Distribution Module

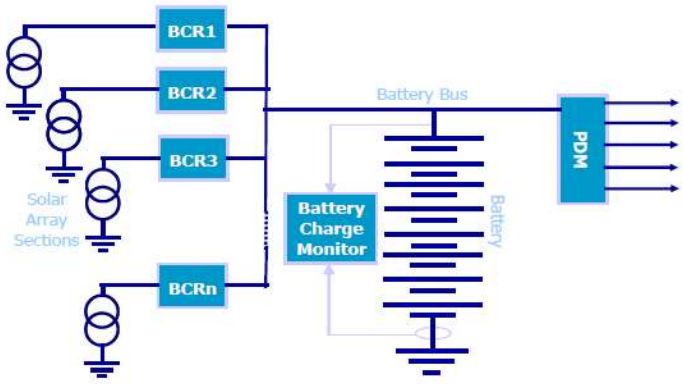

Figure 2-11: MPPT with Battery Bus [8]

Inclusion of MPPT is used when the Maximum Power Point (MPP) of the array is changing significantly while the spacecraft is in sunlight. That is why for interplanetary trajectories or missions that involve a significant travel period, this system is usually used.

The main drawback is the efficiency level associated with the converter. This introduces the main inefficiency of the power system, which is one of the key points where the research is focused.

Performance Comparison

It is clear that the present conditions favour a MPPT based power system as the array characteristics are changing over most of the mission life.

In Clark et al [8] a comparison is presented for a LEO small satellite mission with fixed 3-axis solar array obtaining results showed in Figure 2-12

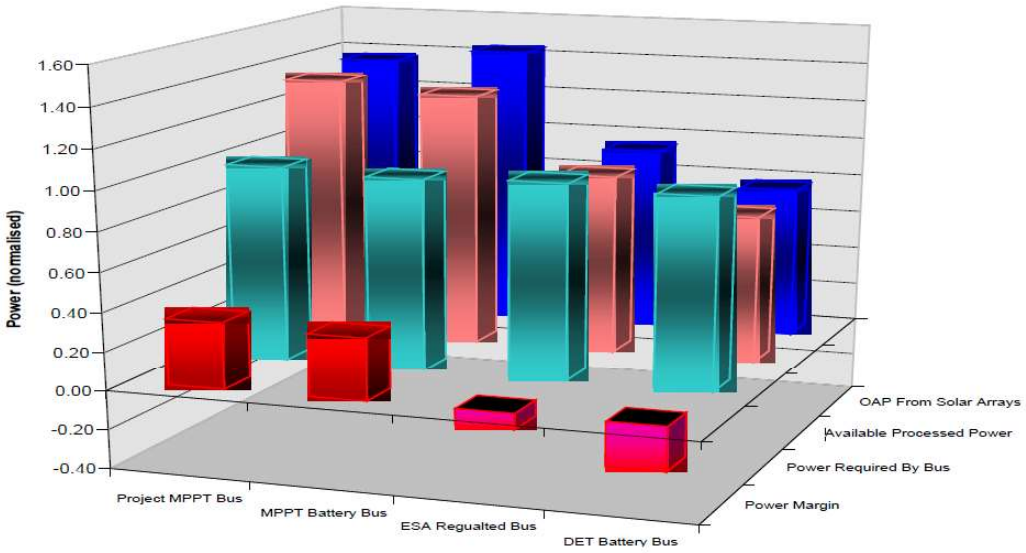

Figure 2-12: Comparison between different architectures for a defined mission [8]

Blue (back) bars indicate the amount of power captured by the arrays. The most important data is the power margin. For the same size solar arrays, DET falls significantly short of the power requirement.

2-3-3 Power Distribution

Distribution system consists of many elements such as cabling, fault protection, and switching gear in order to turn on and off the different loads.

While selecting the type of power distribution it is necessary to focus the attention on keeping power losses and mass at a minimum while ensuring survivability, cost, reliability and power quality. Figure 2-13 shows a lumped equivalent circuit for power distribution modelling.

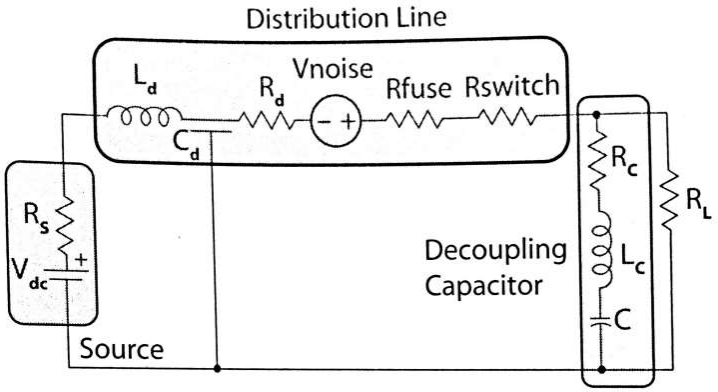

Figure 2-13: Power Distribution Equivalent Circuit [3]

DC source is represented by a simple battery and series resistance R_s. For distribution line representation there are several elements: lumped inductance of the line L_d, noise pickup, capacitance from parallel lines C_d and resistance from the line R_d. Also common elements like fuses or switches are represented by two resistances R_{fuse}[c] and R_{switch}. It is usually necessary to add a decoupling capacitor at the load in order to minimize the transients caused by varying loads. This capacitor is represented by a RLC series branch (C, L_c, R_c).

Regarding the type of connection, it depends on how the power transmission is achieved. Usually for low power applications, Printed Circuit Board (PCB) are used together with Integrated Circuit (IC)s. Also, wires can be used for some connections and depending on the power to be transmitted, PCB transmission would no longer be possible. For wire transmission, the model proposed is more accurate.

Problems with wires are the classical ones. If the cables are long enough, they could act as an antenna picking up noise and radiating out noise to the rest of the equipment. Power loss is also present if the current is high and this fact is one of the key points in the power design.

Concretely, for such low power applications, problems are reduced. The main issue regarding the distribution system will be the space and weight constraint. It will be necessary to work at low current and to use the shortest way to transmit the power to the load. Usually, PCB support plus some short wiring is used in these kinds of devices. PCB use significantly reduces the electromagnetic coupling as well as the line inductances and capacitances.

Distribution systems can be either centralised or decentralised. Centralised systems regulate power to all spacecraft loads attached to the main bus and the decentralised systems place converters at each load separately, called Point of Load (POL). Decentralised systems are usually employed in this kind of small satellites but instead of placing the converters in the load itself, they are usually placed inside the main core of the EPS or PMAD system, allowing different POLs for different load characteristics.

Fault protection within the EPS system focuses on detection, isolation and recovery. Its main purpose is to isolate a short-circuit that could eventually damage the equipment or cause loss of the mission [18].

2-3-4 Real System Examples

It has been identified that two approaches exist: Modular Scalable systems and Flexible one-board systems.

Modular Scalable Systems

For this kind of systems, the EPS is assembled by adding similar modules to one mother core, the so called plug-and-play systems. Each power requirement must be satisfied

[c] In low power, fuses are not usually used as protection element

by adapting the different input, transmission and output modules to the required characteristics.

Analysing the two main examples, the first one is a probed EPS design developed by ClydeSpace in 2006 using the PPT and regulated bus architectures [8]. The second one was developed in 2013 by the University of Toronto with the aim of improving the power range to enable missions requiring higher power [?].

First example by ClydeSpace employs MPPT Battery Bus architecture and they used dedicated MPPT modules for each solar panel for versatility reasons. It is used only for small CubeSat applications. Configuration is illustrated in Figure 2-14. The BCDR performs the MPPT algorithm for each solar array tracking the maximum point of its curve. Three channels for power distribution are used (3.3V 5V and one battery voltage channel). The micro controller (μC) performs the control action for the whole system. The BCR uses a Flyback DC-DC converter topology allowing efficiencies close to 90% even at low power levels (3W per MPPT). Depending on the load power requirements, it is possible to adjust the number of BCR modules as well as the number of solar cell strings.

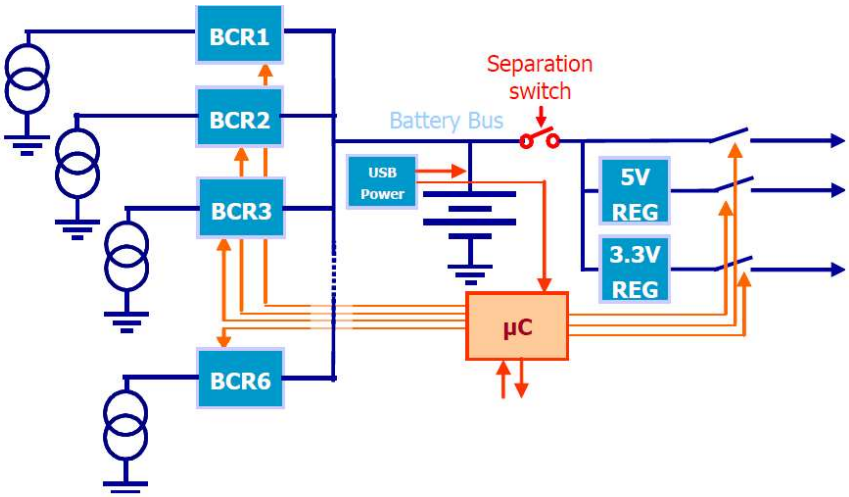

Figure 2-14: ClydeSpace Proposed Architecture [8]

REG represents the Power Conditioning Module (PCM) and consists of two DC-DC converters that regulate the output voltages to 5V and 3V. They can be used in parallel with additional units if higher current is required.

This manufacturer also experimented with architecture changes and proposed a regulated bus set at the MPP voltage during periods of high power demand. Figure 2-15 shows the changes implemented in the previous arrangement. The bus voltage must stay within certain limits (in this case between 22V and 40V). This kind of architecture is known as Regulated Bus architecture, where the battery has no longer a complete control over the bus voltage. As mentioned in section 2-1, this kind of system works better when the power collection is more uniform (SADA powered arrays).

Second example is related to a wider power range and not only limited to small spacecraft applications. The range this system is able to deal with is from 1W up to 1kW.

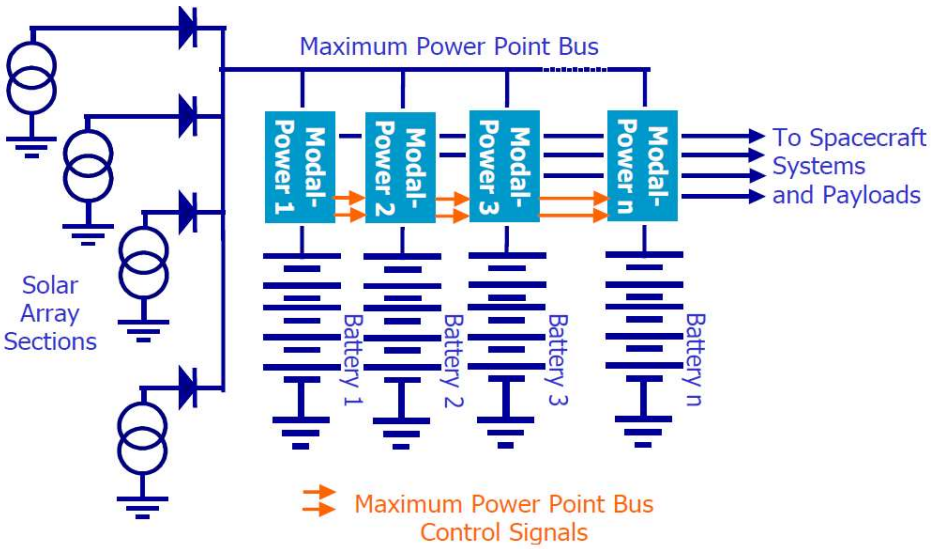

Figure 2-15: ClydeSpace Proposed Architecture Modification [8]

The system is divided in several functional modules attached to a mother board that performs the main and support functions, this is called Modular Power System (MPS). Each module is 50mm x 55mm and weights around 30-40g.

Block diagram of the system is shown in Figure 2-16. This system has two operational modes, one for high power and other for low power. For high power, the system is employed as MPPT with battery bus. For missions that have short solar cell strings, where the nominal solar cell voltage overlaps the nominal voltage of the spacecraft, the DET architecture is more appropriate in terms of efficiency. In the last case, parallel regulation is performed by using a high efficiency BCDR. In Figure 2-17 it is possible to see the different module sizes and shapes when the system is assembled.

The different kind of modules inside the MPS are:

- **Solar Array Battery Regulator (SABR):** It is a synchronous buck converter configured to charge the batteries between 5V to 34V while accepting solar array voltages up to 65V. It operates at efficiencies above 95%. It also performs the peak MPPT by using a dual control approach that allows also to control battery charge. Paralleling different SABR units is possible in order to allow scalability.
- **Switched Power Node (SPN):** These modules are directly connected to the main voltage rails of the power subsystem (either regulated or unregulated) and distribute the power to the spacecraft subsystems. The μSPN represents the same system for low power load requirements. They also perform fault protection and incorporate soft-start devices.
- **Solar Array Telemetry and Filtering (SATF):** It is used to decouple the solar array sizing and configuration from the SABRs. Used for input filtering, muxing (integrating two signals) and monitoring the solar array conditions. Filter is needed in order to attenuate switching noise produced by the SABR.

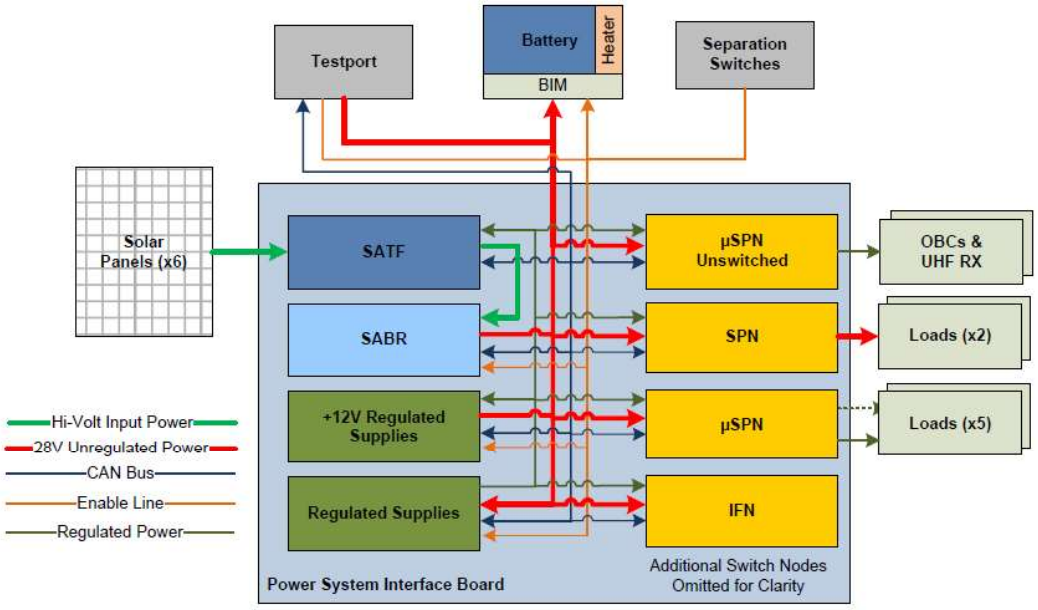

Figure 2-16: Block Diagram of the MPS [9]

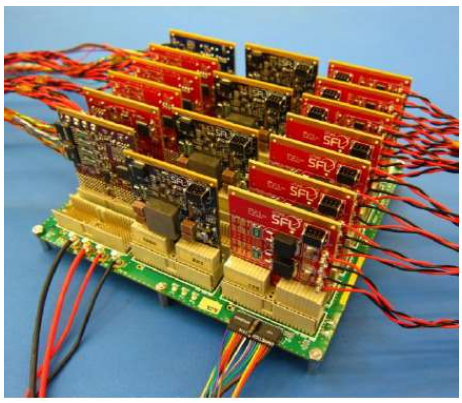

Figure 2-17: Assembled MPS [9]

- **Interface Node (IFN):** This module is used to provide mission specific functionalities (not standard equipment or extra functionalities).
- **Battery Interface Module (BIM):** It is placed between the battery and the main power bus to provide battery protection and monitoring. Used when MPS is used in high power operations.
- **Battery Charge and Discharge Regulator (BCDR):** Provides parallel regulation during DET operation. In addition to the BIM functions, it also allows to control the main bus voltage.

MPS systems have been used in a wide spectrum ranging from Mars rovers (MESR

[d]) to small CubeSats (CanX-7 [e]). Figure 2-18 shows two images describing two of the projects where this design was tested.

(a) MESR picture

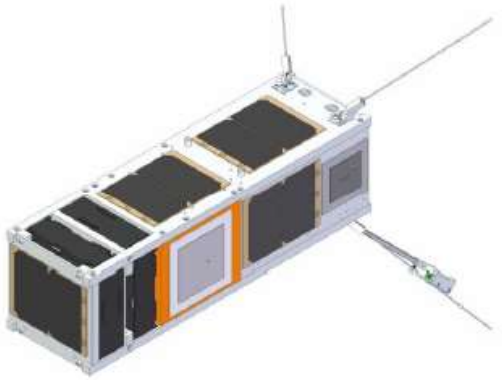

(b) CanX-7 CubeSat

Figure 2-18: Application missions of MPS [9]

Flexible One-board Systems

These systems still have modular architecture, but instead of adapting the number of modules, the EPS board is already capable of dealing with a broad range of power. Physically, it consists of one/two boards depending on the design approach.

Two examples are found in the literature. Notani et al [1] developed a flexible EPS design for 1U to 12U CubeSats. Then, Shah et al [19] and Singh et al [20] improved the design showed in Notani et al[1] by adding some extra features. Second example is associated with the Aoxiang-Sat[f], the first launched 12U scientific CubeSat. It was mainly developed by the Northwestern Polytechnical University of Xi'an and it was designed to deal with 1U/20U CubeSat systems so it is actually a really close example to analyse [10].

Analysis of the first system described in Notani et al [1] which can be configured for 1U to 12U CubeSat range is pursued. The employed architecture is described in Figure 2-19. The prototype developed in this work has different parts:

- **Flexible Battery Charging Module (FBCM):** They interface directly with the solar panel strings and the storage device. They direct all the energy to the storage cells and are able to deal with a wide range of voltages and number of

[d]Mars Exploration Science Rover is a six-wheeled rover designed to support autonomous science prospecting and in situ geological analysis operations [9].

[e]CanX-7 is a 3.5 Kg nanosatellite with the mission of demonstrating a drag sail for de-orbiting nanosatellites and microsatellites from LEO at the end of their mission [9].

[f]The Aoxiang-Sat was launched by China's Long March VII vehicle on June 25 2016, the telemetry data at the time of paper publication showed that the EPS performed well during the three months of orbit lifetime that the satellite had [10]

batteries. Single inductor non-inverting buck-boost converter is used due to the wide input-output characteristics.

- **Flexible Digital Point of Load (FDPOL):** Connected to the unregulated battery bus from the battery or solar panels. They are user configured in order to achieve a variable POL voltage. Each FDPOL module is connected to a regulated DC voltage bus with a fixed voltage determined by the requirements of the mission. Either buck or boost converters are used depending on the desired voltage in the POL to which it is connected.
- **Digital Controller:** EPS core is a digital controller which interfaces with the different modules and functionalities (FBCM, FDPOL, state of health, fault protection, etc.). In this prototype controller used is TI TMS320F28335 DSP, it takes the feedback and gives out control signals.

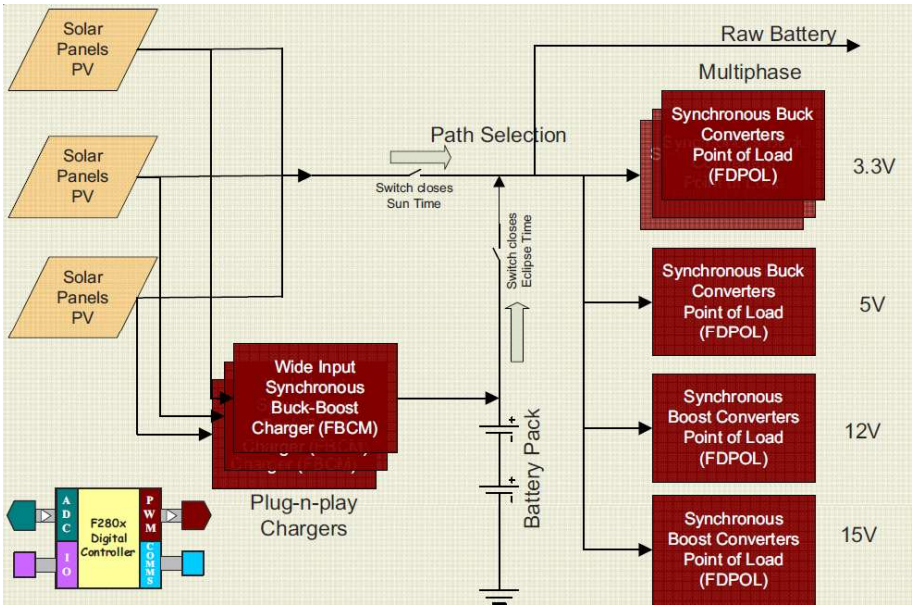

Figure 2-19: Flexible and Configurable EPS Architecture [1]

As it can be observed, the employed architecture is an MPPT battery bus type. By following the scheme in Figure 2-19, it is also evident that during illumination, the solar panel voltage is applied to the main bus. Another remarkable fact is that this system was initially designed for a CubeSat with body mounted panels so the power collection is irregular and depends on the satellite position.

This system could also be an example of the previous case (Modular Scalable Systems). FBCM, FDPOL and batteries could be added in parallel to achieve higher powers. In this case, a fully assembled prototype is used to deal with a precise range of powers with all its components embedded in one PCB. Figure 2-20 shows the developed prototype designed for a LEO CubeSat.

EPS developed in Peng et al[10] was implemented in the Aoxiang-sat deployed on June 25 2016 with excellent performance during the satellite life time. It is also a scalable

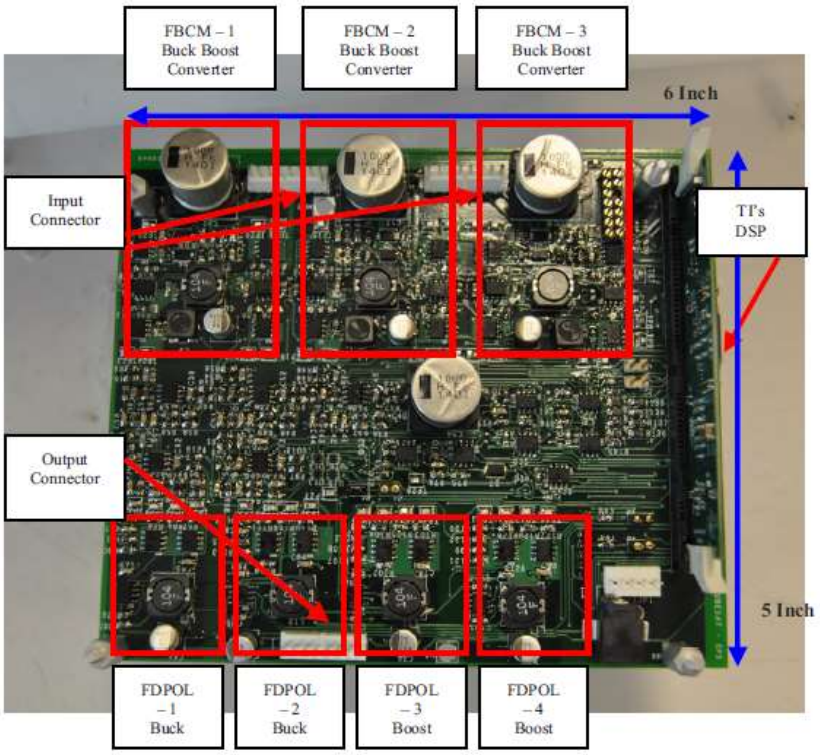

Figure 2-20: CubeSat EPS Prototype with FDPOL and FBCM [1]

system for Multi-U CubeSat application, suitable for 1U up to 20U operation. The developed prototype is again implemented by using one PCB (and also again could be implemented in a modular way).

The architecture employed in Peng et al [10] is described in Figure 2-21. The main components of the EPS subsystem are: Power converter with MPPT, Micro controller (MCU), Distribution (DC-DC power distribution), Separation switch and Health monitoring.

- **Separation switch:** It is used to trigger the power ON after the CubeSat is deployed.
- **Distribution system:** Convert bus voltage to secondary voltage (in this case 5V and 3.3V).
- **Health monitoring:** EPS status is monitored by different kind of circuitry that senses voltage, current and temperature.
- **Power conversion with MPPT:** In order to maintain a stable bus voltage, DC-DC topology with a synchronous buck-boost (or Four Switch Buck-Boost) is used.
- **MCU controller:** The micro controller is in charge of several functions (ON/OFF

control, PV input power monitoring, critical mode protection, etc.) and is directly connected with the OBC by using a I^2C communication protocol[g].

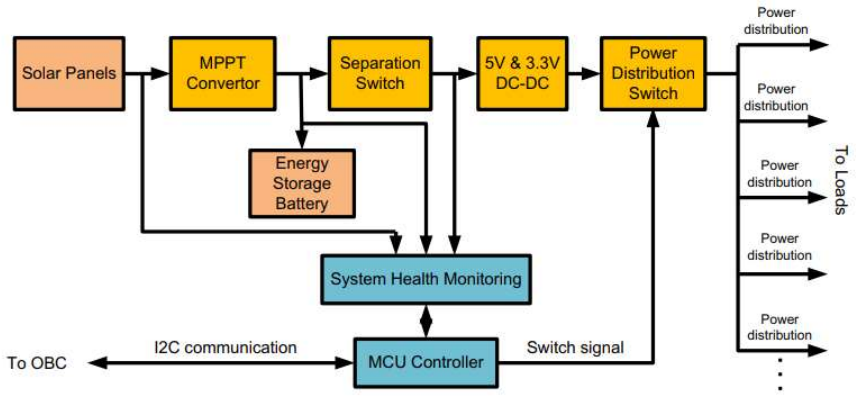

Figure 2-21: Aoxiang-sat EPS Architecture [10]

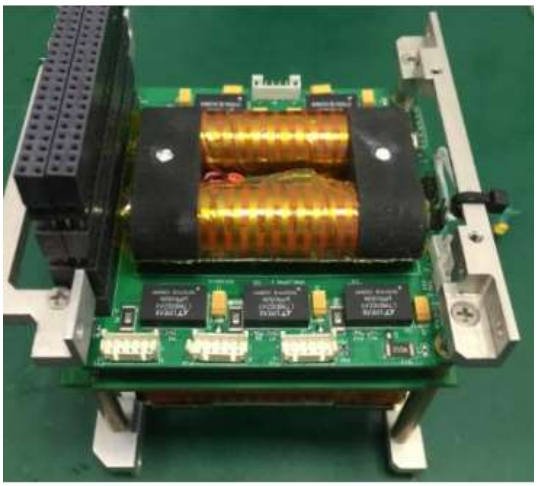

Figure 2-22: Aoxiang-sat EPS prototype [10]

The main difference from the previous example is that the system employs a MPPT regulated bus architecture. Even if the Aoxiang-sat was designed for LEO operation, the bus voltage is set in a range between 6.5V and 8.4V (for the power budget exposed in 2-21). Figure 2-22 shows the EPS shape included on board of the Aoxiang-sat.

2-4 Summary

In this chapter the main parts of an EPS subsystem in CubeSats have been described. Solar array and ESS key points have been described. Power Management and Distri-

[g] I^2C is a serial protocol for two-wire interface to connect low-speed devices like micro controllers, EEPROMs, A/D and D/A converters

bution issues were treated in depth, explaining different architectures for regulation and control of the power flow as well as the main points of the distribution system. Finally, a literature review of some real projects was pursued, differentiating between plug-and-play and one-board designs.

Chapter 3

EPS Basic Design

The objective of this chapter is to set the boundary conditions of the Electrical Power System (EPS) design and to select the basic architecture of the system. The necessary data is basically the power input and output that the system has to handle as well as the characteristics of the studied CubeSat types. It is also necessary to choose a proper architecture for the system and to set the main functional parameters (modularity, type of converters, etc.).

The basis of the design is established based on LUMIO [4] and MARIO [5, 6] missions. These reports provide detailed data about their operation and can be useful in order to set the edges of the design.

3-1 CubeSat Functional Characteristics

Present work deals with a specific type of CubeSat for beyond-LEO missions. Power generation issues are critical in this kind of missions and they constrain the CubeSat power source design. For interplanetary transfer, the thruster problem also arises, which needs special attention in terms of power delivery.

In order to analyse the problem, an upper limit in functional typology is set: MARIO CubeSat typology is proposed as upper limit in topology and functional characteristics due to the following reasons:

- **Deployable Solar Array:** The deployable Solar Array allows higher solar collection than the body-mounted panels so the power production will be the highest possible (only depending on the number of mounted panels).
- **Solar Array Drive Actuator (SADA) usage:** SADA allows a more regular power acquisition. It varies the angle of the solar arrays in order to reduce the inclination angle and keep the solar panel normal to the Sun irradiation direction. Figure 3-1 depicts how SADA system works.

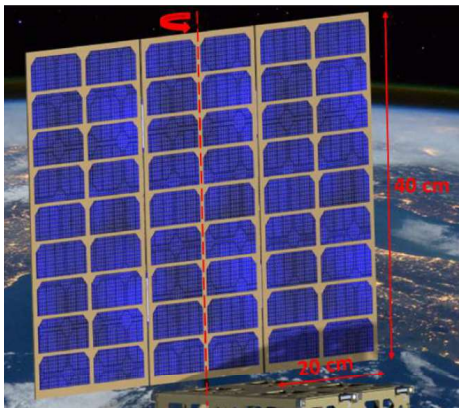

Figure 3-1: MARIO Tri-folded Solar Array with SADA mechanism [5, 6]

- **Interplanetary transfer:** For achieving transfer and deep space cruise, MARIO utilizes an Ion Thruster[a], so the power consumption increases when using this kind of equipment.
- **Size:** MARIO size is 16U, with this dimension being the upper limit in this work.

As for the lower limit, the changes are the size (12U is considered) and the exclusion of Ion Thruster. The proposed typology still has deployable solar panels and SADA (essential elements for energy collection when moving away from the Sun).

3-2 Power Boundaries

Once the typology of device under study has been bounded, it is necessary to set the power conditions under which the EPS will work. At first, the electrical power system is conceived as a black box with input and output powers. Before starting the design of the converter, a proper range of power must be defined, and once again, LUMIO and MARIO missions are employed as references, marking the lower and upper boundaries of load power operations respectively. Figure 3-2 shows the overall power flow diagram.

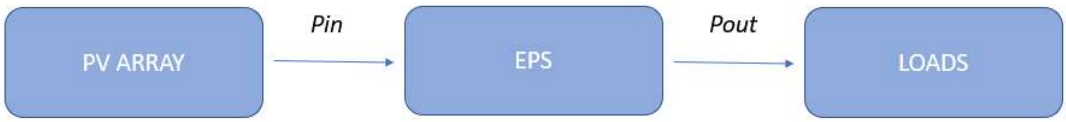

Figure 3-2: Power flow diagram

Boundaries must be defined in terms of Generation and Consumption. Both missions are analysed in order to obtain the peak values of power in the different stages of the mission.

[a] An ion thruster creates thrust by accelerating ions with electricity

3-2-1 Generation

For proper confinement of the problem, higher and lower limits have to be identified. Generation boundaries directly depend on the properties of the solar panel (efficiency, type of technology, etc.).

- *Higher limit:* It is clear that MARIO CubeSat [5, 6] will have the highest generation due to the greater size of its solar array. Maximum solar collection will happen immediately after the deployment near the Earth with Beginning of Life (BOL) characteristics (without degradation). Figure 3-3 identifies MARIO power curve for generation and consumption over the whole low-thrust transfer phase. Approximately, 120W is the value obtained in the initial time for the total power available.

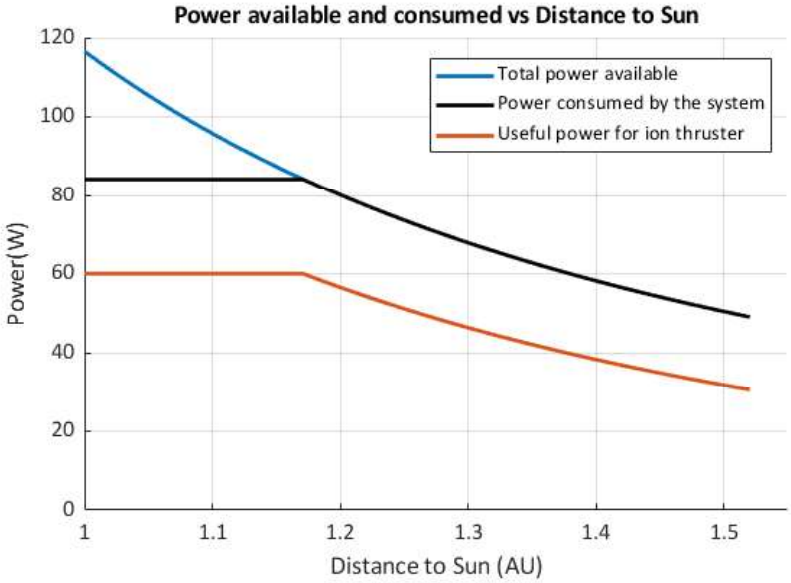

Figure 3-3: Power representation for ion thruster vs Distance to Sun [5, 6]

- *Lower limit:* The minimum average generation is found for LUMIO [4], whose average power production is 28W. Despite this fact, the lower limit for generation is not as important because the system has to be prepared to handle low or even null power production.

Once the main data has been obtained, a gross estimation is applied in order to take into account future improvements in solar panel efficiencies. By applying a 20% improvement to the higher limit (conservative value for the sake of security), a gross value of 150W[b] generation for MARIO mission is obtained.

[b] Real value is 144W but for the sake of simplicity, 150W is adopted

3-2-2 Load Consumption

Load consumption has a huge range of possible values due to the payload and systems dependence. In order to settle the limits for the reference missions, load consumption of both missions is analysed in terms of consumed power. MARIO mission includes an Ion Thruster that will be a critical point.

- *Higher limit:* MARIO CubeSat will have the highest consumed power due to the size and subsystem arrangement. It is possible to analyse the power consumed during normal operation for each of the phases of MARIO life cycle by checking Table 3-1. Each operation mode represents the different combination between subsystems depending whether they are switched on or off. As observed, the maximum power requirement occurs during the interplanetary transfer operation mode in which the Ion Thruster fires, and the value is 84.4W. For reliability reasons the considered value will be 100W.

Table 3-1: MARIO power requirements for the different operation modes [5, 6]

OPERATION MODE	POWER [W]
Deployment	7.24
Detumble/Desat	24.54
Earth Burn	26.63
Earth Communication	35.54
Earth Orbiting	12.64
Interplanetary Transfer	84.54
Int. Transfer + Communication	79.54
Int. Transfer Communication	43.54
Mars Capture	30.54
Mars PL	34.43
Mars Communication	45.62
Mars Eclipse	12.73
Mars ADCS and PROC	24.53
Safe Mode	10

- *Lower limit:* After the deployment of the satellite, subsystems start working and the CubeSat is not supposed to switch off all the subsystems (0 W consumption). There exits one operation mode called Safe Mode where the system operates under minimum consumption and only the essential subsystems are switched on (On-Board Computer (OBC), EPS, etc.). Table 3-2 shows operation mode power for both missions. Adopted value will be 8.995W, approximately 9W.

Power limits have been sized for the reference missions considered. Obviously, one of the aims is flexibility, so the obtained values are not rigid and higher power values may be considered in order to assess the flexibility and reliability features of the system.

Table 3-2: Safe mode operation power for LUMIO and MARIO

	LUMIO	MARIO
Safe Mode Power [W]	8.995	10

3-3 Phase definition

For phase definition, it is necessary to set some functional parameters. The objective missions have common points in terms of mission stages. Thus, it is possible to define three main stages:

- *Launch and Early Operation (LEOP):* The spacecraft is located near the Earth and the EPS may deal with eclipse conditions where the sunlight is not incident on the spacecraft.
- *Transfer:* Interplanetary or lunar missions have a transfer stage where sunlight is always present and its intensity changes only with the distance from the Sun. Moreover, systems including SADA ensure continuous power generation.
- *Main orbit:* Once the spacecraft is inserted in the desired final orbit for scientific observations, operation under sunlight conditions and eclipse periods are foreseen.

Focusing on Figure 3-3, where the available and consumed powers during transfer phase of MARIO is depicted, it is possible to notice that,

1. *Total power available > Total consumed power:* This working conditions will occur during the Deployment and Transfer stages. The EPS under design must dissipate or adjust the drawn power in order to meet the load consumption.
2. *Total power available = Total consumed power:* Under these conditions, as part of the Transfer stage and Mars orbit, it is necessary to obtain the total power provided by the solar array, so an Maximum Power Point Tracking (MPPT) system (converter + algorithm) is necessary.

Trading off the last two classifications, the EPS operational phases can be defined. Table 3-3 shows the different characteristics for each stage of the EPS operation.

As it can be observed in Table 3-3, when the Total Available Power is greater than the Total Consumed Power, converter interfaced with the solar panels is adjusted to draw the exact power needed by the loads from the Photovoltaic (PV) array. This is achieved by controlling the current in the input of the converter and instead of following the Maximum Power Point (MPP) point, the desired current and voltage is imposed in order to draw the exact power.

Also some voltage levels for the main bus are defined. The bus voltage levels will follow the battery voltage levels in order to properly manage the charging and discharging of the battery.

Table 3-3: Operating conditions of the system during different stages of mission

		LEOP + (Total available power > Total consumed power) CHARACTERISTICS
1		*Initially charged battery*
3	*Earth Eclipse*	*Battery discharging: Battery feeds the load* *Battery charging: MPPT algorithm is applied in order to satisfy loads and battery* *Battery charged: Current control mode is applied, supplying the exact amount of current the loads need*
		Transfer + (Total available power > Total consumed power) CHARACTERISTICS
1		*No battery usage*
2		*Current control mode: power adjusted to satisfy required power by the loads*
		Transfer + (Total available power = Total consumed power) CHARACTERISTICS
1		*No battery usage*
2		*MPPT mode: main bus regulated, MPP voltage in PV array*
		Main Orbit + (Total available power = Total consumed power) CHARACTERISTICS
1	*Sunlight MPPT regulation*	*Battery charging: MPPT algorithm is applied in order to satisfy loads and battery* *Battery charging: Current control mode is applied, supplying the exact amount of current the loads need*
2	*Eclipse*	*Battery discharging: Battery feeding the load*
3		*Peak mode: Battery helps the main supply*

Once the different operational modes of the EPS have been defined, an architecture can be developed to ensure proper working and achieve desired performance.

3-4 EPS system requirements

Considering sections 3-1 to 3-3 it is possible to put together all the analysis and set the EPS main characteristics. Table 3-4 lists the EPS system requirements.

Once the EPS requirements have been set and described, it is possible to initiate the design process. In present chapter only the basic design features are going to be set, while the detailed design will be assessed in following chapters.

3-5 Architecture selection

Definition is based on the examples presented in Chapter 2. The design is based in previous works even if none of them was suitable for the kind of mission this system design deals with. That is the reason why the proposed architecture has an innovative shape and may use different kind of equipment. Figure 3-4 shows the different blocks and interactions of the architecture scheme. System employed will be a battery bus voltage with MPPT usage.

The different parts of the architecture are:

- **Array Conditioning Unit (ACU):** Its main aim is the decoupling of the solar array and the EPS system. It senses the PV system voltage, current and temperature in order to have the required information for power control. It also filters the

Table 3-4: EPS system requirements

ID	Requirement	Rationale
EPS-001	The EPS shall handle a maximum load power of 100 W.	MARIO peak power consumption.
EPS-002	The EPS shall handle a minimum load power of 9 W.	LUMIO minimum power consumption.
EPS-003	The EPS shall provide overcurrent protection in POL points.	Prevent failure.
EPS-004	The EPS shall be able to handle voltage and current oscillations (ripples) up to 1% of their average value at maximum allowed load.	Power quality requirement.
EPS-005	The EPS shall be able to limit the generation when power generation exceeds load requirement.	Simplicity of the system and security and to avoid electrical energy dissipators.
EPS-006	The EPS shall provide overcharge protection to the battery, limiting the maximum SoC of the battery to 80%.	Protection of battery and prolongation of battery life.
EPS-007	The maximum deph of discharge shall be no more than 60%.	Protection of battery and prolongation of battery life.
EPS-008	The EPS shall limit the charging current to specified levels by the battery manufacturer.	Battery life protection.
EPS-009	The EPS shall assure a current and voltage oscillation up to a maximum value of 1% of their average value.	Proper feeding of POL converters and provide proper voltage and current dynamics in the battery terminals.
EPS-010	EPS shall handle a maximum generation power of 150W.	MARIO peak power generation.
EPS-011	The EPS shall limit oscillation (ripples plus harmonic content) in generation terminals up to 5%	Power quality assurance, capacitor size constraints and failure prevention.

harmonics produced by the main converter avoiding its back propagation towards the PV array.

- **Converter type 1:** This converter is in charge of controlling its input current and voltage to obtain the desired power from the PV panels, controlling the main bus current between certain boundaries, performing the MPPT algorithm for MPP tracking, and regulating the battery charge/discharge procedure. Depending on the operational phase of the EPS, the converter varies its working conditions. Detailed design is presented in the following chapters.

- **Battery Monitoring Unit (BMU):** As the name itself indicates, it is in charge of the battery integration and monitoring. It senses the battery State of Charge (SoC) by means of frequency sweep and communication with the Digital Signal Processing (DSP) unit which has the battery model inside its memory. This module design is outside the scope of this work.

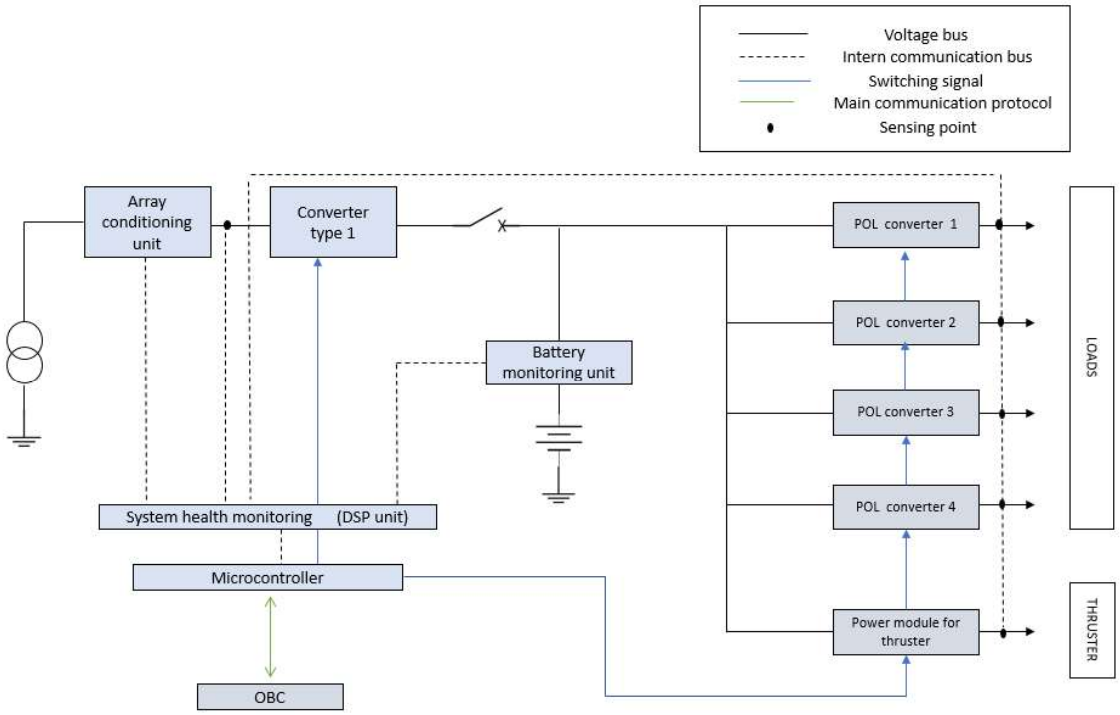

Figure 3-4: Proposed architecture

- **POL converters:** It sets the Point of Load (POL) voltage levels. In this case, desired voltage levels are 3.3V, 5V, 12V and 24V. They can switch on and off the branch in which they are connected if their loads are not in use. They also damp undesired transients in the loads. Each branch is monitored for system health assessment and protection devices are also implemented. The selected voltage levels are usually employed in the state of the art systems. However, depending upon the load variation and current constraints, voltage levels could be changed.

- **Switch:** It is used in order to switch on the whole system once the spacecraft reaches the deployment point.

- **Power module for thruster:** This device is used for electrical thruster power supply and it is out of the scope of this work.

In addition, there exist some devices for monitoring, processing and communication inside the EPS physical model.

The *system health monitoring unit* is a DSP device with integrated memory. It performs measuring actions and commands some basic operations such as emergency actions and SoC determination.

EPS board also includes a *microcontroller*, which is mainly in charge of the low level control of the system. The microcontoller is directly connected with the *OBC* through

a communication protocol, which will probably be a I^2C protocol due to its lower power consumption.

Communication and interface design is out of the scope of this work and just some main features are indicated.

3-6 Main converter typology

The main converter (type 1) has several objectives:

- *Perform MPPT algorithm in order to work in the MPP of the PV curve*
- *Control input current on the system*
- *Control battery charging current for battery damage prevention*
- *Deal with broad power range*

In order to accomplish such objectives, different topologies for dc-dc converters exist. The main characteristic will be the ability to step up and down the input voltage because of the wide spectrum of power during the mission. Both Buck and Boost converters are discarded for this reason.

Flyback type converters are an isolated type of converters which use a transformer in order to achieve such an isolation. For this reason, they are not usually employed when the work takes place under limitations of weight and space.

Another possible solution is to use a boost converter with a linear regulator[c], which allows to generate higher and lower voltage. Despite this fact, they have really poor efficiency values compared to classical systems without linear regulator.

There exists a group of converters which are called inverting converter which also allows to step up and down the voltage. Buck-Boost and Cúk converters belong to this group. Typologies of these two converters are depicted in Figure3-5. Cúk converter has a higher amount of components (one more capacitor and inductor) and due to mission requirements on space and weight, Buck-Boost converters are preferred over this type of converters.

For converters which are not inverting and are able to step up and down the input voltage, there exist two converters typically used for this kind of applications which are non-inverting buck-boost converter and single-ended primary-inductance converter (SEPIC) [12]. Figure 3-6 depicts these two kinds of converters. Non-inverting Buck-Boost is preferred over SEPC for this kind ofsystem because of the lower level of reactive components (inductors, capacitors).

[c] A linear regulator is an electronics device which allows to maintain a steady voltage

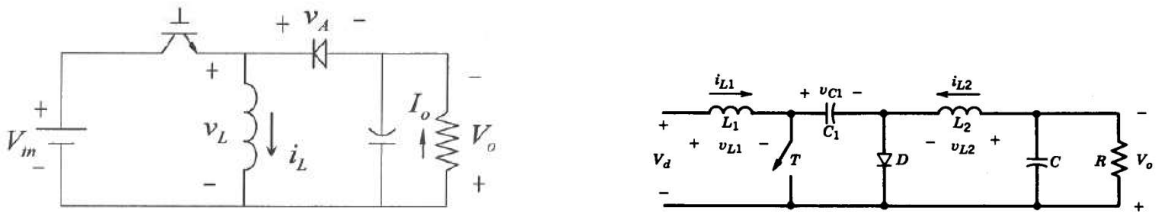

(a) Buck-Boost converter

(b) Cúk converter

Figure 3-5: Inverting converters [11]

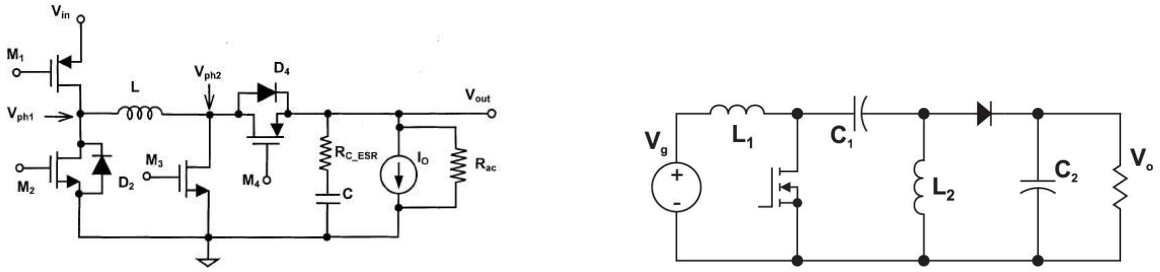

(a) Non-inverting Buck-Boost converter

(b) SEPIC converter

Figure 3-6: Non-inverting converters typologies considered [12]

Normally, these kind of converters are implemented in an IC (theory of System on a Chip (SOC))[d], so the idea of inverting the poles of the converter is not suitable for these kind of embedded systems. That is why, normally for this kind of applications, non-inverting buck-boost converter is used. In spite of its better behaviour and its easier adaptability to embedded systems, its working principle is more complex. That is the reason why for this kind of nascent stage of the research work, a simpler system is firstly used. The system is going to be simulated with the buck-boost inverting dc-dc converter type.

3-7 POL converters typology

These kind of converters should manage the voltage level of the different load points. These levels will be be 3.3V, 5V, 12V and 24V.

The type of converter will depend on the battery voltage level and the risk of overvoltage inside the main voltage bus. If the voltage level of the point of load is lower than the minimum (cut-off) battery level, the employed converter will be a step-down (buck) converter. If the voltage is higher than the fully charged battery voltage level plus a overvoltage margin, employed converter will be a step-up (boost) converter. If

[d] A SOC is an integrated circuit that contains all the required circuitry and components of an electronic system on a single chip. Following [12] inversion of poles is not possible when working with these kind of systems.

the voltage level is within the boundaries of fully charged/fully discharged battery, a buck-boost converter is employed (or non-inverting buck-boost converter). Figure 3-7 represents the Buck and the Boost types for POL use.

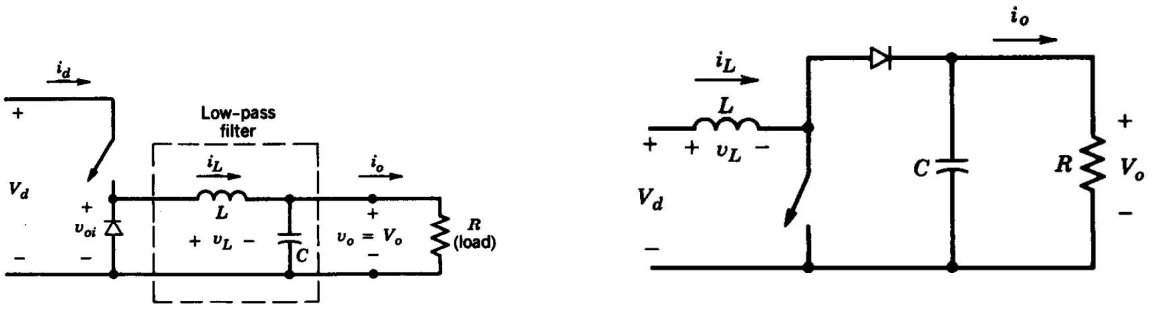

(a) Standard Buck converter **(b)** Standard Boost converter

Figure 3-7: Standard dc-dc converters [11]

3-8 Summary

This chapter defined the main characteristics of the EPS system. The boundaries in terms of specific characteristics, power generation and load consumption power were specified. Operational phases have also been defined in terms of their particular characteristics, setting the system architecture according to them. Finally, the basic design of the system has been set, defining the main components and their functions. Little attention is paid to the communication protocols and interface systems and on the other hand, the two main types of converters, that are employed, are characterised.

One of the main points which is detailed in this chapter has been the definition of the main type of architecture employed: Centralised system, MPPT usage with battery bus voltage.

EPS main schematic represents a block diagram and definitive physical design can vary from the essential design.

Chapter 4

EPS model development

Present chapter deals with the proposed model of the system. It is necessary to build the main components of the proposed architecture, generation equipment, and storage for both case studies. For every component in the system,the basic working principle is also explained in order to build a whole picture adressed to those readers with basic knowledge in Electrical Engineering principles. It is clear that an expanded explanation would include every expression demonstration. However and exhaustive explanation is discarded in this work but the readers are invited to refer to Mohan et al [11].

Te aim of this model is to simulate some of the most important Electrical Power System (EPS) functional phases. The software used for simulation will be Matlab-Simulink. It is a well known software for signal simulation and, by adding Simscape package, it is also able to simulate physical systems. Inside Simscape it is possible to find a library called Power Systems, which offers a wide range of specialised blocks for power system simulation. Figure 4-1 shows the employed library location inside Simulink libraries.

4-1 Converter models and working principles

As mentioned in Chapter 3, converter types will be either Buck, Boost or Buck-Boost, depending on their output voltage and main bus voltage level. As it will be described in following chapters of this work,the Boost converter type will not be necessary for the system under study.

Different converter models have been built taking into account ideal components due to the nascent stage of the research work. Additionally the savings in computation time are also taken into account.[a].

[a] In future steps of the work it would be necessary to take into account parasitic elements, quality factor of inductances, etc.

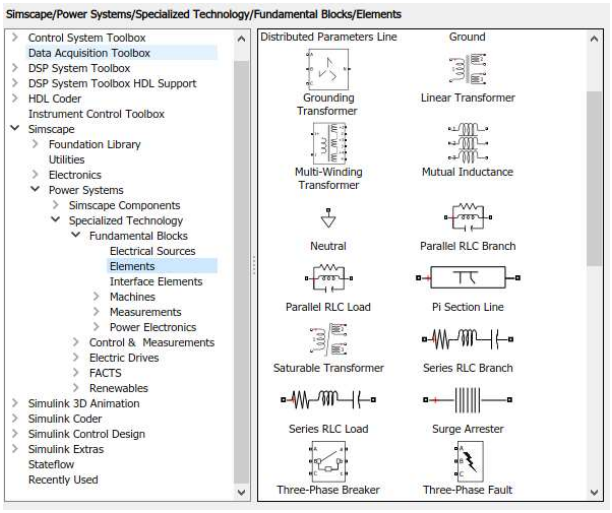

Figure 4-1: Simulink library for Power System simulation

Regarding transistor modelling, which is common to every converter in the model, a typical MOSFET transistor is employed due to its broad applicability. In future research works, the transistor type could be different depending upon renew requirements.

The main working principle in dc-dc converters relies on stepping-up or stepping-down some of their electromagnetic parameters (current and voltage). This is achieved by controlling the switch or switches, in this case a MOSFET transistor, by modifying its gate signal. Gate input signal is obtained by intersecting the desired control signal (error signal) with a sawtooth signal (with amplitude $\hat{V}_{st}$), whose periodicity frequency is set at the desired switching frequency. Figure 4-2 shows how this gate signal is obtained where v_{st} is the oscillating signal at frequency f_s and the control signal $v_{control}$.

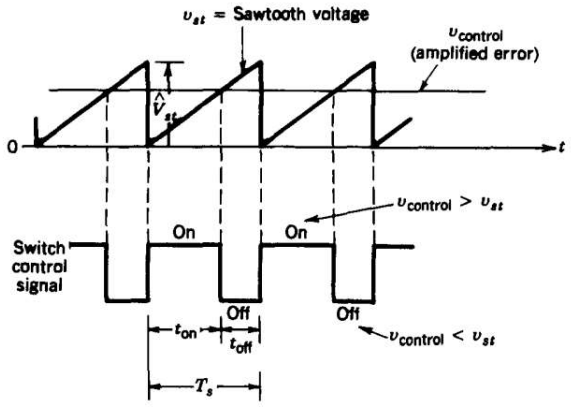

Figure 4-2: Gate input signal determination [11]

The most important parameter in these kind of devices is called Duty Cycle (D), which is the ratio between the time when switch is conducting (t_{on}) and the total switching period (T_s). Figure 4-3 shows the Duty Cycle determination process for a Buck converter, where V_d and V_o are constant dc input and output voltages, respectively.

Duty cycle expression follows equation 4-1 and its value is within the interval [0, 1].

$$D = \frac{t_{on}}{T_s} = \frac{\hat{V}_{st}}{v_{control}} \tag{4-1}$$

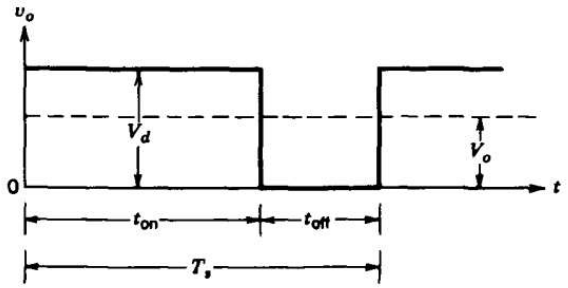

Figure 4-3: Duty cycle determination method [11]

Input and output parameters of the converter depend on the Duty Cycle, which at the same time also depends on the type of converter which is being used. Continuous Conduction Mode (CCM) is assumed, which means that the current in the inductor is always greater than zero ($i_L > 0$) for every steady-state working condition.

4-1-1 POL Buck converter

In Figure 3-7, Buck converter typology is depicted and described. This converter is aimed to step-down the input voltage, providing a lower voltage at the output terminals of the converter. Main relationship between input and output parameters is given by equation 4-2.

The main working principle and parameters are described by the electrical circuit when the switch is on and off, making the main parameters to vary depending on the circuit defined by the working conditions.

$$D = \frac{V_d}{V_o} = \frac{I_o}{I_d} \tag{4-2}$$

Figure 4-5 illustrates the two working conditions and the electrical circuits of the converter for both settings (when transistor is on and off) by assuming that inductor current i_L flows continuously.

The circuit equations, which are given by the typical inductor and capacitor equations are expressed in equations 4-3 and 4-4, respectively. The equations describe the behaviour of the inductor and the capacitor which are evaluated for the different working conditions and provide the characteristic output curves that are employed for ripple evaluation.

$$v_L = L\frac{di_L}{dt} \tag{4-3}$$

$$i_C = C\frac{dv_o}{dt} \tag{4-4}$$

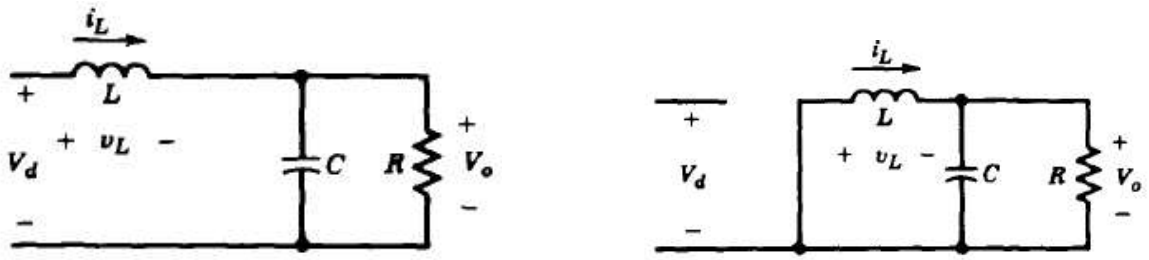

(a) Transistor conducting **(b)** Transistor not conducting

Figure 4-4: Converter circuits for both operating conditions in Buck converters [11]

Characteristic curves of i_L and v_o are presented in order to evaluate their ripple (variation respect to the mean value) in Figure 4-5. Analysis of the ripples of i_L and v_o is critical to evaluate system behaviour and set parameters to obtain the desired performance. Ripple must be limited to a maximum value in order to ensure power quality. Ripple values are ΔI_L and ΔV_o for current and voltage respectively[b].

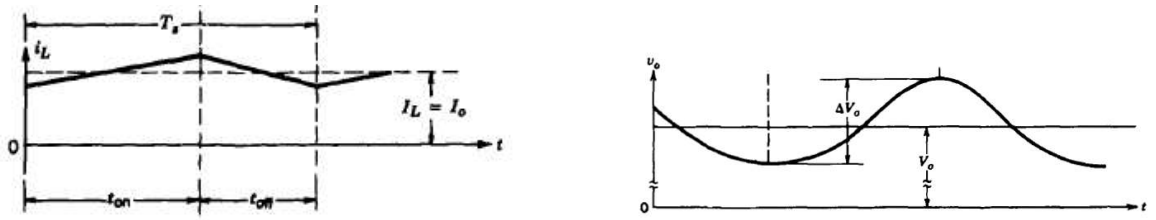

(a) i_L waveform **(b)** v_o waveform

Figure 4-5: Output waveforms in Buck converter showing ripple values [11]

$$\Delta I_L = \frac{V_o}{L}(1-D)T_s \tag{4-5}$$

$$\Delta V_o = \frac{1}{C}\frac{\Delta I_L T_s}{8} \tag{4-6}$$

A point to note is that there exists a low-pass filter comprised by the inductor and the capacitor inside the converter. This filter has a cut-off frequency which attenuates higher harmonic amplitudes. With f_c being the cut-off frequency for the filter, it is required that $f_c \ll f_s$ so the harmonic component of the voltage is attenuated. For the input current, similar phenomenon holds and another filter may be necessary. Figure 5-11 depicts the low-pass filter effect, where v_o and v_{oi} are the output and input filter voltages respectively.

[b]For more details refer to Mohan et al [11], Chapter 7

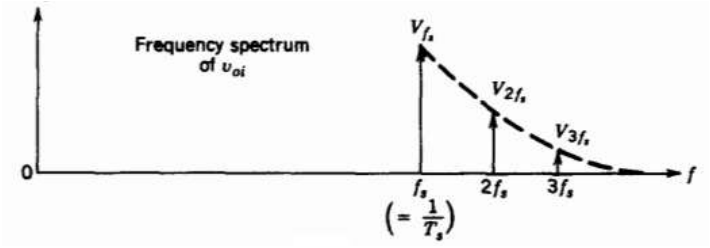

(a) Input filter harmonic content

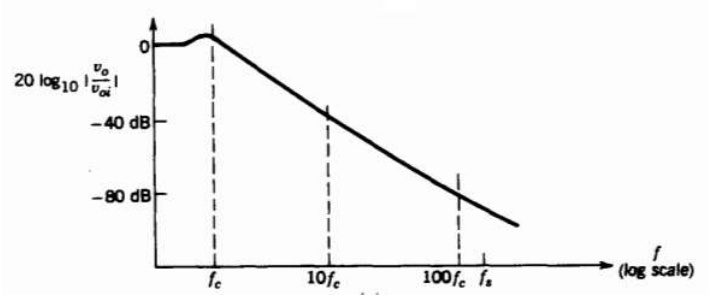

(b) Bode diagram between input and output voltages

Figure 4-6: Low-pass filter action [11]

Figure 4-7 describes the Simulink model for the POL-Buck converter. Connections labelled 2 and 3 are attached to the main distribution bus and the others labelled 1 and 4 are attached to the load bus.

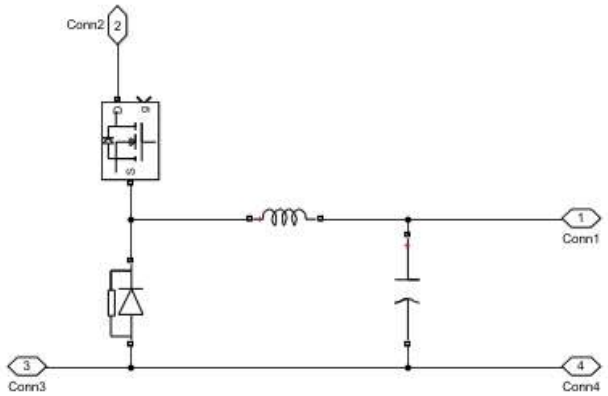

Figure 4-7: POL-Buck converter Simulink model

4-1-2 POL and Main Buck-Boost converter

The converter typology is the same for the 24V POL converter and the main converter performing the Maximum Power Point Tracking (MPPT) algorithm and controlling the main parameters of the distribution system [c]. In Chapter 3 the typology was described,

[c] As it was commented in Chapter 3, the usual employed converter is the non-inverting one. For the sake of simplicity, this type is used in this stage of the research.

and now the focus is on the working principle.

The Buck-Boost converter can be obtained by cascading the two basic converters (Buck and Boost). The aim of this converter is to both step-up and step-down the voltage in order to deal with a broader voltage range. The current behaviour in the inductor will be the sum of I_o and I_d. The duty cycle variation is explained in equation 4-7. When D is greater than 0.5, the voltage is stepped-up and is stepped-down if $D < 0.5$.

$$\frac{V_o}{V_d} = \frac{I_d}{I_o} = \frac{D}{(1-D)} \tag{4-7}$$

The circuit depending upon the working conditions of the switch also changes and Figure 4-8 depicts both electrical circuits with their parameters (for i_L greater than zero). From Figures 4-8 and 4-5 it is possible to observe the inverting characteristic where the poles are inverted. Equation 4-7 employed for Buck converter also holds for Buck-Boost converter, but the different configuration of its components make the characteristic parameter curves to be different.

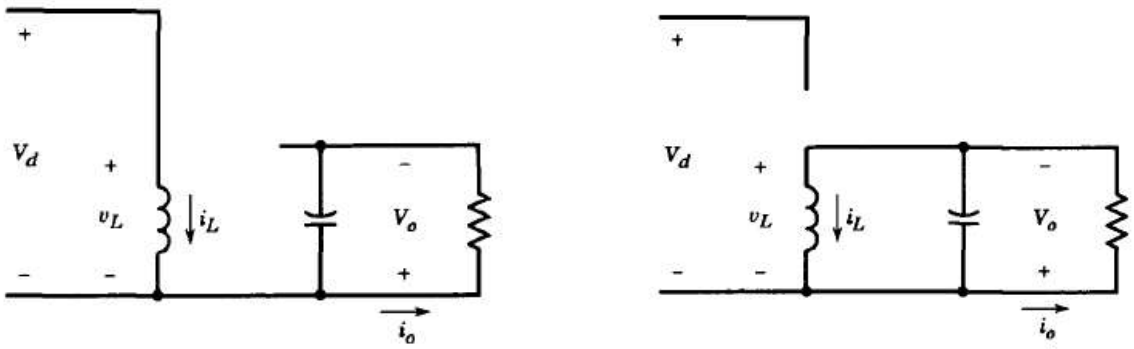

(a) Transistor conducting **(b)** Transistor not conducting

Figure 4-8: Converter circuits for both operating conditions in Buck-Boost converters [11]

The main current and voltage curves and ripples are depicted in Figure 4-9. It can be observed that the curves are a bit different and the ripple expressions depend mainly on the same parameters. It is inversely proportional to switching frequency f_s and to the inductance in case of the current and to the capacitance in case of the voltage.

In this kind of converter a low-pass filter is also present, so the harmonic content of output parameters will depend on the filter cut-off frequency. A filter may also be necessary in the input in order to avoid undesirable effects of the harmonic content of the input current.

Figure 4-10 shows the Simulink model for this converter type. Connection labels are attached to different parts depending whether the converter is working as a Point of Load (POL) converter or as the main one.

In following Chapters, it will be necessary to limit the ripple of the main output and input signals. In addition to the ripple values, some harmonics will also be present and

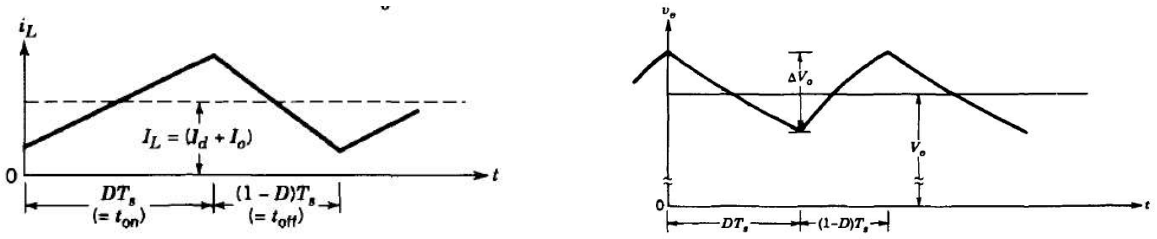

(a) Inductor current waveform **(b)** Capacitor voltage waveform

Figure 4-9: Main parameters waveforms for Buck-Boost converters [11]

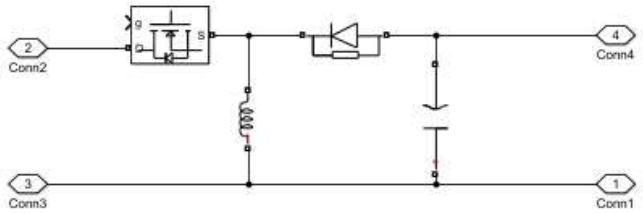

Figure 4-10: Buck-Boost converter Simulink model

it will be necessary to tune the main filter of the converters. This harmonic content is linked with the ripple values since both depend on the inductance and capacitance as well as the switching frequency. This tuning is done to obtain the desired values of the deviation from the mean value of the signal.

4-2 PV generation system model

For Photovoltaic (PV) array model implementation, an already implemented block is available in the Simulink library. This PV module contains the essential model of the PV technology.[d]. In Chapter 2, some fundamentals are provided. In this section, the main equations, inputs and outputs will be explained.

The main circuit describing the PV module behaviour is studied. It doesn't have any differential equations and the main equation describing its behaviour is given by the so called diode equation (see eq. 4-8). Figure 4-11 represents the equivalent circuit and equations 4-8 and 4-9 describe the behaviour of the model.

$$I_d = I_o \cdot [exp(\frac{V_d}{V_T}) - 1] \tag{4-8}$$

$$V_T = \frac{kT}{q} \cdot nI \cdot N_{cell} \tag{4-9}$$

[d] https://es.mathworks.com/help/physmod/sps/powersys/ref/pvarray.html

- I_d: Diode current.
- V_d: Diode voltage.
- I_o: Diode saturation current.
- nI: Diode ideality factor, it is a number close to 1.
- k: Boltzmann constant $\simeq 1.3806 JK^{-1}$.
- q: Electron charge $\simeq 1.6022e^{-19}C$.
- T: Cell temperature in Kelvin.
- N_{cell}: Number of cells connected in series in a module.

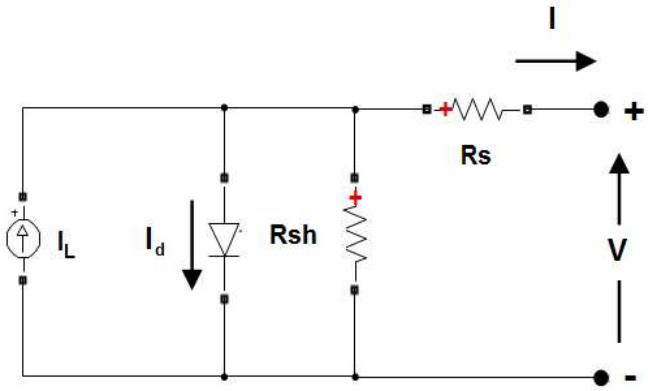

Figure 4-11: Equivalent circuit of the PV model

Resistances R_{sh} and R_s represent the real system behaviour, taking into account two phenomena occurring inside the PV cells. The former represents the bulk resistance of the silicon wafer, the resistance between metallic contacts of the front and back surfaces, and the resistance of the terminal contacts. The latter is associated with the leakage currents due to the p-n junctions non-linearities and impurities inside the cell.

Irradiation and temperature heavily influence the PV curves' performance. Lower irradiation levels reduce the available energy in the array and it is one of the most critical issues in power collection. Figure 4-12 shows the effect of the different values of irradiation on the I-V curves. Regarding the temperature effects, for decreasing temperature the open-circuit voltage (V_{oc}) increases and the short-circuit current (I_{sc}) decreases marginally. Figure 4-18 shows the effect of temperature in I-V curves.

It is necessary to describe the connection strategy between cells for the two different case studies. In [5, 6] and [4] it is possible to find the characteristics of solar arrays designs for for MARIO and LUMIO missions, respectively. The connections are described by a simple computation taking into account the already designed solar arrays, with one module of the explained model equal to one string. Figures 4-14 and 4-15 depict the connection strategy of the two CubeSats under study.

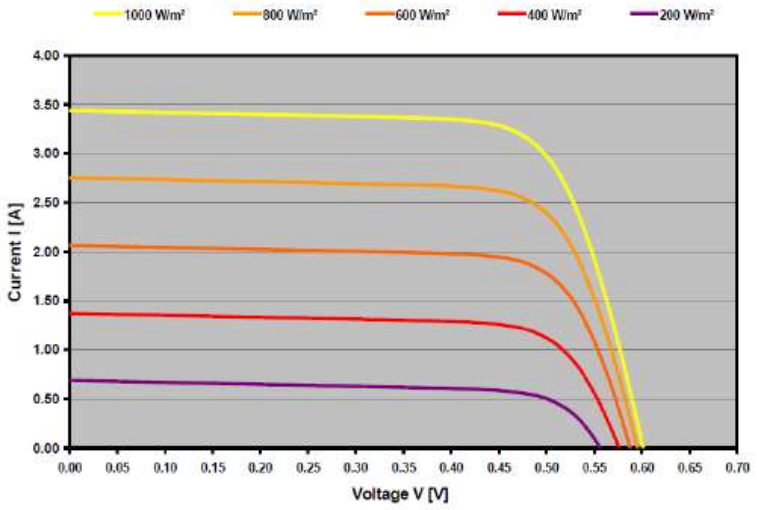

Figure 4-12: Irradiation effect for different levels of incident irradiation in a PV array [13]

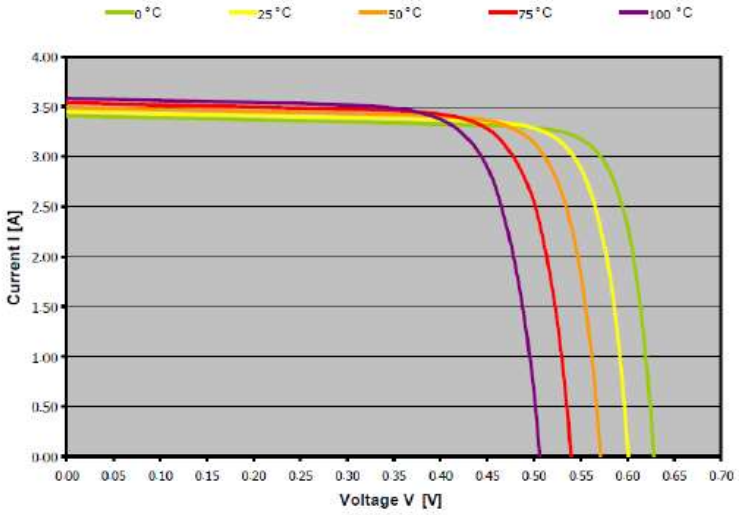

Figure 4-13: Temperature effect for different levels of PV array temperatures [13]

Solar cells employed for the satellites have been defined in previous stages of their design. Employed COTS equipment is AzurSpace 3G30C Advanced 30% Triple Junction GaAs Junction Solar Cell [e] whose main characteristics are described in Tables 4-1 and 4-2. The characteristic parameters of the solar cells degrade over the mission lifetime due to the accumulation of radiation dosage [f]

Once all the characteristics are known and connections are described it is possible to implement the model block for Simulink. Figure 4-16 shows the block inputs and

[e] http://www.azurspace.com/images/0003429-01-01_DB_3G30C-Advanced.pdf

[f] The number of radiant-energy particles emitted from or incident on a surface in a given period of time, divided by the area of the surface.

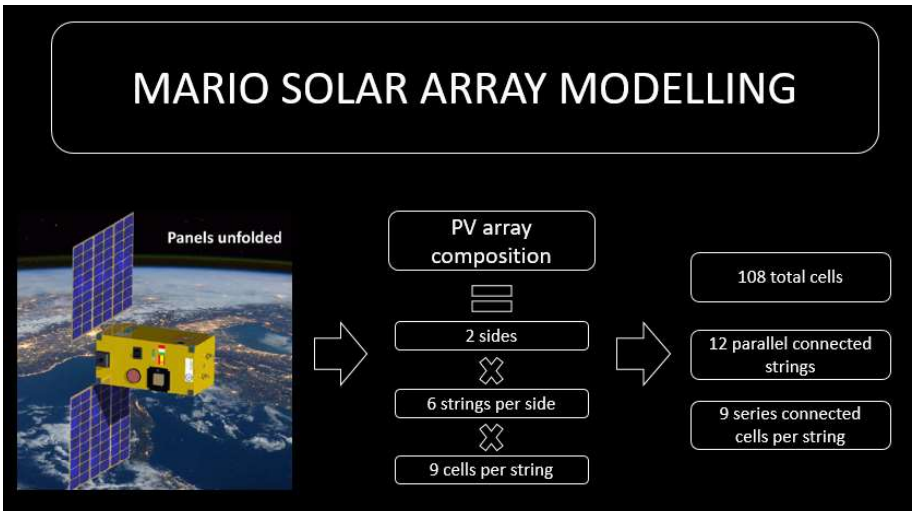

Figure 4-14: MARIO solar cells connections description

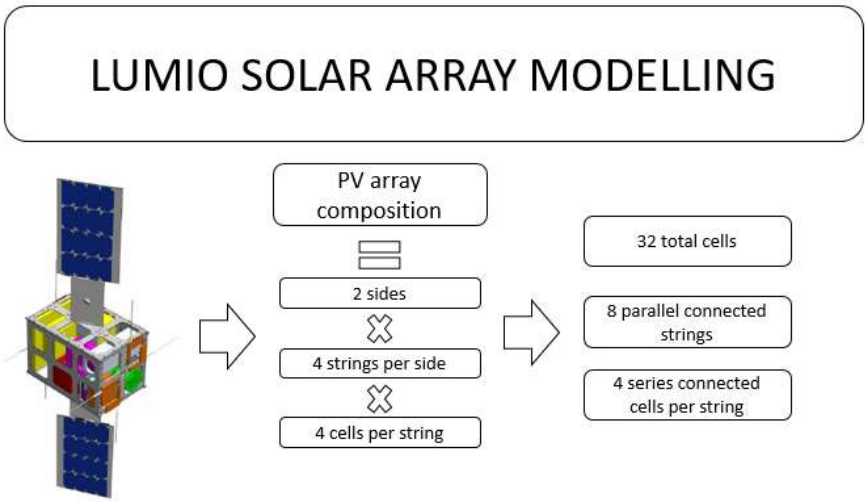

Figure 4-15: LUMIO solar cells connections description

outputs, with:

- *Input signal 1*: Irradiation value
- *Input signal 2*: Temperature value
- *Output signal 1*: Measurements, mainly voltage and current in PV output.
- *Power output*: Positive bus and negative bus connected to the main circuit.

Inside the block, it is possible to model the connections and the main characteristics of the PV array. As an example, MARIO PV array under BOL conditions is implemented. Figure 4-17 shows the main parameters for the PV block which automatically provides

Table 4-1: Solar cell electrical characteristics

Electrical data	*BOL*	*2.5E14*	*5.0E14*	*1.0E15*
Average Open Circuit Voc [mV]	2700	2616	2564	2522
Average Short Circuit Isc [mA]	520.2	518.5	514.0	501.9
Voltage at max. Power Vmp [mV]	2411	2345	2290	2246
Current at max. Power Imp [mA]	504.4	503.2	500.6	486.6
Average efficiency [%]	29.5	28.6	27.8	26.5

for irradiance 1367 W/m^2 and temperature 28°C

Table 4-2: Solar cell temperature characteristics

Temperature gradients	BOL	2.5E14	5.0E14	1.0E15
Open circuit voltage $\Delta Voc/\Delta T \uparrow [mV/^oC]$	-6.2	-6.5	-6.6	-6.7
Short circuit current $\Delta Isc/\Delta T \uparrow [mA/^oC]$	0.36	0.33	0.35	0.38
Voltage at max. power $\Delta Vmp/\Delta T \uparrow [mV/^oC]$	-6.7	-6.8	-7.1	-7.2
Current at max. power $\Delta Imp/\Delta T \uparrow [mA/^oC]$	0.24	0.2	0.24	0.28

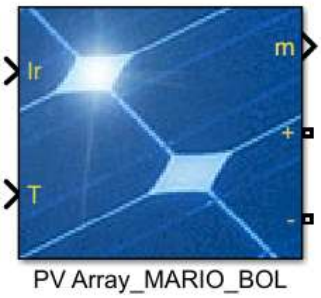

Figure 4-16: PV array model block

the PV curves necessary for the correct characterisation of the PV array (I-V and V-P curves) shown in Figure 4-18. The curves show the values for two different irradiation values. For the given parameters, maximum power production is close to the maximum power that the system can handle (150 W).The PV array model in Simulink can be either user defined or chosen from a given set.

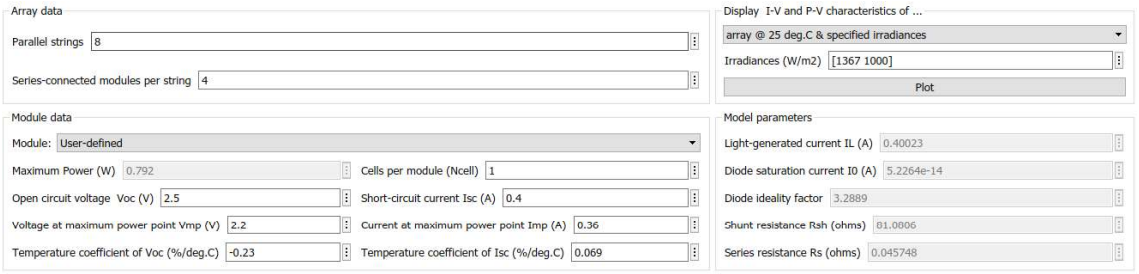

Figure 4-17: PV array model basic data

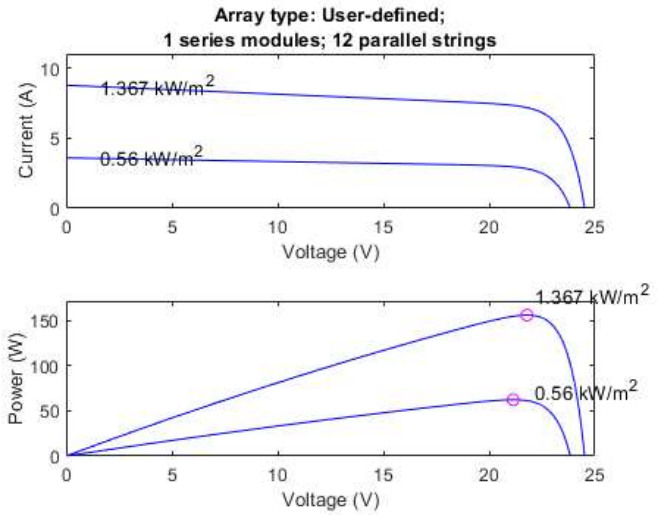

Figure 4-18: PV array model curves for BOL at 25 °C

For each scenario and case study, temperature, irradiation and type of solar panel (depending if LUMIO or MARIO is under study) will change, allowing to simulate the generation during different scenarios of different missions. It will be necessary to know the maximum power point in each scenario for the different irradiation and temperature values.

In order to get the Maximum Power Point (MPP) for each case, a Simulink test is developed. Main principle behind this test system is the variation of the load at array terminals which allows to sweep the current and voltage values, thereby varying the load from open-circuit to short-circuit conditions. Unfortunately, Simulink power systems do not have a proper block for simulating a variable load, thus a custom system is designed. Figure 4-19 shows the device for MPP tracking.

The two load branches simulate open-circuit and short-circuit conditions, with R_{high} being a very high resistance and R_{low} being a small one. The switch is controlled by a ramp signal, which varies from 0 to 1 with a 0.1 slope. The transistor will allow the current to flow in the short-circuit branch, going form a very low current flow to a very high one.

The PV array will provide two plots which will allow to identify the MPP of the array under test. First one will be the Power-Time plot, which will show the MPP of operation with respect to the time. Once the time instant of MPP is known, it will be possible to check the second plot, the IV-Time plot, which provides the maximum current and maximum voltage in the MPP by checking the time instant when the maximum power is achieved. Figure 4-20 and 4-21 show both plots for MPP determination in particular temperature and irradiation conditions.

Once this parameters are known, it is possible to simulate the PV array for the maximum generation conditions. On the one hand, in MARIO mission, these parameters will play a more important role because of the dramatical decrease of irradiation and temperature. On the other hand, for LUMIO, irradiation and temperature don't change

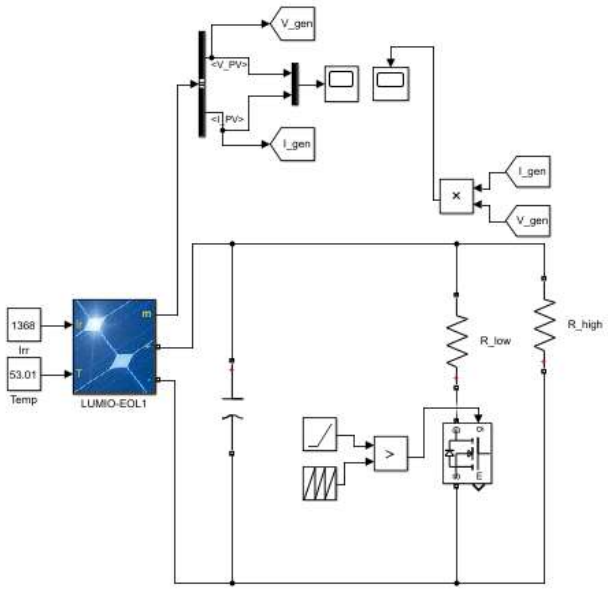

Figure 4-19: Custom system for MPPT

Figure 4-20: PV array power over time for variable load

significantly, so a more uniform generation is achieved.

4-3 Energy storage system model

The storage system is modelled by a Simulink specific block which simulates the dynamic behaviour of the battery. Technology used will be Li-ion type. The model inside

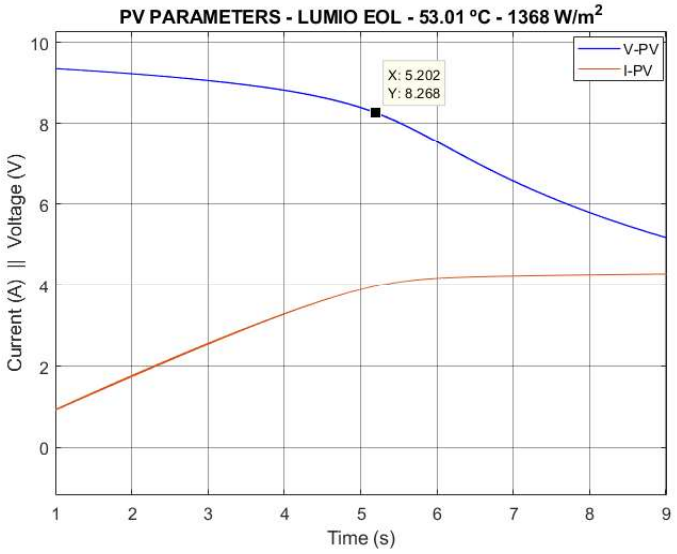

Figure 4-21: PV array characteristics over time for variable load

the block[g] is described in Figure 4-22. For Li-ion technology, there exist two equations describing charge and discharge dynamics. Equations 4-10 and 4-11 describe their State of Charge (SoC) behaviour. The dynamic equations and the parameters in the model are described as follows:

Discharge model (i^*>0)

$$f_1(i^*, i_t, i) = E_o - K \cdot \frac{Q}{Q - i_t} \cdot i^* - K \cdot \frac{Q}{Q - i_t} \cdot i_t + A \cdot exp(-B \cdot i_t) \tag{4-10}$$

Charge model (i^*<0)

$$f_2(i^*, i_t, i) = E_o - K \cdot \frac{Q}{i_t + 0.1Q} \cdot i^* - K \cdot \frac{Q}{Q - i_t} \cdot i_t + A \cdot exp(-B \cdot i_t) \tag{4-11}$$

- E_{batt}: Non-linear voltage of the battery [V].
- E_0: Constant voltage [V].
- $Exp(s)$: Exponential zone dynamics [V].
- $Sel(s)$: Battery mode, represents $Sel(s)$=0 during battery discharge and $Sel(s)$=1 during battery charge.
- K: Polarization constant [Ah^{-1}].
- i^*: Low frequency current dynamics [A].
- i: Battery current [A].

[g] https://es.mathworks.com/help/physmod/sps/powersys/ref/battery.html

- i_t: Extracted capacity [Ah].
- Q: Maximum battery capacity [Ah].
- A: Exponential voltage [V].
- B: Exponential capacity $[Ah^{-1}]$.

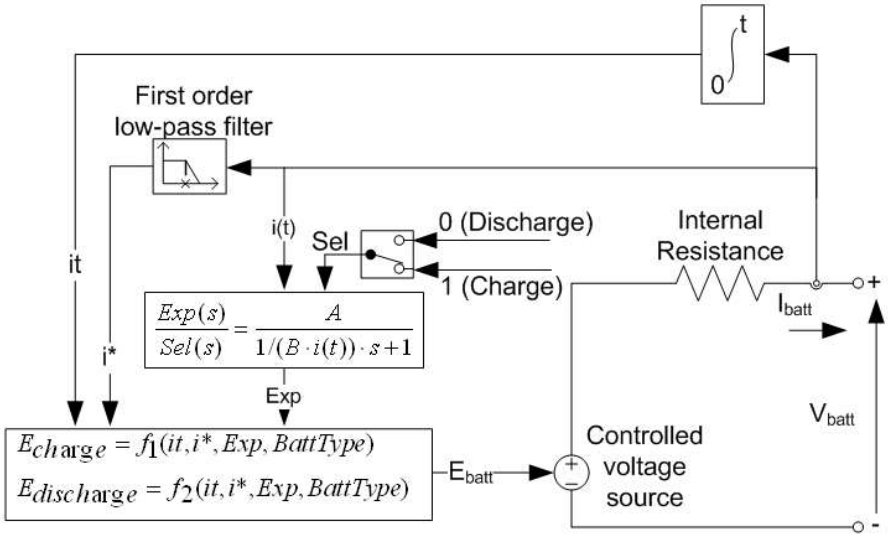

Figure 4-22: Battery model inside the block

In order to understand the battery working conditions and behaviour, charge/discharge characteristics must be studied. A random discharge curve has been generated in order to explain and identify the main areas of the curve. Figure 4-23 shows a random generated discharge curve. Three main areas are identified:

1. **Exponential area**: Represents the exponential voltage drop when the battery is being discharged from 100% SoC. This voltage drop depends mainly on the battery type.
2. **Nominal area**: Main working region of the discharge curve. Represents the energy which can be extracted from the battery until reaching a point below the nominal voltage.
3. **Total discharge area**: Represents the total discharge of the battery when the voltage decreases very fast. This region is usually avoided.

When the battery current is negative, it means that it is being recharged, and instead of the discharge characteristic, charging curves are used. Figure 4-24 shows a charging curve for Li-ion and Lead-acid batteries.

As a particular remark, it is interesting to compare last two curves with the one shown in Figure 2-4. It can be observe both curves exhibit similar behaviour.

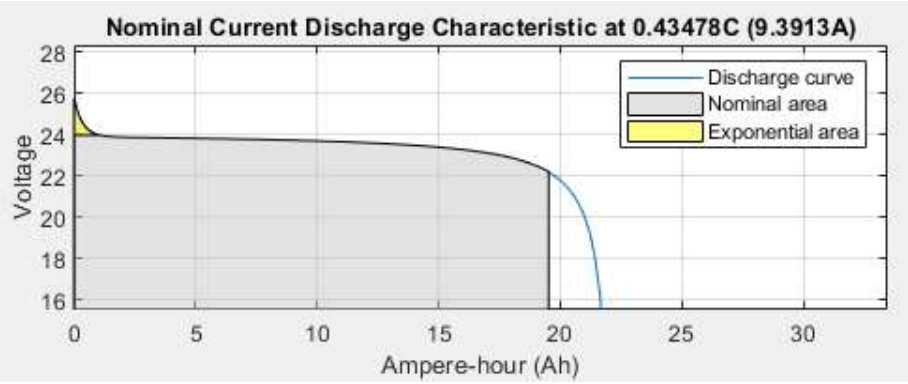

Figure 4-23: Random generated discharge curve

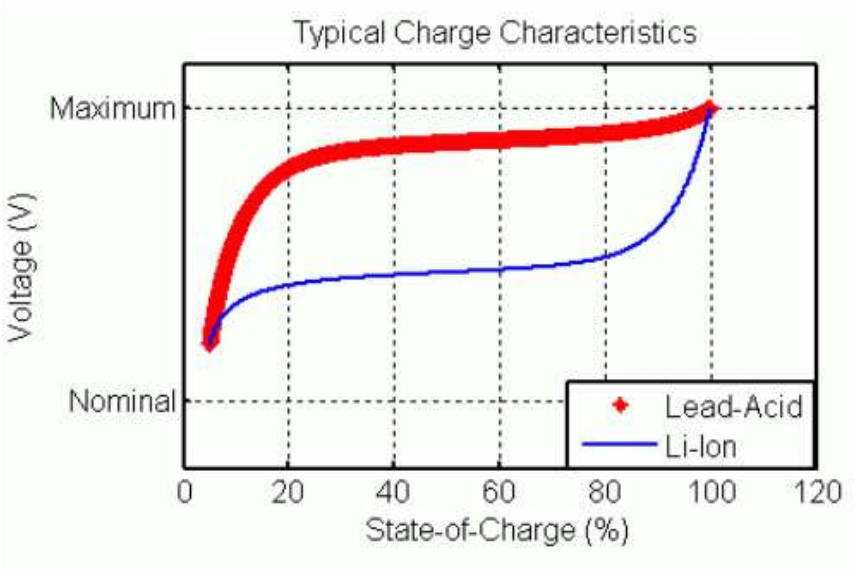

Figure 4-24: Charging curves

Once the characteristic curves have been explained, some of the most important parameters and variables of the storage systems should be described in order to provide a comprehensive vision of the model.

- *(C-rate)*: Discharge current is usually expressed as the C-rate in order to normalise battery capacities. A C-rate is a measure of the rate at which a battery is discharged relative to its maximum capacity. A 1C rate means that the discharge current will discharge the entire battery in 1 hour (i.e. for a battery with a capacity of 100 Ah, this equals to a discharge current of 100 A).
- *State of Charge (SoC) [%]*: It is a well-known characteristic and it indicates the battery capacity as a percentage of the maximum capacity. It is calculated by integrating the current in order to determine its variation with time.
- *Depth of Discharge (DoD) [%]*: Percentage of battery capacity that has been

discharged. Usually for values around 80% of DoD, the term depth discharge is used, which is a condition to be avoided.

- *Terminal Voltage [V]*: The voltage between battery terminals for an applied load, that varies the SoC and the charge/discharge current.
- *Open-circuit voltage [V]*: The voltage between battery terminals with no-load applied. It is varying only with the SoC.
- *Internal resistance [Ω]*: Resistance within the battery. As internal resistance increases, efficiency of the battery decreases and thermal stability is also reduced. Its physical meaning differs from type to type and it is due to the particularities of the chemical process, contacts, etc.
- *Cut-off voltage [V]*: Voltage which normally defines the empty state of the battery.
- *Nominal capacity (Ah for a specific C-rate)*: Total Ah available when battery is discharged at a certain discharge current.
- *Nominal energy (Wh for a specific C-rate)*: The total Wh available when the battery is discharged at a certain discharge current (C-rate) from 100% SoC to the cut-off voltage. Obtained by multiplying the nominal capacity [Ah] by the nominal voltage [V] of the battery.
- *Cycle life (for specific DoD value)*: Number of discharge-charge cycles the battery can experience before it fails to meet specific performance criteria.

Energy storage system parameters were designed in previous stages and some data is available in references [5, 6] and [4]. This sizing considered possible eclipse situations and peak power supply, however an in-depth analysis was not performed due to the nascent stage of the mission. Table 4-3 shows the battery capacities computed for LUMIO and MARIO missions. The battery DoD will be computed in next chapters in order to check optimal battery design.

Table 4-3: Battery capacities for LUMIO and MARIO missions

	LUMIO	MARIO
Battery Capacity [Wh]	160	119.8

For battery modelling, GomSpace battery cells are employed[h]. They are usually grouped in stacks of several cells in order to achieve the desired capacity for the battery [i]. Now, LUMIO battery parameters which are more precisely determined, is modelled. By checking the data sheets, it is possible to model the whole stack from the single cells for the given battery capacity. Equations 4-12 and 4-13 describe the number of cells

[h] https://gomspace.com/UserFiles/Subsystems/datasheet/gs-ds-nanopower-battery-17.pdf

[i] https://gomspace.com/UserFiles/Subsystems/datasheet/gs-ds-nanopower-bpx-3-18.pdf

necessary for the whole battery stack. Table 4-4 presents the results by rounding the cells number to the closest even number.

$$P_{cap}(cell) = V_{nom}(cell) \cdot I_{cap}(cell) \tag{4-12}$$

$$N.cells.stack = \frac{P_{cap}(stack)}{P_{cap}(cell)} \tag{4-13}$$

Table 4-4: Required number of cells in one stack for LUMIO

Single cell characteristics		Required capacity [Wh]	Cell number in the stack
Nominal voltage Vnom [V]	3.7	160	15
Nominal capacity Icap [Ah]	2.6		
Nominal capacity Pcap [Wh]	9.62		

The connection strategy of the cells is now studied. The criteria for connection type is determined by several factors. The buck converter is the most simple type of dc-dc converter, being the most convenient converter to use. The main bus voltage depends directly on the battery voltage, with its value being critical for the choice of the converter. With the POL fixed voltages 24V, 12V, 5V, and 3.3V, thus the ideal choice for the main bus voltage should be above the POL voltages. However, the ability to convert the main bus voltage into the lowest voltage level is a critical factor especially since 3.3V being the lowest one. Additionally a better behaviour can be obtained if the difference between the PV array voltages and the main bus voltage is small. Finally a trade-off among these factors is performed to stablish the connection strategy of the battery. For LUMIO, the battery connection strategy is to connect five series cells in two parallel strings as described in Figure 4-25.

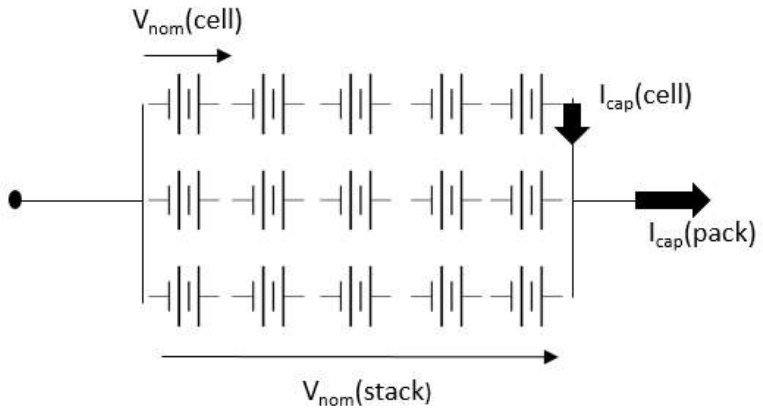

Figure 4-25: Connection strategy of LUMIO battery

Once the connection of the cells is defined, it is necessary to compute the parameters of the whole battery stack. Following the main equations for parameter estimation

provided by the manufacturer data sheet, nominal voltage, nominal capacity and energy capacity are computed for the whole stack. Equations 4-14, 4-15 and 4-16 provide the necessary parameters. Table 4-5 shows the computed parameters for the stack. Rated capacity results are lower than the reference once due to the applied rounding. A lower number of cells (15 cells) is preferred because of the weight and space constraints.

$$V_{nom}(stack) = V_{nom}(cell) \cdot N.series.cells \tag{4-14}$$

$$I_{cap}(stack) = I_{cap}(cell) \cdot N.parallel.strings \tag{4-15}$$

$$P_{cap}(stack) = V_{nom}(stack) \cdot I_{cap}(stack) \tag{4-16}$$

Table 4-5: LUMIO battery stack characteristic parameters

Battery stack characteristics	
Vnom(stack) [V]	18.5
Icap(stack) [Ah]	7.9
Pcap(stack) [Wh]	144.3

For MARIO battery, parameters and connections are estimated by using the same method as before. Table 4-6 represents battery values for MARIO. Again, cell number is rounded down because of the space and weight criteria.

Table 4-6: Required number of cells in one stack for MARIO

Single cell characteristics		**Required capacity [Wh]**	**Cell number in the stack**
Nominal voltage Vnom [V]	3.7	119.8	12
Nominal capacity Icap [Ah]	2.6		
Nominal capacity Pcap [Wh]	9.62		

Connection of the different cells is performed similar to that of the LUMIO battery. In this case, the number of cells to connect is 12, thus it has been decided to connect them on six series cells in two parallel strings. The connection is justified because by connecting the cells in three parallel strings, the nominal voltage achieved is close to 12V, so in order to preserve the security of the 12V POL, only two strings are considered. Figure 4-26 shows the connection schema for MARIO battery pack.

The battery pack characteristics are again calculated following equations 4-14, 4-15 and 4-16 providing the values tabulated in Table 4-7.

The Simulink model of the battery is now described. Figure 4-27 shows its main outputs which are the power connections and the measurements port. Measurements provided automatically by the port are mainly SoC, terminal voltage and charge/discharge current (depending if current is positive or negative).

In the settings box, two main tabs are available: main parameters and discharge. It would be also possible to create other two tabs for ageing and temperature simulation,

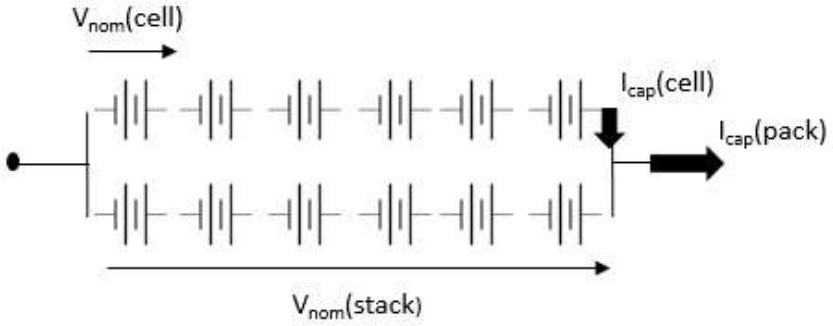

Figure 4-26: Connection strategy for MARIO battery

Table 4-7: MARIO battery stack characteristic parameters

Battery stack characteristics	
Vnom(stack) [V]	22.2
Icap(stack) [Ah]	5.2
Pcap(stack) [Wh]	115.4

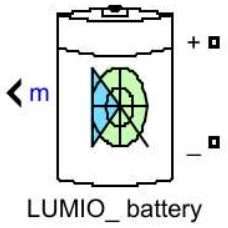

Figure 4-27: Battery model block

however this two characteristics are not of the interest for current simulations. First choice is the battery type, which is clearly Lithium-ion type. Then, main parameters such as rated capacity and nominal voltage are inserted. The battery response time refers to voltage dynamics and can be observed when a current step is applied and default value is applied. The initial SoC value will vary depending on the case study. Figure 4-28 shows the main interface of the main settings tab.

Discharge curves for the single cell are provided in their data sheets and despite this fact, no precise data is provided for particular areas of the curves. In this case, it is particularly difficult to estimate the whole stack charge and discharge curves, so the approximation given by the block is used in order to have an appropriate model. Discharge curve tab illustrated in Figure 4-29, shows the parameters which are estimated from the main ones. The main parameters for the discharge curve are provided and it is possible to plot the exact curves of the battery discharge behaviour.

Figure 4-30 depicts two curves, first one shows the voltage-capacity behaviour and the main operational areas of the battery discharge. Second curve represents the capacity

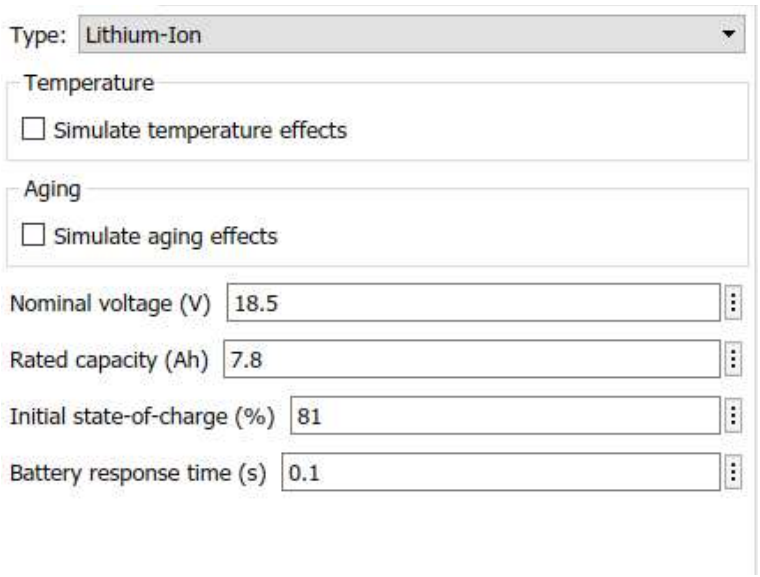

Figure 4-28: LUMIO main parameters selection, including battery type, rated capacity and nominal voltage

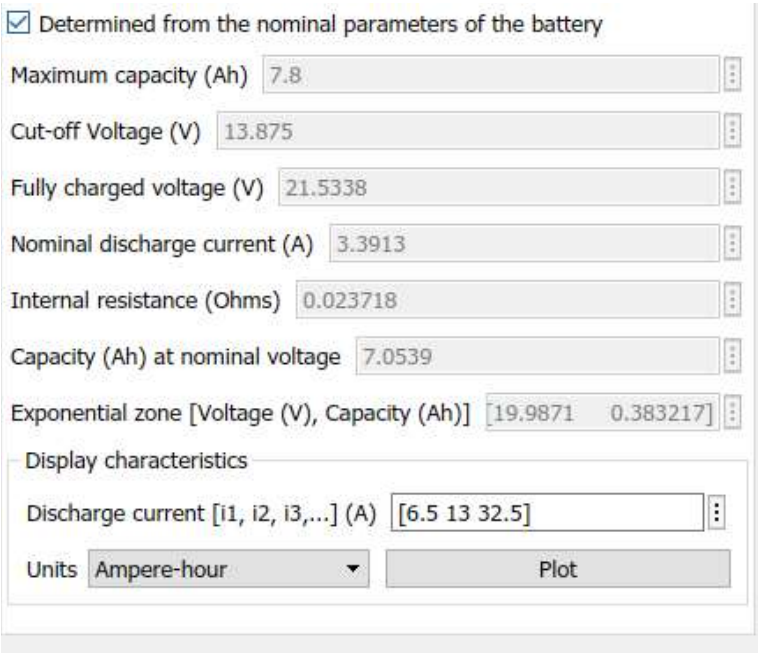

Figure 4-29: LUMIO battery discharge curve estimated from the main data of the battery stack

for a certain discharge current. The smallest one is rated capacity current of the battery. This means, that with such a current, the battery will be discharged within an hour. Also, the main parameters of the model behaviour are provided in the plot (i.e. polarization constant (K), Exponential voltage (A), Exponential capacity (B), etc.).

Since the cut-off voltage is 13.875V, which is lower than 24V, the POL converter for the 24V bus should be of the Buck-Boost type in case LUMIO CubeSat would use it.

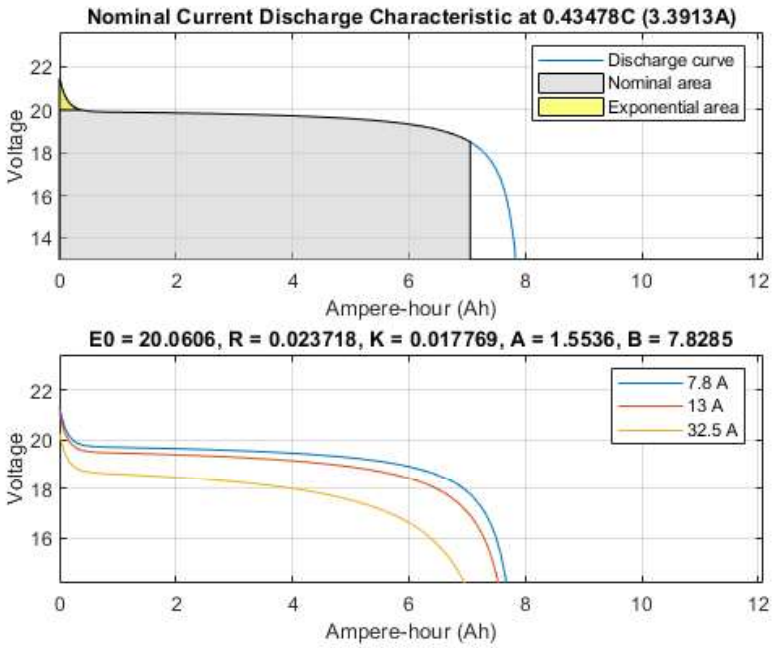

Figure 4-30: Discharge curves. Top: Voltage-Capacity plot showing the different operational areas. Bottom: Capacities for certain discharge currents.

It is also probable that the DoD of the battery would be selected such that the battery would operate above the cut-off voltage condition. However, the converter type will still be Buck-Boost for security issues.

4-4 Load model

Power consumed by the loads in the different stages of the mission is provided in the references [5, 6] and [4]. Simplest way to model a load is a classic resistance, which will be directly attached to the output of the different POL converters depending on the voltage requirement of the load. Depending upon the type of connection of the different loads, (series or parallel) which at the same time depends on the maximum allowable current and voltage level per POL, the resistance of the different loads is chosen in order to provide the required load power.

The load distribution for MARIO mission is pursued. No previous work on this issue has been performed before due to the early stage of the research. First step should be load definition and description. For every subsystem, a determined power is required as well as a certain voltage level in some cases, which are mainly obtained from the data sheets of the components. For systems which do not have a voltage level specification, voltage level is selected for setting a maximum current of 2A per bus as specified for some of the most important COTS EPS manufacturers[j]. Subsystems have particularities which

[j]Generally manufacturers use 2A of max. allowable current per bus. Example: https://gomspace.com/UserFiles/Subsystems/flyer/gomspace_nanopower_p60_flyer.pdf

must be commented in detail:

- *P/L-CAM:* Main payload of the system. Its power consumption is estimated from similar components but still not defined accurately in this stage of the research.
- *P/L-PROC:* Component performing this task is used for several processing tasks, PL, GNC and ADCS[k]. Particularly for Payload image processing, its power consumption limits are pushed until higher levels, going from 2.3W to 6W. Voltage level is specified at 3.3V.
- *EPS:* Component under design in the present work. Consumption will be very low because the components to be fed are small electronics and controllers. Power values and voltage level are estimated.
- *COMMT-HGA, COMMT-LGA, COMMR:* The communications component groups all the necessary systems for data transmission: High Gain Antenna (HGA), Low Gain Antenna (LGA), and Receiver[l]. LGA is used during mission stages when the spacecraft is near the Earth up to a certain point, when data transmission switches to the HGA, which is able to transmit from longer distances. This systems are attached to the same voltage level, working within a voltage range of 9V-28V. Power consumption is specified for every component.
- *OBC & CDH:* The terms OBC and CDH stand for On-board Computer and Command and Data Handling respectively[m]. They constitute the main brain of the spacecraft, with consumption power being 5W. Allowable voltage range is 4.5V-16V.
- *ADCS RW:* Altitude Determination and Control (ADCS), is achieved by using different devices. Reaction Wheels (RW)[n] are actuators used to influence the rotational motion of a spacecraft. According to the principle of angular momentum conservation, a torque is exerted onto the spacecraft if the wheel speed is changed. The ratio between acceleration of the wheel and the spacecraft is equal to the ratio of their moments of inertia. Its power consumption depends on the speed of the internal motor, with average consumption of 18W. Voltage range is not specified.
- *ADCS SENSORS:* In this load, it is possible to find the rest of devices for ADCS function: Star Tracker[o], Star Sensor[p], and the Inertia Measurement Unit (IMU)[q]. Even if they are different loads, they are described together due to the aim sharing. They total power consumed is 6W, they can be connected in parallel. Common voltage for proper operation is 5V.

[k] https://gomspace.com/UserFiles/Subsystems/datasheet/gs-ds-nanomind-z7000-13.pdf
[l] https://www.jpl.nasa.gov/cubesat/pdf/Brochure_IrisV2.1_201611-URS_Approved_CL16-5469.pdf
[m] http://aacmicrotec.com/products/spacecraft-subsystems/avionics/siriuscdh/
[n] https://www.vectronic-aerospace.com/space-applications/reaction-wheel-vrw02/
[o] http://hyperiontechnologies.nl/products/st400-star-tracker/
[p] http://www.spacequest.com/attitude-determination-control/ssoc
[q] https://www.sensonor.com/media/1132/ts1524r9-datasheet-stim300.pdf

- *EPROP:* This load refers to the Electrical Propulsion for Transfer phase. It is an Ion thruster with with a power processing and control unit attached to it, to ensure stable power supply. The power requirement of the thruster is adapted to the power availability, having a really high consumption during some periods of the mission. In order to have a proper model it will be attached to a 24V bus, consuming a current higher than 2A, with this value is not adapted to reality. Power considered for simulation is 72W
- *CPROP:* The employed system is bi-propellant engine [r]. Power consumption for this system comes from the ignition devices, valve openings, catalyst transformation, telemetry, etc. Average consumed power is 14W, being the voltage range for every component (telemetry, valves and heaters), within 9V and 12.6V.
- *TCS:* Temperature Control System (TCS) controls temperature inside the spacecraft, consisting of a simple resistance providing requested heat amount. Its value is estimated in 10W.
- *MECH:* This load refers to the SADA actuator for solar array angle adjustment. The employed model is customized for the mission.
- *AOCS-PROC:* Altitude and Orbit Control System (AOCS) use the same device as the payload processing unit. Voltage range does not change but power is lower due the lower processing requirements.

Table 4-8 shows the main loads which should be supplied by the EPS during the different stages of the mission and their characteristic values of power and voltage.

Table 4-8: MARIO load definition and characteristics

Subsystem	Nominal power [W]	Standby power [W]	Voltage level [V]	Remarks
P/L-CAM	4	0.1	5	Science
P/L-PROC	6	0.1	3.3	Science Processing unit
EPS	1	0.1	3.3	Power supply and distribution
COMMT HGA	31	0.1	24	Communications High Gain Antenna
COMMT LGA	23	0.1	24	Communications Low Gain Antenna
COMMTR	12	0.1	24	Communications Reciever
OBC & CDH	5	0.5	5	Main computer and data handler
ADCS RW	18	0.6	12	Reaction Wheels
ADCS SENSORS	6	0.2	5	Star tracker, Sun sensor, IMU
EPROP	72	0.1	SPECIAL (24)	Electric propulsion
CPROP	14	0.01	12	Chemical propulsion (primary + RCS)
TCS	10	0.01	12	Thermal control system
MECH	2	0.01	3.3	Deployment and Solar array orientation
AOCS-PROC	2.3	0.01	3.3	Altitude and Orbit Control System

Once the necessary data has been obtained for every subsystem which represents a load, it is possible to get the interface between MARIO EPS and the loads. Connections represented in Figure 4-31. Every load will have its own unidirectional switch with the exception of the essential ones (OBC, EPS, etc.).

[r] http://www.cubesat-propulsion.com/wp-content/uploads/2017/08/X17025000-data-sheet-073117.pdf

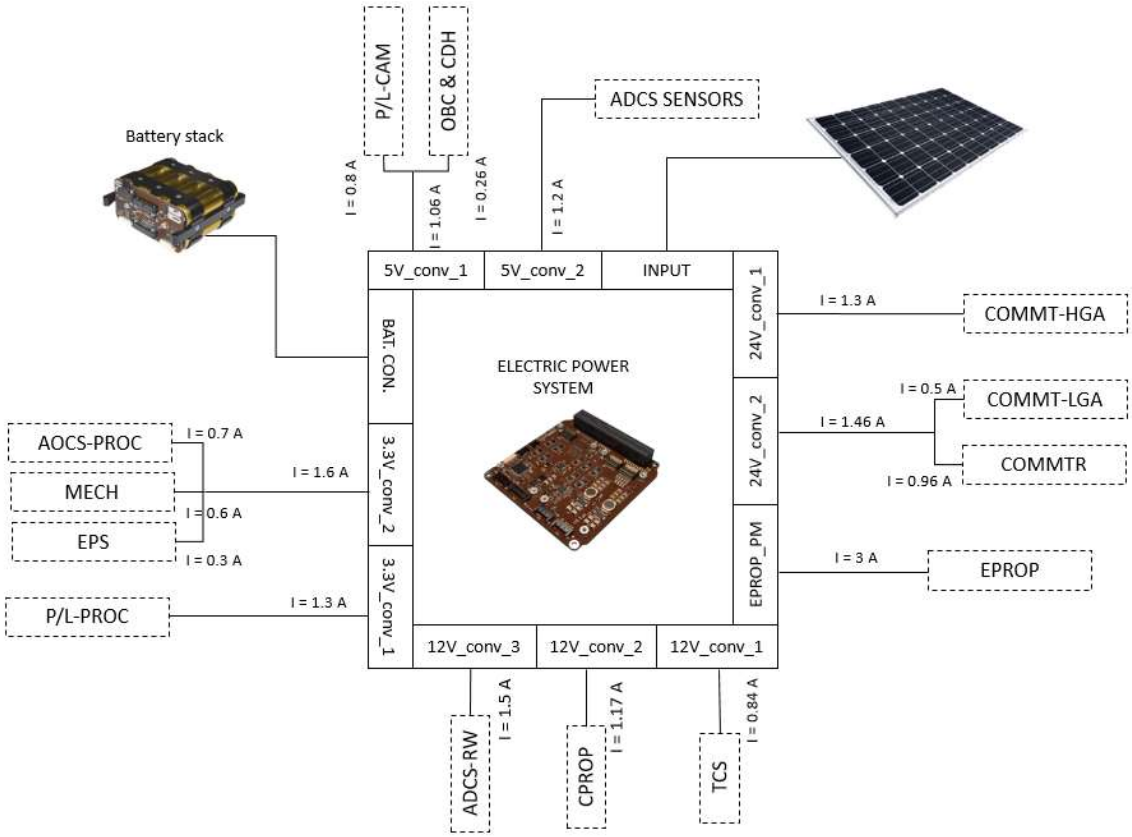

Figure 4-31: MARIO load connection in order to have a maximum current of 2A per bus

For LUMIO the main difference from the MARIO design is the absence of 24V bus. There exist some common points between the two spacecraft loads such as chemical propulsion, SADA actuator, AOCS processing unit, etc. Payload is also similar in terms of power as well as the thermal control system. Main differences between MARIO and LUMIO are listed below:

- *Absence of Electrical Propulsion*: LUMIO mission does not require the electrical propulsion and EPS will not use the special port required for this kind of thrusters.
- *Data transmission*: Communication equipment is simpler due to the absence of long distance communication.
- *Reaction wheel*: The employed reaction wheel is smaller due to the reduced size of the spacecraft, so power consumption is also lower. This fact has an influence also in the ADCS sensors which consume less power.

Figure 4-32 shows the connections between the different systems in LUMIO mission using the same board as MARIO.

As it was commented at the beginning of the section, loads are modelled as resistances. Equivalent resistances will depend on the current and voltage of the loads (which at

Table 4-9: LUMIO load definition and characteristics

Subsystem	Nominal power [W]	Standby power [W]	Voltage level [V]	Remarks
P/L-CAM	3.6	0.2	5	Science
P/L-PROC	3.96	0.1	3.3	Science processing unit
EPS	1	0.1	3.3	Power supply and distribution
COMMT-RF	18	0.1	12	Radio frequency transmissor
COMMT-TRANSP	2.5	0.1	3.3	Reception transponder
OBC & CDH	1.3	0.1	5	Main computer and data handler
ADCS-RW	3.5	0.5	12	Reaction Wheels
ADCS-SENSORS	3.18	0.1	5	Star tracker, Sun sensor, IMU
CPROP	15	0.06	12	Chemical propulsion (primary + RCS)
TCS	15	0	12	Thermal control system
MECH	2	0.1	3.3	Deployment and Solar array orientation
AOCS-PROC	2.3	0.01	3.3	Altitude and Orbit Control System

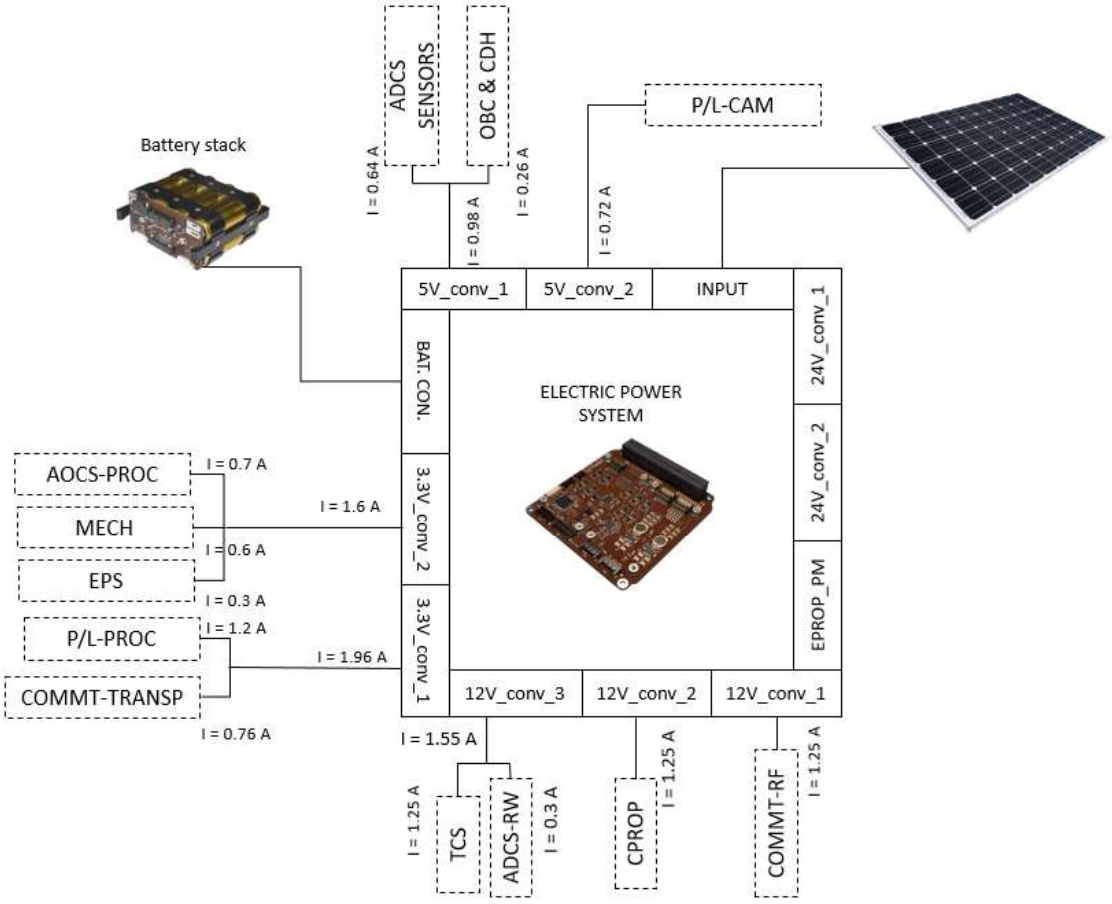

Figure 4-32: LUMIO load connection in order to have a maximum current of 2A per bus

the same time depend on the power consumed). Tables 4-10 and 4-11 describe the equivalent resistances and their related parameters for both case studies.

Equivalent resistances are represented as a resistor branch with the specified resistance value. Each converter will have its load model with the corresponding loads for each converter. As an example, LUMIO load corresponding to $3.3V\_conv\_2$ is described. It is a good example because it has two switched loads and one unswitched, which

Table 4-10: MARIO loads equivalent resistance

Subsystem	Nominal power [W]	Voltage level [V]	Consumed current [A]	Equivalent resistance [Ω]
P/L-CAM	4	5	0.8	6.25
P/L-PROC	6	3.3	1.82	1.82
EPS	1	3.3	0.3	10.89
COMMT-HGA	31	24	1.29	18.58
COMMT-LGA	23	24	0.96	25.04
COMMTR	12	24	0.5	48
OBC & CDH	1.3	5	0.26	19.23
ADCS-RW	18	12	1.50	8.00
ADCS-SENSORS	6	5	1.2	4.17
CPROP	14	12	1.17	10.29
EPROP	72	24	3.00	8.00
TCS	10	12	0.8	14.40
MECH	2	3.3	0.6	5.45
AOCS-PROC	2.3	3.3	0.7	4.73

Table 4-11: LUMIO loads equivalent resistances

Subsystem	Nominal power [W]	Voltage level [V]	Consumed current [A]	Equivalent resistance [Ω]
P/L-CAM	3.6	5	0.72	6.94
P/L-PROC	3.96	3.3	1.2	2.75
EPS	1	3.3	0.3	10.89
COMMT-RF	18	12	1.5	8
COMMT-TRANSP	2.5	3.3	0.76	4.36
OBC & CDH	1.3	5	0.26	19.23
ADCS-RW	3.5	12	0.29	41.14
ADCS-SENSORS	3.18	5	0.64	7.86
CPROP	15	12	1.25	9.60
TCS	15	12	1.25	9.60
MECH	2	3.3	0.61	5.45
AOCS-PROC	2.3	3.3	0.7	4.73

means that two unidirectional switches are attached to the loads which are switched off (or in stand-by) during some stages of the mission. Switches are controlled by applying a positive signal to the gate signal available in the block. Figure 4-33 shows the load Simulink model employed for the described load.

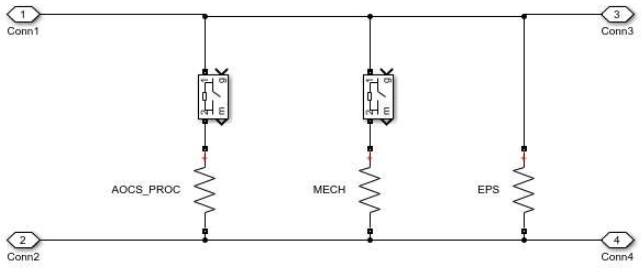

Figure 4-33: 3.3V _ conv _ 2 load Simulink model for LUMIO

Before proceeding forward, a check simulation is performed in order to verify that the equivalent resistances represent the appropriate values of the consumed current and subsequently the power. A very simple Simulink simulation containing the model described in Figure 4-31. It represents the system, as described in Figure 4-34, including a 3.3V source and the measurement blocks necessary to obtain the data. As observed in Figure 4-35, the results coincide with the design and the equivalent resistances method complies with the power consumed by the loads.

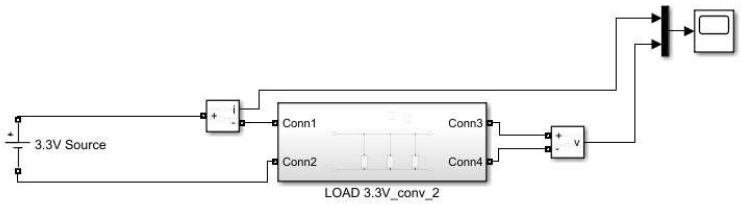

Figure 4-34: Equivalent resistances method checking model

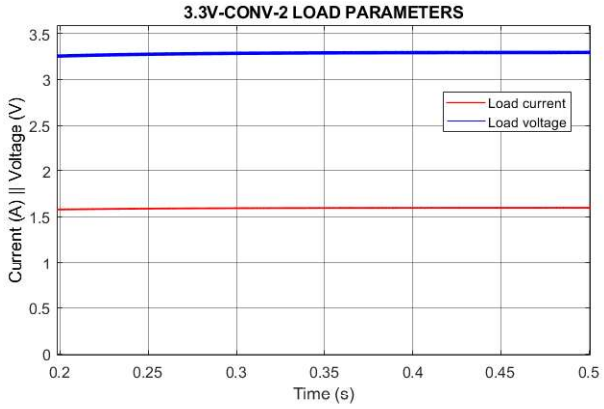

Figure 4-35: Current consumed and voltage applied to the 3.3V _ conv _ 2 load

4-5 General EPS model

Once every system has been explained, they are assembled together to form the whole EPS model. Every component is modelled as a subsystem, which is a more organized method to build bigger systems. General model is depicted in Figure 4-36 .

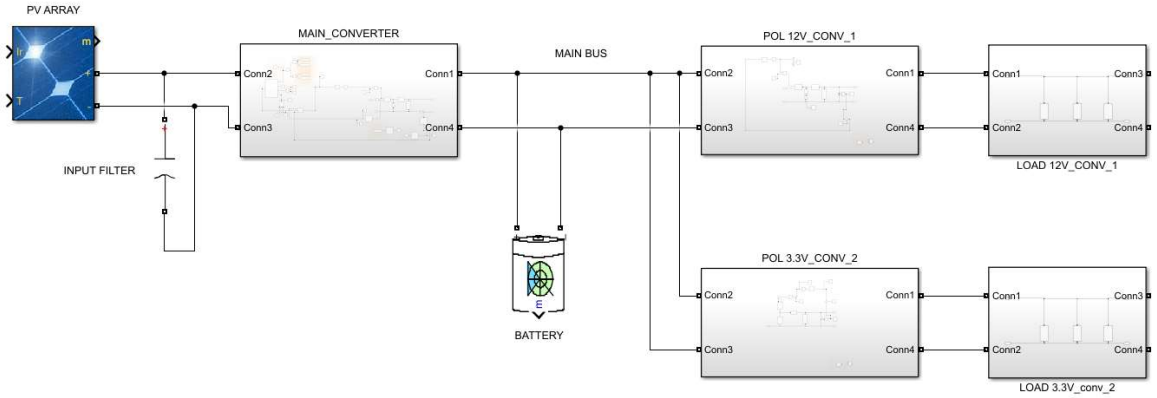

Figure 4-36: EPS general model showing each component as a subsystem

Notice that the only component which has not been explained is the input filter between the PV array and the main converter. Its function is to filter the input current harmonic content acting as a first order low-pass filter. It has to assure an accurate power collection from the PV system.

4-6 Summary

This chapter dealt with the main parts of the EPS system and described their work principles.

Main converters were described and modelled indicating their characteristics, working principle and Simulink aspect. Buck-Boost converter will be used for the Main and 24V POL converters while for the rest of the POL, Buck type converter will be used.

PV array model uses a predefined Simulink block, which main parameters were described and selected from real system data sheets and construction, in order to have an accurate model for simulation process. Irradiation and temperature will be the varying parameters during the different scenarios of the mission.

For energy storage systems, a predefined block was also used. Characteristic features of the battery as well as model parameters have been described. Connection strategy of the batteries is set in order to have an appropriate voltage on the main bus with the aim of using as many Buck converters as possible due to their simplicity compared to the Buck-Boost one. Parameters of the model were selected, whilst neglecting Ageing and Temperature in this stage of the work.

Loads are modelled by equivalent resistances consuming the same power as the employed equipment. Connections of the different loads were determined, obtaining the voltage required for their proper performance consuming maximum current of 2A per converter. Equivalent resistances method is then proved by simple simulation checking.

General EPS model is finally depicted and explained.

Chapter 5

EPS basic control

Electrical Power System (EPS) under design needs an appropriate control logic to properly manage the generated, stored and consumed power. The control logic developed for the system is placed at a low-level control stage which is aimed to control stability and main regulation of the system. In a future developed physical system, this control level will be performed by a microcontroller inside the EPS Printed Circuit Board (PCB). In higher control levels, other situations are taken into account involving different subsystems of the spacecraft. Higher level control is executed by the On-Board Computer (OBC) providing some signals employed for EPS control.

Basic control for the EPS is achieved by regulating the different converters. They allow the control of several parameters of the EPS system by modifying the gate signal of the switches inside the device. Main converter and POL converters have different tasks, which have been explained before. For Point of Load (POL) devices, their main aim is to adapt the output voltage to the desired level for proper subsystem feeding. For the main converter some of its control tasks were listed in previous chapters, but it is necessary to expand them:

- *Maximum power point tracking*: The MPPT algorithm must be performed in every moment of operation, providing maximum power characteristics of the Photovoltaic (PV) array curves. It is not directly run by the converter itself, but receives the reference value to adapt the input parameters to the Maximum Power Point (MPP) value of current and voltage.

- *Adapt power consumption to load demand*: There exist some periods during the mission where power generation provided by operating in the MPP, results in excessive amount of energy which will not be used. In this phase, the converter shall adapt the power input to the load requirements to avoid power dissipation inside the electrical system.

- *Control battery charge/discharge*: Converter must regulate the battery dynamics in order to avoid overcharge. Battery input current shall be monitored to avoid fast charge and discharge, which is harmful for battery health.

Obviously, the control implementation for simulations is implemented in Matlab-Simulink. Simulink blocks are mainly used and some Matlab scripts are used in addition to facilitate the implementation.

Some notes about control basics are explained, providing the reader the basic concepts taken into account in the system design.

The control design is explained in three stages. First, the POL converter control is explained, followed by the explanation of the Main converter control and finally the explanation of the general model with the implemented control.

5-1 Control basics

In this section, basic knowledge about control systems is provided in order to have a proper picture about the developed work. In Chapter 4, main working principle of the converters was described starting from a repeating signal (v_{st}) and a control signal ($v_{control}$). The aim of the controller is to provide the proper $v_{control}$ which requires an adequate duty cycle (D), which at the same time is translated into the desired behaviour of the converter. The main working principle of the system is illustrated in Figure 5-1. It represents the main idea behind the control design.

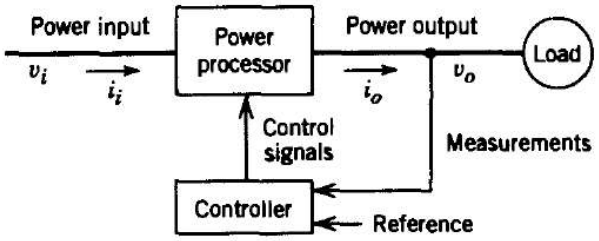

Figure 5-1: Working diagram for a generic converter [11]

Going deeper into the converter, another block diagram can be defined. Now, the switch input signal is highlighted as the main output of the control system. Figure 5-2 shows the block diagram for the switch control inside the converter. The sawtooth signal voltage v_{st} is compared with $v_{control}$, providing the desired gate signal for the switch, with constant output voltage V_o. The only difference between the presented block diagram and the implemented one is that instead of an amplifier a real control device is used.

Employed control device is called PID controller which is a well-known device. It is an acronym of Proportional, Integral and Derivative, which means that it is composed by the three actions.

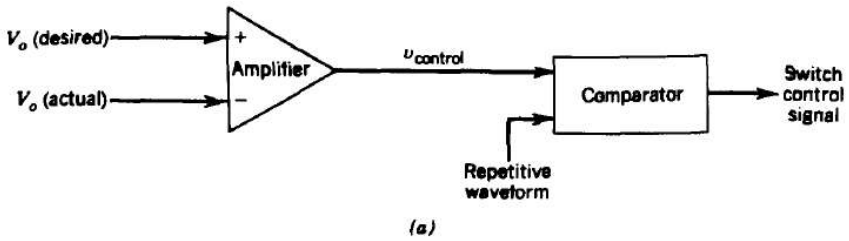

Figure 5-2: Switch control block diagram [11]

- **Proportional (P):** It is mainly an amplifier of the input signal, which is just multiplied by a gain value. Despite its simple effect, it is mainly responsible for stability[a] of the system. It tends to generate an off-set value called position error.
- **Integral (I):** As its name indicates, it is basically an integral. By integrating the value of the input signal, the position error is eliminated, reaching the exact desired operating point. It mainly influences the dynamic response of the system.
- **Derivative (D):** It can be understood as a "prediction" of the future state of the variable or in other words, a state of change of the input.

Figure 5-3[b] illustrates the main working principle of the PID controller which substitutes the amplifier block of Figure 5-2 for the control system under design.

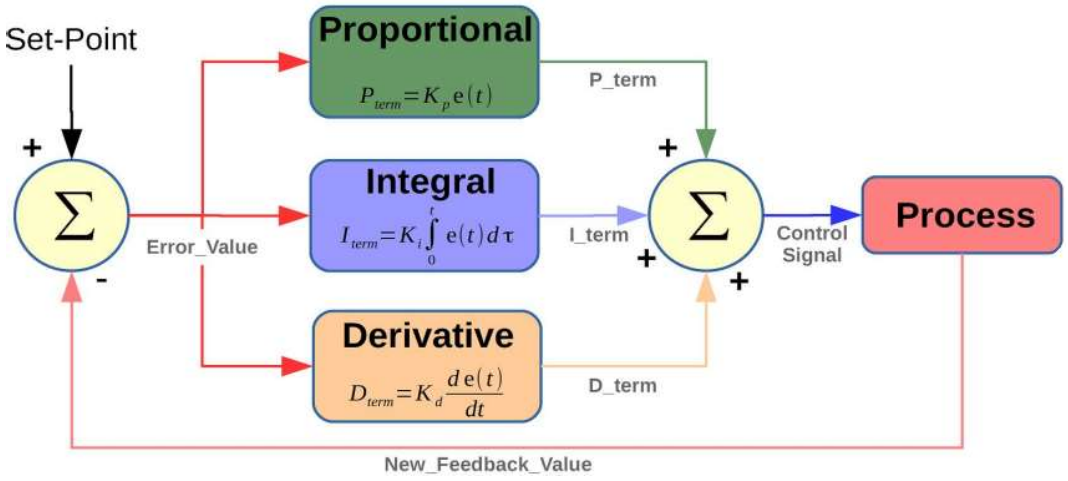

Figure 5-3: PID working principle

For the aim of the present work, only proportional and integral action are used. This is for the sake of simplicity of the system because by using a PI controller, necessities of the system are covered without the derivative action.

[a] Stability is accomplished when system reaches an operating point. Not stable systems oscillate and tend to infinite.

[b] http://students.iitk.ac.in/roboclub/lectures/PID.pdf

Employed control logic changes depending on the converter operation. Variables are controlled by a closed-loop which provides feedback of the actual value of the controlled variable. Reference value and actual value provide the error which is the input for the PI controller. The controller provides the desired control value which is saturated within a range for duty cycle limitation. Figure 5-4 represents the employed method.

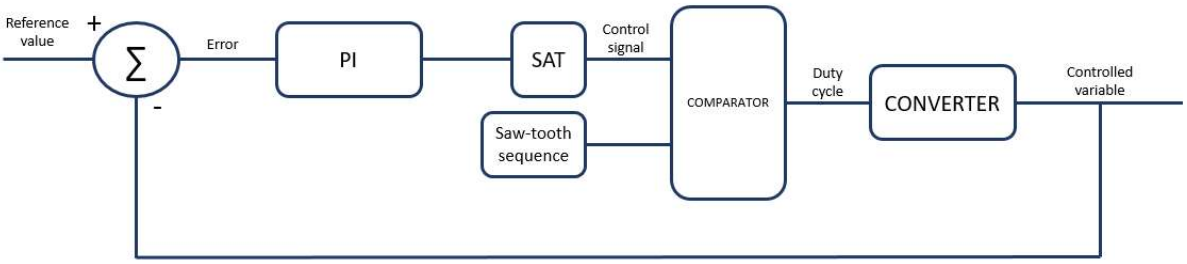

Figure 5-4: Employed control logic

Saturation is set in the interval [0.5 , 0.95] in order to assure the proper operation of the converter. If the duty cycle is close to 0 or 1, it may happen that the switch is not able to turn on and turn off inside the specified switching period.

Usually, for controller parameters tuning, the small-signal linear model of the system is necessary, which can be performed once the circuit topology has been chosen. This method encompasses the representation of converter parameters by a sum of a steady-state or DC component and a small signal or AC component.

Once the linearised model of the converter has been obtained, it is possible to compute the desired controller parameters, ensuring stability and the dynamic response to possible disturbances. This task can be performed by computing the closed loop transfer function including the controller parameters. This step is avoided in this work due to system complexity. It was found that an empirical controller tuning coming from the control theory was more time-effective, obtaining good results in the system response and stability.

Method for PI controller parameters tuning followed several steps:

1. Proportional gain was selected to stay inside the stability limits with integral action equal to zero.

2. Integral gain is selected in order to have the desired dynamic behaviour (speed in system response) ensuring that system still inside the stability limits.

Obviously, system parameters have not been selected yet, and this procedure was applied once the components of the different converters are chosen. System parameters will be selected in the next chapters taking into account the desired response of the system.

5-2 POL converter control

For control implementation on POL converters, a Buck type converter is selected since it is the most common type in this type of converters. Controlled variable in POL converters will be the output voltage, setting the reference value. Reference value will be the desired voltage for each converter, 3.3V, 5V, 12V or 24V. It must be implemented inside the model described in Figure 4-7 since it is necessary to measure the voltage at the output terminals of the converter. Figure 5-5 shows the implemented control system inside a buck converter.

It can be observed that the reference values are selected by the user by the configurable variable POL_x_ref, with x between 1 and 4.

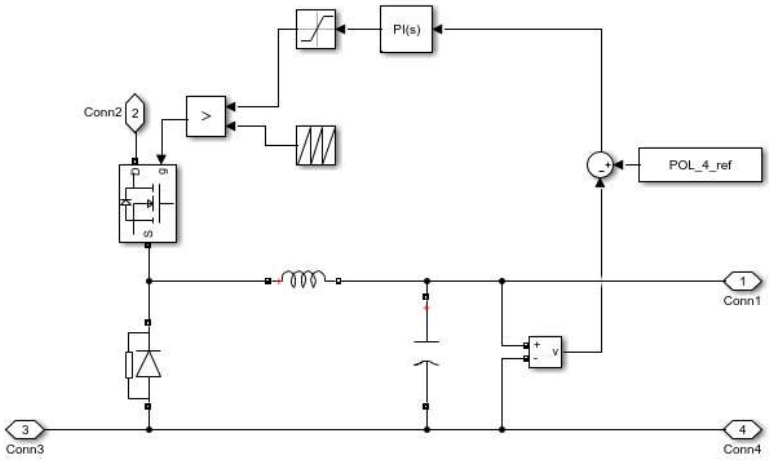

Figure 5-5: Buck converter Simulink control implementation

For Buck-Boost POL converter, the control scheme is very similar to that described for Buck type. The main difference lies on the results, which provides a different duty cycle for the same reference value due to the different behaviour of the converter. Figure 5-6 depicts the control implementation inside a POL Buck-Boost converter for the 24V load bus.

5-3 Main converter control

The main converter have to accomplish the objectives described at the beginning of this chapter. Control method employed is more complex than the one implemented for the POL converters due to the complexity of its tasks. Controlled variables now are currents, and they are controlled depending upon the aim of the control mode.

The control modes are explained below:

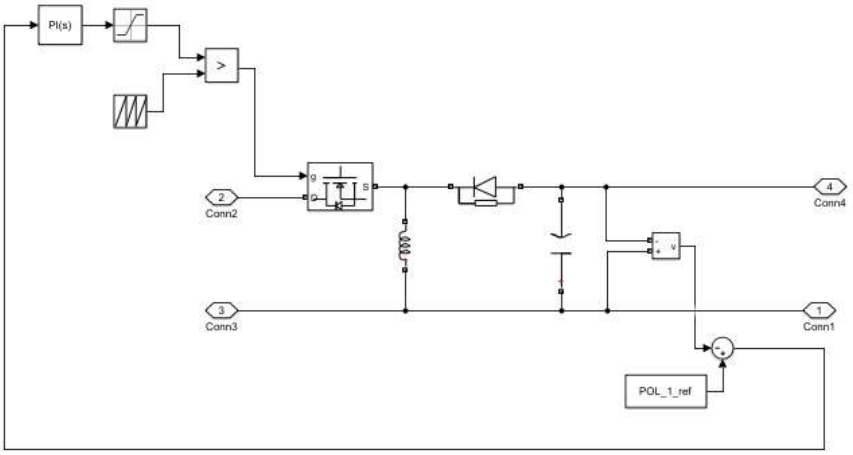

Figure 5-6: Buck-Boost POL converter Simulink control implementation

- *Input current control*: Current input is controlled when generation is set at the MPP operation. This operating condition is known as **maximum generation mode control**.
- *Output current control*: Current supplied to the main bus is regulated in order to meet load or load plus battery power requirements. This operating condition is called **adjusted power mode control**.

Depending on the objective of the converter, the control mode will be selected, allowing the device to accomplish its mission in every stage of its operation.

Adjusted power mode: It is employed when the generation at the MPP exceeds the requirements of the load and battery is completely charged or does not need to be charged. It is also employed when charging current exceeds the allowable charging current of the battery, and there exists enough power capacity to feed the loads and charge the battery in the new generation point. The controlled variable will be the output current of the converter I_o and the reference value will vary depending on the control function. For load adjustment, reference value will be the current consumed by the loads I_{load}. If the battery charging current needs to be limited, reference value will be provided by: $I_{load} + I_{max.bat}$.

Maximum generation mode: It operates when it is necessary to exploit the whole generation available in the source. Input current is set at the maximum power current value, positioning the operating point exactly working at the MPP of the curve and providing the MPP parameters at the input terminals of the converter. An MPPT algorithm must be implemented in order to track this MPP during the whole mission life. This algorithm will provide values of the MPP parameters I_{mpp} and V_{mpp}. Controlled variable will be the input current of the converter I_d and reference value will be set at I_{mpp} value.

Up to this point, the procedure to implement the control for the two modes by using the control logic described previously is known. The main problem is now how to switch between the two control modes when control change is necessary. A selection algorithm must be developed in order to set the selection criteria for each method. A Matlab function will provide a binary logic value (0 or 1) which will be directed to a selection switch. The switch will select the error value applied to the PI controller which will control the converter's duty cycle. Figure 5-7 represents the block diagram which describes the logic employed for mode selection.

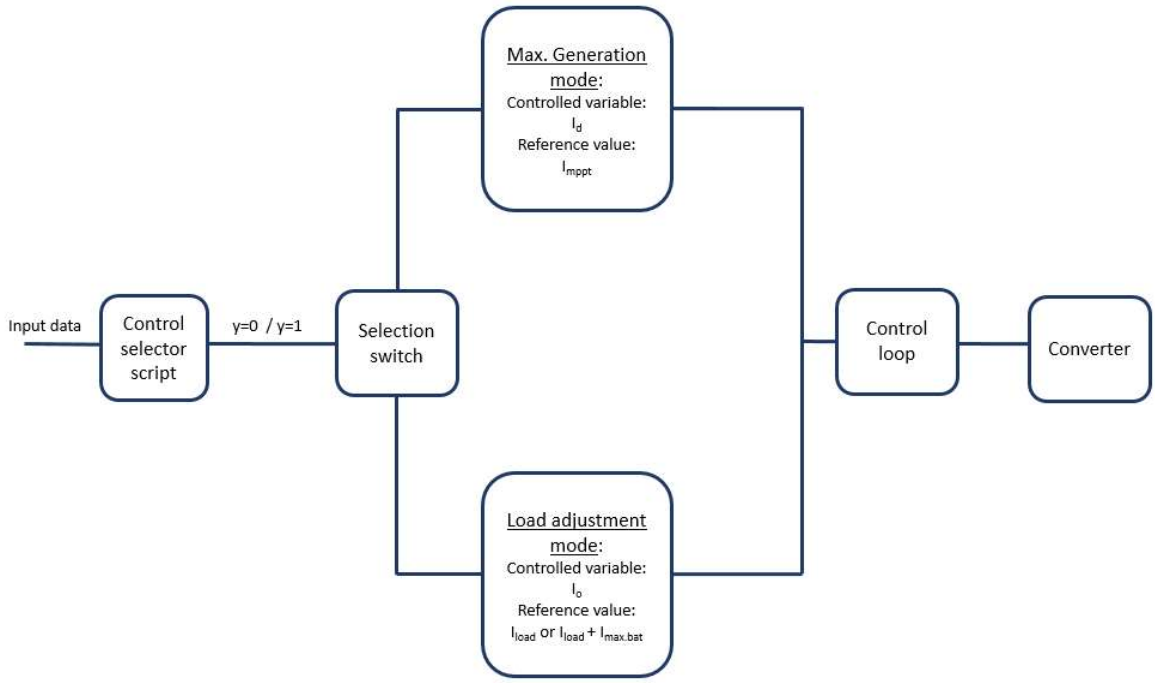

Figure 5-7: Block diagram for mode selection logic

The main conditions which define the control mode are the generated power in the MPP (P_{gen}) and the power consumed by the loads (P_{load}). Other conditions regarding battery overcharge and charging current are taken into account. Control selector is also affected by external instructions coming from the higher control levels (i.e. battery needs to be recharged). If operation at the MPP is required, control indicator y becomes one and for load adjustment operation y becomes zero. Instructions for control selection can be ordered as follows:

1. If $P_{load} > P_{gen}$: Maximum generation mode $y = 1$.
2. If $P_{load} < P_{gen}$: Several situations.
   - 2.1. If $SoC < SoC_{max}$ and $Charge\_req <= 1$ and $I_{bat.charge} < I_{bat.charge.max}$: Maximum generation mode $y = 1$.
   - 2.2. Else: Load adjustment mode $y = 0$.

Regarding condition 2.1, some remarks need to be made. Three conditions must be satisfied. First one is related to the State of Charge (SoC), which is upper bounded by a value SoC_{max} defined to avoid overcharge of the battery. Second condition is related with an external instruction which is activated when battery charge is necessary (i.e. after an eclipse period) and it is sent from a higher control level. Third condition regulates the maximum charging current, limiting its value up to a value specified by the battery manufacturer in order to avoid harmful effects $I_{bat.charge.max}$.

All this control system must be implemented in Simulink. The control structure is now depicted and explained by decomposing it in several parts, describing the different elements and their parameters. Figure 5-8 shows the whole control system actuating on the Buck-Boost converter. As it can be observed, there are three main different zones in the control architecture.

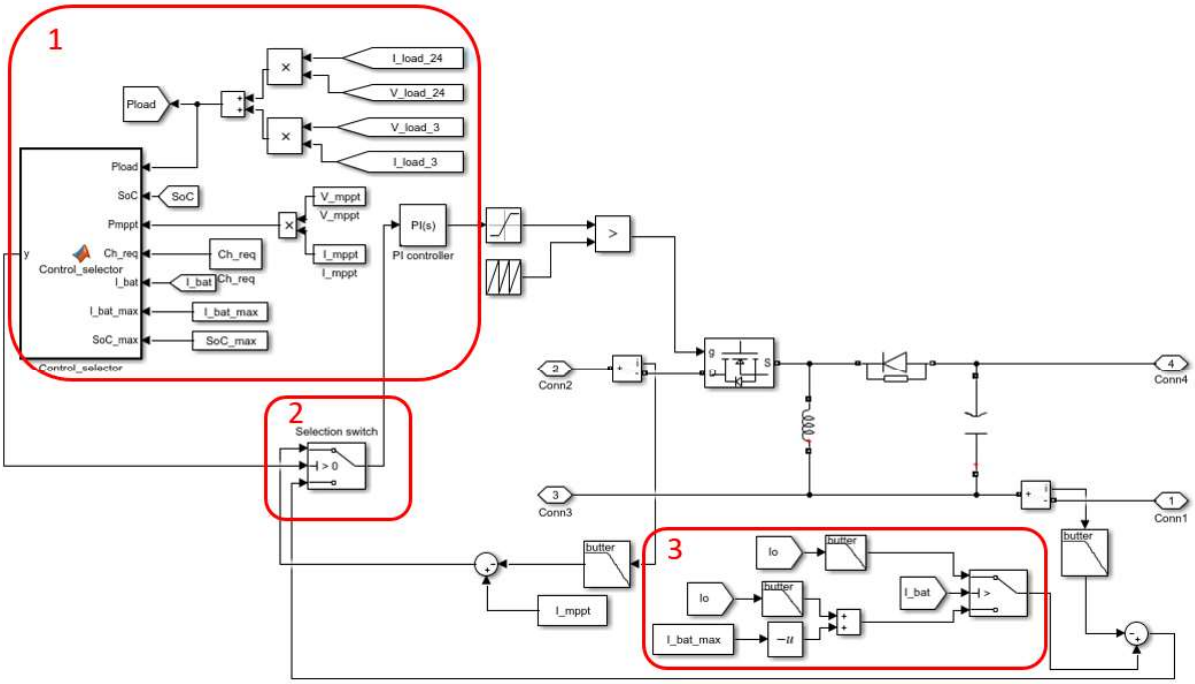

Figure 5-8: Simulink control system for Main converter operation

Zone number one represents the control selector method. Several variables are directed towards the main block `Control _ selector`, which are the necessary parameters to run the described algorithm for control selection. Power of the load is directly computed inside the area by multiplying the different load currents and voltages and then, multiplying them in order to get the total load power P_{load}. Also generated power at the MPP (P_{gen}) is computed there by using the same method as for P_{load} computation. The other input parameters are the external variables `Charge _ req`, `SoC _max` and `I _bat.charge.max`, and the internal variables (which are changing with the simulation time) SoC and I_{bat}. Inside the main block, it is possible to find a Matlab function which has the previously defined variables as input arguments and the mode selector binary parameter y and as output argument.

Zone two represents the mode selector switch, having three inputs and one output. Switch works in a very simple way: if central input (y) is greater than zero, maximum generation method is applied (input signal will be the error between input current and MPP current), and if it is zero, load adjustment method is used. Output signal will be one of the two methods' error signal which will be then applied to the control loop.

Zone three is implemented in order to get the reference value of the load adjustment method. As it was commented before, this can have two values: I_o or $I_o + I_{bat.max}$. This task is achieved by using a switch with control variable I_{bat}. Notice that I_{bat} will have negative values when battery is charging. When I_{bat} is lower than $I_{bat.max}$, it means that the reference value will be I_o, but if that maximum battery current value is overcome, the battery current will not longer be the the maximum value, changing the reference value to $I_o + I_{bat.max}$. Of course, when I_{bat} is greater than $I_{bat.max}$, control mode switches to the load adjusting method.

Labels with trapezoidal form represent the internal variables coming from the Simulink model and they have two meanings:

- Go to: Assign a variable to the label's name.
- From: They take the value assigned to the "Go to" equivalent label.

In Figure 5-9, it is possible to check the meaning for the two kinds of labels.

Figure 5-9: Labels employed for variable assignment

For measured current variables, a Butterworth filter is used. The filter is tuned at a certain cut-off frequency above which the harmonic content is attenuated. This action is implemented in order to filter the harmonic content present in some of the variables. Filters are tuned with the aim of having a clear signal for error computation, so the control will be more precise. Figure 5-10 shows the non-filtered signal and Figure 5-11 shows the filtered signal for a generic input current. As it can be observed, input current is affected by the switching harmonics before filtering it, so the filtering action is needed in order to get a proper error signal.

5-4 General model with control parameters

Finally, model and control schemes are ready to be tested in simulations. A new model that includes the necessary signal for control performance is established by improving the model presented in Chapter 4. This scheme will be followed for future simulations.

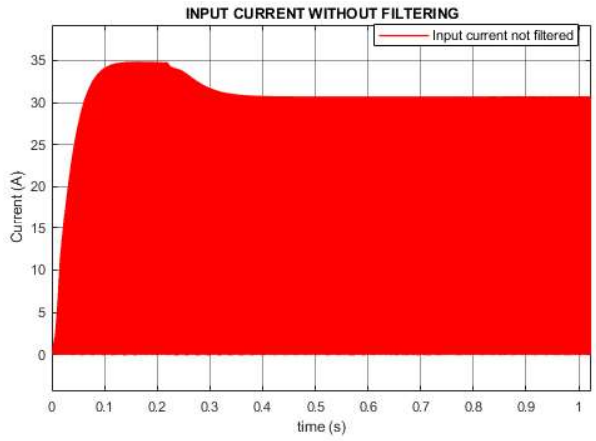

Figure 5-10: Generic input current before filter action

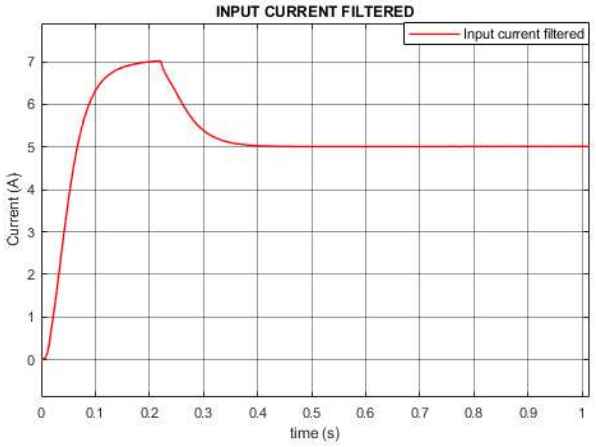

Figure 5-11: Generic input current after filter action

5-5 Summary

Chapter has described the main concepts and designs regarding control and regulation of the EPS system.

At first, main concepts were described including basic control logic and employed controllers. Once these elements were described, converter's control was explained for the two main converter types.

For POL converters, output voltage is controlled in order to follow the desired load bus voltage values. Main converter is controlled in a more complex way, switching between two main control modes: Maximum generation mode and Load adjustment mode. The former method is employed when operation at MPP is needed while the latter is used when generation at MPP overcomes system requirements. Switching between the two methods is achieved by a simple algorithm taking into account system the parameters and external settings imposed by the designer. Finally, general model with all the variable measurement is presented in order to have a generic picture of the system.

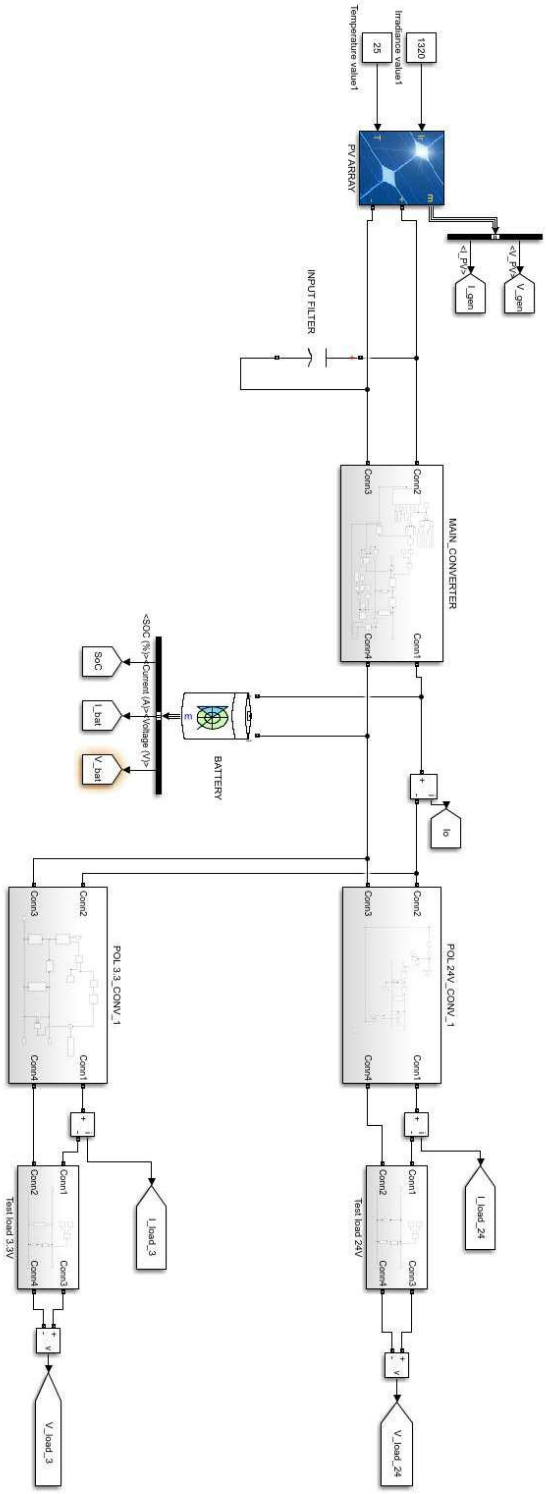

Figure 5-12: General model with control parameters

Chapter 6

Converter parameters design

The present chapter deals with the set-up of component parameters in the employed converters. Also switching frequency is set, taking into account the limitations of the present work.

The main critical points in the power quality will be at the generation terminals, battery terminals and load buses. It is worthy to mention that the components are considered ideal, so the frequency response differs from the real one which will be evaluated during the breadboarding phase. This assumption is considered for sake of simplicity as well as to save computational power during the simulation.

Three main parameters affect the oscillation of the signals:

- *Ripple limitation:* Converter parameters and switching frequency have an influence in the current and voltage ripples. This value, is inversely proportional to the switching frequency and to the inductance or capacitance.
- *Harmonic content:* In addition to the ripple of the signal, a periodic signal is added. Harmonic content comes from the switching of the converters. This content is filtered out by the existing filters inside the converters. Some external devices will also be necessary in order to be able to remove the input current harmonic content.
- *Controller transient*: Converters can be coupled by inserting transient signals coming from their design. This signal is only present during transitions between two steady-states.

In order to have a good response in the main points, the following elements which have an influence on the behaviour need to be analysed.

- *Point of Load (POL) converters:* They mainly affect the load characteristics. Depending on the voltage level which the converter has to impose, the parameters

will vary. A restriction on the current level also exists, so the converters will be modelled for maximum allowed current level in order to assure a proper behaviour at the feeding point.

- *Main converter:* Its design has a great influence in the battery terminals. Also, the setting of its parameters taking into account the generation is necessary.
- *Input filter*: It is in charge of input current filtering, acting as a classic low-pass filter. The cut-off frequency of the filter will vary inversely proportional to the capacitance value. The higher the capacitance, the greater is the filtering of the harmonic content.

For the design of POL converter parameters, the system is decoupled. Decoupling is performed in order to be able to simulate all the converters in a quicker way, due to the lack of computational power that simulation would require if a high amount of converters is simulated at the same time.

Regarding switching frequency of the converters, some issues must be taken into account. First one is the simulation stage of the work. In this kind of computational simulations, switching frequency cannot be very high due to algebraic loops constraint. In bread-boarding test phase, switching frequency can be higher than in computational simulations. Moreover, if the switching frequencies are too high, switching losses in the converter will increase, affecting the efficiency of the converter. The system works properly for a switching frequency of 5 kHz in every converter in the model. Switching frequency influences the ripple of the currents and voltages, but in this case, ripple will be compensated by selecting the inductance and capacitance values.

6-1 POL converter parameters

In POL converters, the most important objective is to limit the oscillation in the load voltage and current. Ripples will be the highest when the applied load is the maximum allowable load. The system must be decoupled and the controller for voltage level setting is tuned in order to get a stable and fast behaviour.

A random working condition is selected, where the battery will have a specific voltage level. This voltage level does not affect the ripples in the converters and only the duty cycle is affected. It shall be adjusted for each type of converters.

The converter tuning is performed in an empirical way due to the harmonic content present in the signal. The lower the cut-off frequency, the lower is the harmonic content($f_s \gg f_c$).

The input voltage is 23V and it is selected from one of the operating conditions. The applied load is the maximum allowed one, resulting in a 2A current flowing towards the load. Figure 6-1 shows the disposition of the converters in the decoupled scenario.

For converter simulation, the controller is tuned for a fast response within stability limits. Test time is set at 5s, which is enough time to see the signal and check appropriated working conditions.

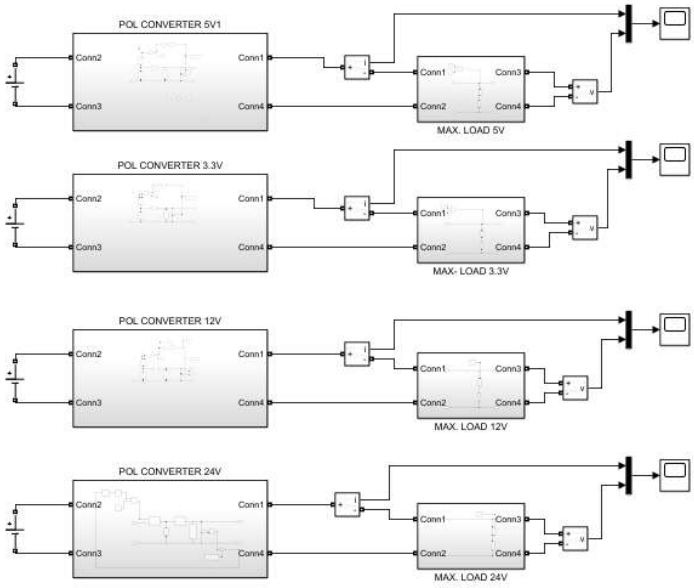

Figure 6-1: Decoupled case study for POL converter design

Ripple values must be limited up to a value. The lesser the ripple (compared to the average vale in %), the better the power quality for the load feeding. A typical value for good power quality is 1% of the average value. This is a really conservative value because in future steps, there will be more disturbance signals in the system which will exacerbate the converter behaviour. Every POL converter typology (3.3V, 5V, 12V and 24V) is going to be tested going from the greatest voltage level to the lowest one.

6-1-1 24V POL converter design

The objective is to limit the maximum oscillation (ripple plus harmonic content) of every parameter signal to 1% of its average value. The 24V POL converter is Buck-Boost type, and its inductance and capacitance are modelled to achieve the objective value.

Inductance is in charge of limiting the current ripple whilst the capacitance will limit the voltage ripple. These values are inversely proportional to the ripple values. The obtained values are listed in Table 6-1.

Table 6-1: 24V POL converter characteristic values

Converter	Av. voltage [V]	ΔV [V]	ΔV [%]	Av. current [A]	ΔI [A]	ΔI [%]	L [mH]	C [mF]
24V _ CONV	24	0.25	1.0	2	0.02	1.0	0.15	1.05

The load current and voltage plots for the given values is shown in Figure 6-2. The converter response is obtained and the waveform of the signal confirms that the the ripple is within the defined limit and ensures good power quality.

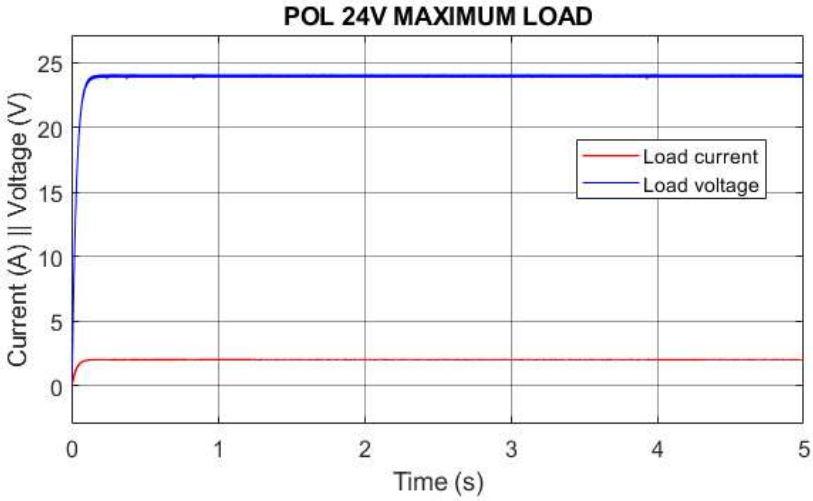

(a) 24V POL total response

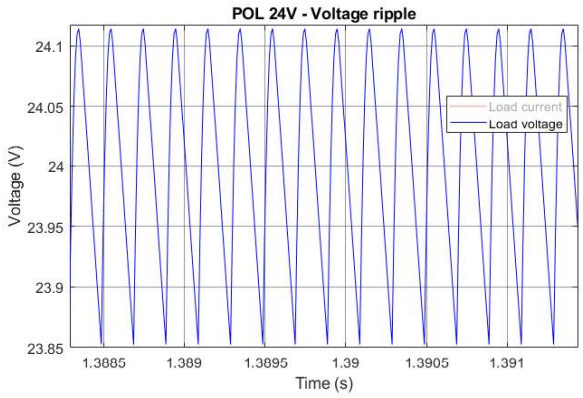

(b) 24V POL voltage oscillation

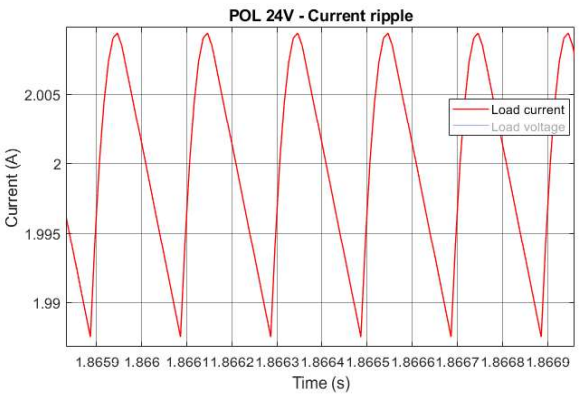

(c) 24V POL current oscillation

Figure 6-2: 24V POL converter response for maximum allowed load

From Figure 6-2, the signals employed for converter design and verification can be obtained. By evaluating the signals, the oscillation value can be verified in Table 6-1.

By subtracting the highest value and the lowest value of the periodic signal, and dividing it by the nominal value, the variation percentage is obtained.

6-1-2 12V POL converter design

For 12V POL converter, the employed method is the same as for the 24V converter design. In this case, the only difference is that for this POL, the employed converter is a Buck type. The obtained waveform will differ a bit from the Buck-Boost type. Finally, the oscillation variation of the signals is computed. Obtained values for 12V POL converter are shown in Table 6-2.

Table 6-2: 12V POL converter characteristic values

Converter	Av. voltage [V]	ΔV [V]	ΔV [%]	Av. current [A]	ΔI [A]	ΔI [%]	L [mH]	C [mF]
12V_CONV	12	0.12	1.0	2	0.02	1.0	0.55	0.45

6-1-3 5V POL converter design

The voltage is set at 5V and the corresponding maximum allowable load current is set. Table 6-3 shows the parameters for 5V POL converter and Figure 6-4 its response and oscillation waveforms.

Table 6-3: 5V POL converter characteristic values

Converter	Av. voltage [V]	ΔV [V]	ΔV [%]	Av. current [A]	ΔI [A]	ΔI [%]	L [mH]	C [mF]
5V_CONV	5	0.05	1.0	2	0.02	1.0	0.55	

6-1-4 3.3V POL converter design

The voltage is set at 5V and the corresponding maximum allowable load current is set. Table 6-4 shows the parameters for 3.3V POL converter and Figure 6-5 its response and oscillation waveforms.

Table 6-4: 3.3V POL converter characteristic values

Converter	Av. voltage [V]	ΔV [V]	ΔV [%]	Av. current [A]	ΔI [A]	ΔI [%]	L [mH]	C [mF]
3.3_CONV	3.3	0.03	0.9	2	0.02	1.0	0.5	1

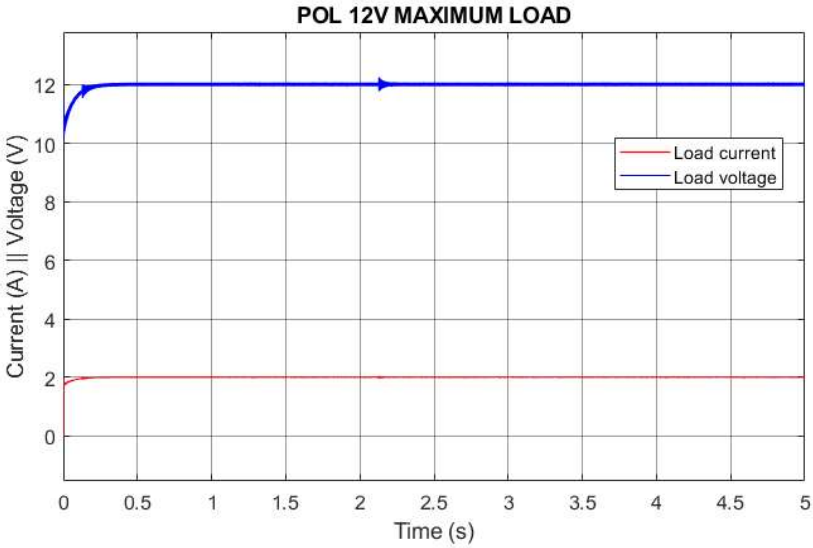

(a) 12V POL total response

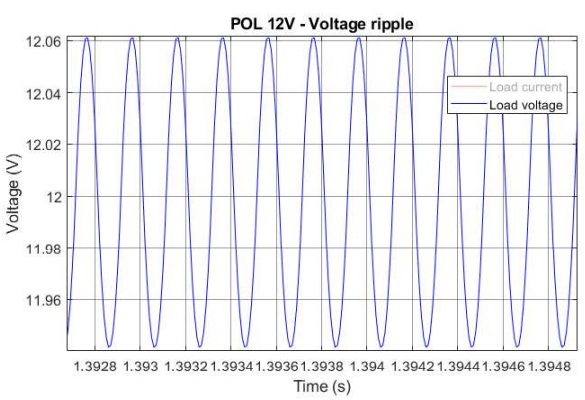

(b) 12V POL voltage oscillation

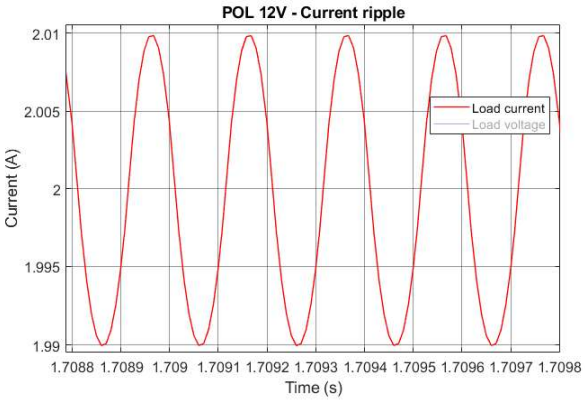

(c) 12V POL current oscillation

Figure 6-3: 12V POL converter response for maximum allowed load

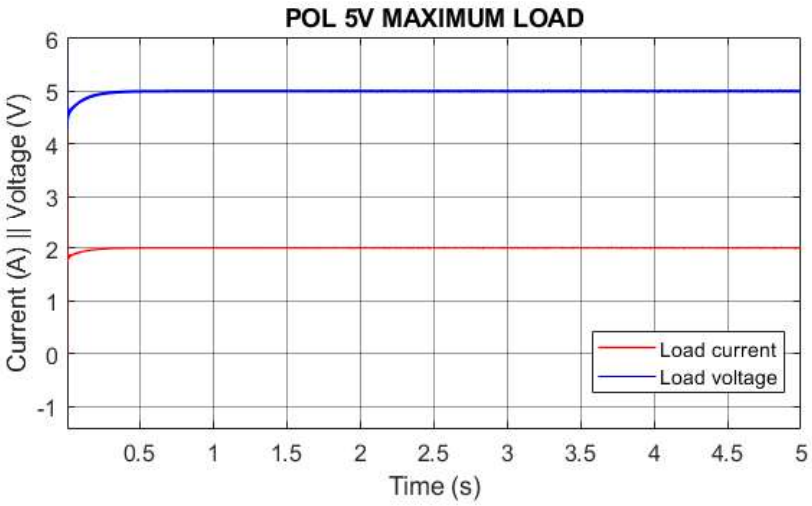

(a) 5V POL total response

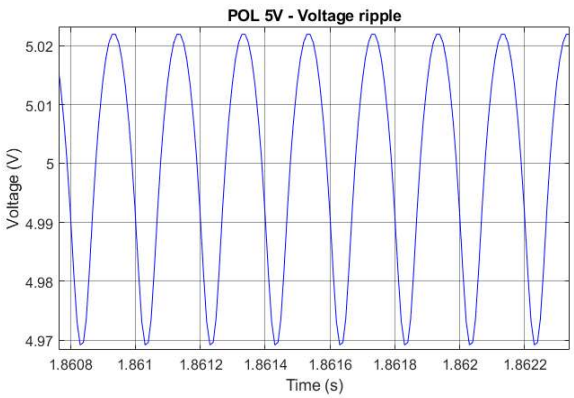

(b) 5V POL voltage oscillation

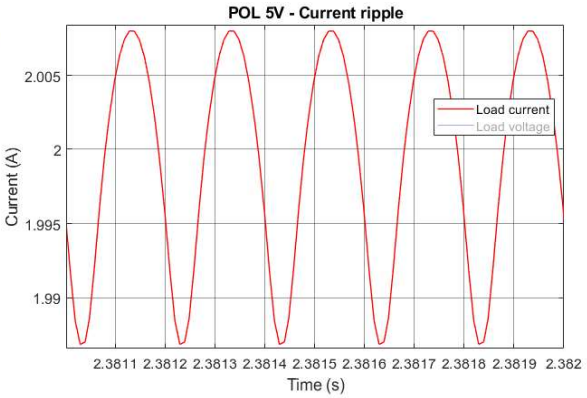

(c) 5V POL current oscillation

Figure 6-4: 5V POL converter response for maximum allowed load

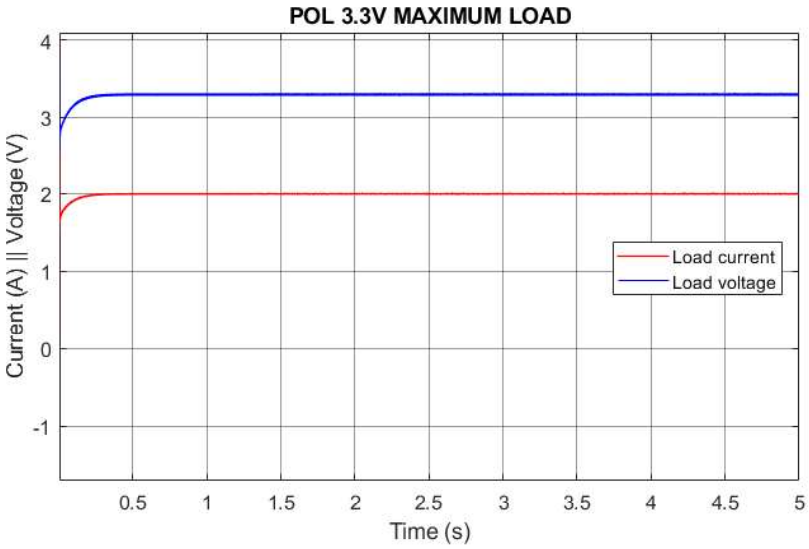

(a) 3.3V POL total response

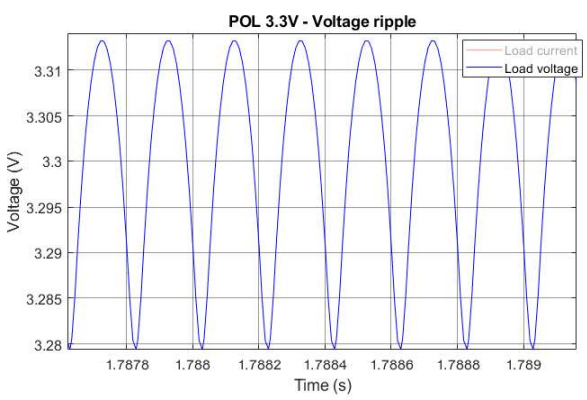

(b) 3.3V POL voltage oscillation

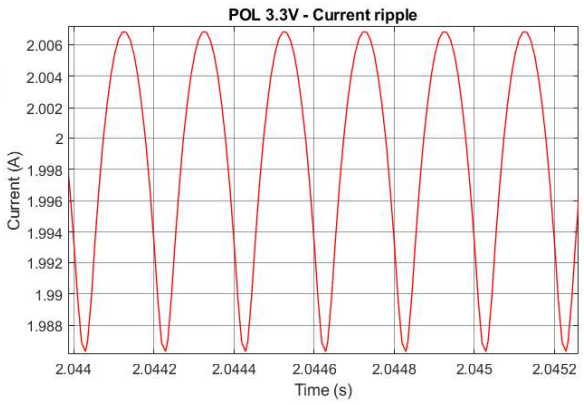

(c) 3.3V POL current oscillation

Figure 6-5: 3.3V POL converter response for maximum allowed load

6-2 Main converter design

The main converter design primarily influences the battery terminal parameters. It is necessary to minimise the oscillations in the battery voltage and current. The batteries are electrochemical devices and they have quite unpredictable transient behaviour in its terminals. Despite this fact, the model provides a current and voltage waveform which can be attenuated by modifying the main converter parameters. The working principle is the same: there will be a ripple and harmonic content in the different signals. From the battery model, it is possible to deduce that some high harmonic content will be inherent to the battery model. This is the reason why the employed Simulink block has a low-pass filter to acquire the low-frequency dynamic behaviour of the battery. The voltage will also have a singular ripple but unlike the current, it is easier to filter. Naturally, the current oscillation will be higher if the charge or discharge current increases.

The converter is designed taking into account the charge limitation. Limits of battery charge/discharge current are given by the data sheet of the battery cells. Table 6-6 shows the maximum values for charge and discharge current per cell.

Table 6-5: Maximum allowable charge/discharge currents per cell

Max. charge current [A]	Max. discharge current [A]
2.5	3.75

Maximum and minimum values are found for LUMIO battery by multiplying the given values by the data sheet by the number of parallel cell strings in the pack. Table 6-6 provides the maximum allowable values for the stack in LUMIO battery.

Table 6-6: Maximum allowable charge/discharge currents for battery pack

Max. charge current [A]	Max. discharge current [A]
7.5	11.25

The charge current will be limited by the control system, but the discharge current will only depend on the load consumption. For a general case with undetermined load, the maximum allowable current ripple should be limited, which will be the upper boundary for this case.

Simulations are designed for setting a 11.25A value of maximum discharge current in the battery terminals. The converter must be tuned in order to get the desired value of oscillation in battery terminals while operating at this maximum current scenario. This value is not determined but it must be a trade-off between capacitor size and ripple value. Even if the inductor normally reduces the current ripple, it is mainly affected by the output capacitor of the converter due to its low-pass behaviour with respect to the current flowing in the main bus.

The main point of the converter is the capacitor value. For this high discharge current,

it is found that the current ripple is really high, so the capacitor needed to limit the current must have a large capacitance, and thus a large size.

Reductio ad absurdum[a] method is performed, by setting the capacitance at a really high value. Inductance shows a very little influence on the battery current when capacitance is set at a very high value of 20 mF. The obtained current and voltage waveforms are shown in Figures 6-6 and 6-7. As it can be observed, even if the capacitance is really high, the oscillation of the maximum discharge current is significantly high (more than 1A) and voltage waveform is very smooth due to the ripple reduction by the capacitor. If we also set a large inductance value, the scenario does not change.

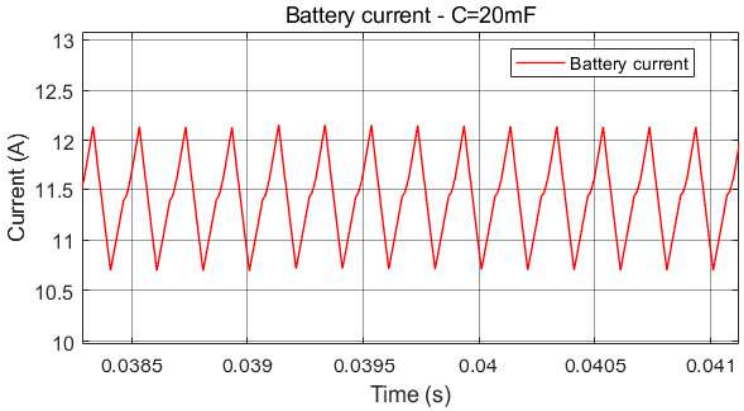

Figure 6-6: Battery current for C=20mF supposition

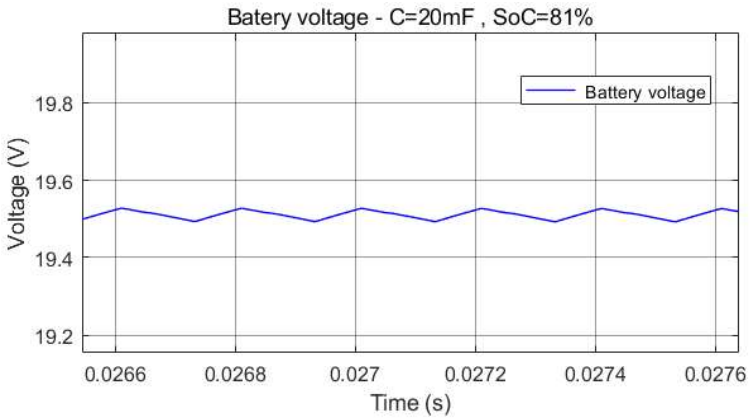

Figure 6-7: Battery voltage for C=20mF supposition

To conclude, for obtaining an acceptable value for current ripple, the output capacitance of the main converter must be very high. To reduce the current ripple value, the design must be carried out using real batteries during breadboarding phase. Thus, the observed undesired behaviour is due to the battery model. In the present design, converter characteristics are set for setting acceptable voltage ripple.

[a]This method is a form of argument which tries to disprove a statement by showing it inevitably leads to an impractical solution.

For voltage ripple, it is found that for higher discharge currents, greater voltage ripple will appear. The highest discharge current is again set and voltage ripple will be limited up to 1%. Voltage level based on SoC of the battery does not affect the ripple.

Even for voltage ripple limitation, high values for output capacitance are found. For a value slightly greater that 1%, the parameters are C=3.3 mF and L=0.05 mH. Capacitance is selected in order to fit a standard commercial value[b] even if the ripple value limitations do not perfectly match. Figure 6-8 shows the new battery voltage waveform. As it can be observed, it is affected by the current waveform which will have a value in the order of 5A oscillation.

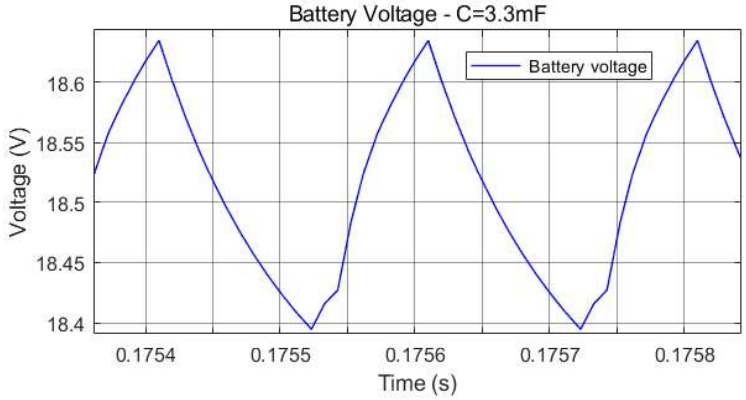

Figure 6-8: Battery voltage waveform for C=3.3mF

6-3 Input filter design

The generation current and voltage are the parameters which depend on the input filter design. The current is mainly affected by this low-pass filter, which shall limit the harmonic content as much as possible in order to get a good power generation.

For filter design, several scenarios are taken into account in order to detect the highest current oscillation. This oscillation will be evaluated for an arbitrarily selected capacitance of 1 mF and the ripple values are described in absolute values (not in percentage of the average value).

- *Maximum generation:* Maximum generation will take place when MARIO CubeSat is operating near the Earth for BOL characteristics.
- *Minimum generation:* It will take place at LUMIO operation when the corresponding irradiation on LUMIO solar arrays is the lowest. It has to be noted that the LUMIO maximum generation capacity is much lower than that of MARIO.
- *Maximum load:* The power requirement during heliocentric transfer with the electric propulsion operating at peak power is considered as the maximum load (around 80W).

[b] https://www.mouser.it/datasheet/2/88/TTA_series-552998.pdf

- *Minimum load:* Minimum load is set at LUMIO safe mode operation (around 9W).

This operation modes are evaluated in the PV array terminals for an input filter capacitance of 1mF. For steady-state oscillations, one graph is obtained for each of the four combinations. Figure 6-9 depicts the oscillation for the different combinations in operation. Table 6-7 shows the overall view of the oscillations peak-to-peak values. As it can be observed, the worst behaviour (maximum oscillation) is obtained for LUMIO generation and the lowest load..

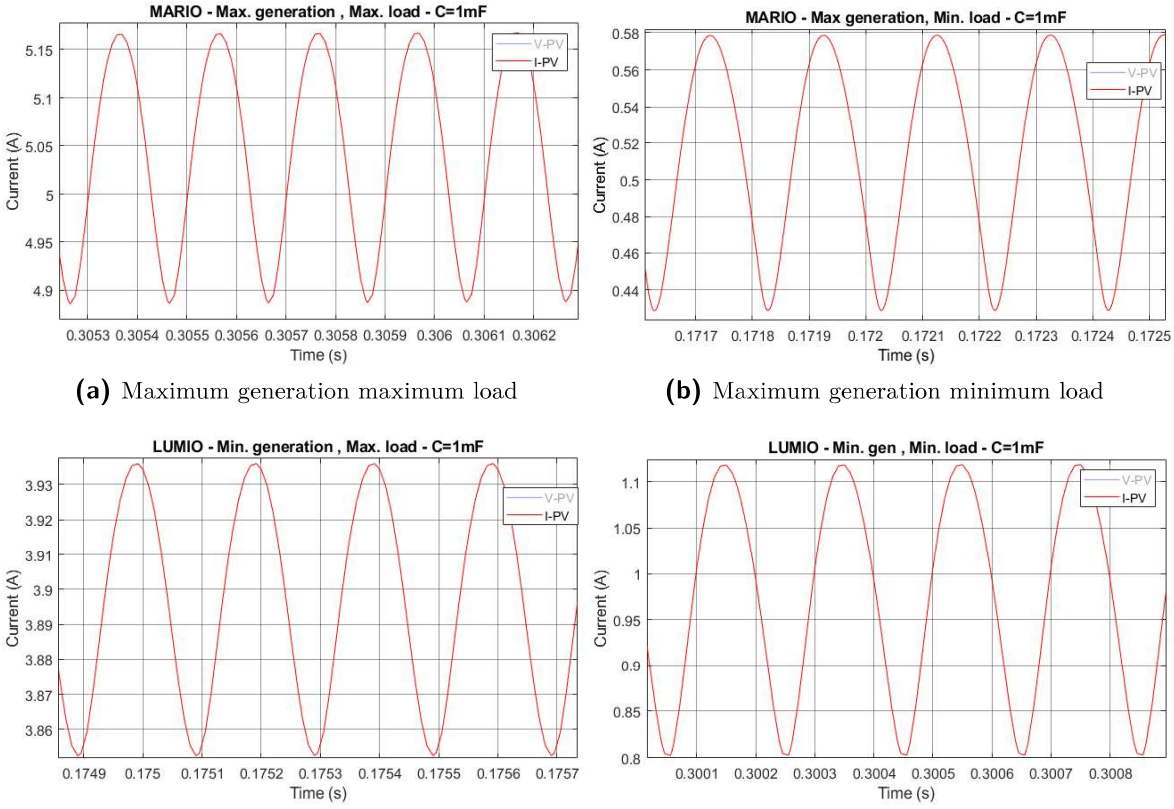

(a) Maximum generation maximum load

(b) Maximum generation minimum load

(c) Minimum generation maximum load

(d) Minimum generation minimum load

Figure 6-9: Input current oscillation values for C=1mF

Table 6-7: Peak-to-peak values in generation terminals for input filter at C=1mF

Operation	Oscillation peak-to-peak values [A]	Worst case
Max Gen - Max Load	0.257	
Max Gen - Min Load	0.15	
Min Gen - Max Load	0.09	
Min Gen - Min Load	0.35	X

The objective value will be in the order of 0.05A (around 5% of the average value) in order to have a clean generation signal. A trade-off between capacitor size and

quality of the signal is performed. The capacitor size obtained (again by referring to a commercial value) is C=4.7 mF, which is significantly large. It provides an oscillation value of 0.065A. Figure 6-10 shows the current oscillation obtained for the defined capacitance value.

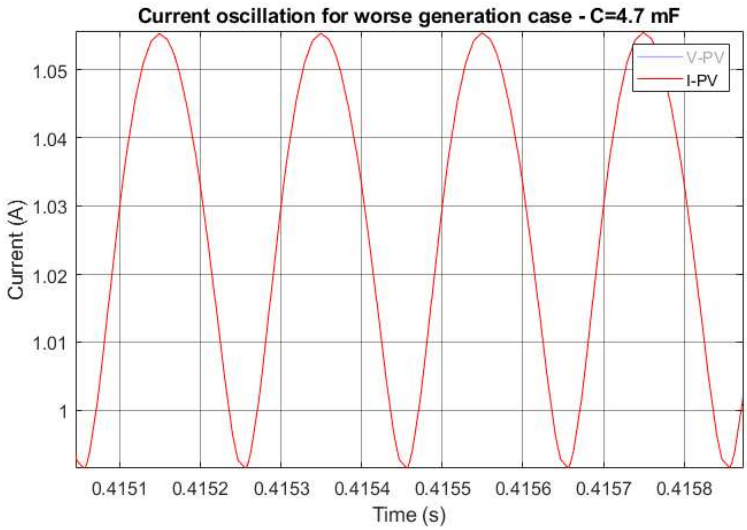

Figure 6-10: Generation current oscillation for worse generation case filtered

6-4 Remarks about converter design

For POL converters design, it is proved that the results are very similar when they are decoupled from the main system when compared to the coupled design. This demonstration of decoupling is achieved by attaching the already designed converters to the general system with the main converter, battery pack and input filter. The aim is that the behaviour of the system does not worsen the load parameters behaviour. In fact, an improvement is expected due to the higher filtering characteristics of the previous filters for some of the control methods.

Figures 6-11 and 6-12 show the behaviour of the 12V converter operating in coupled mode with the rest of the EPS system. As it can be observed, the response is very similar to the decoupled case with a little difference in the initial dynamics, where the signal shows a slightly different oscillation before reaching the steady-state value and also faster dynamics. There is also a very small difference in oscillation, where the ripple is slightly reduced. This value is considered negligible because it is in the order of 0.01 V difference.

For Main converter and the Input filter, significantly high capacitance values are obtained. This fact drives the design towards the use of several main converters and input filters. From the analysis of the examples provided in section 2-3-4, where the designs are breadboarded, Notani et al[1], Shah et al [19] and Singh et al [20] presented some large capacitors are inside the PCB boards. It is observed that they had several input

channels containing several input converters. This paralleling of converters split the PV array in several modules. Each one is controlled by a different input converter, allowing the usage of smaller size capacitors. This issue shall be tested in following stages of the research.

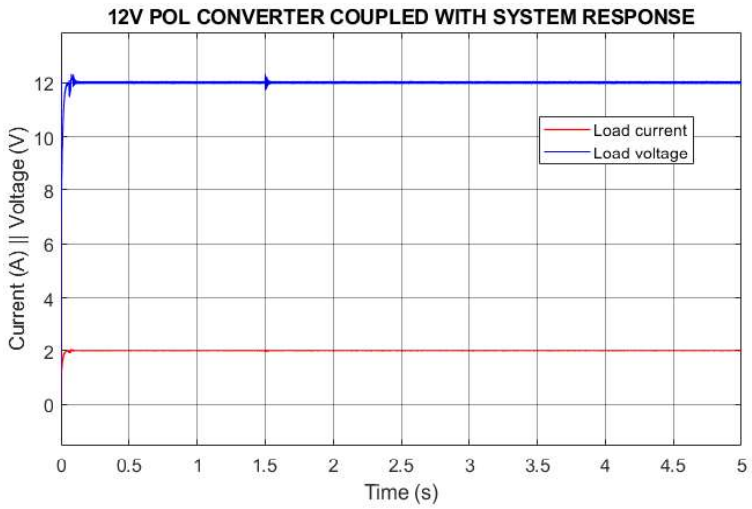

Figure 6-11: POL 12V converter coupled inside the whole EPS system response

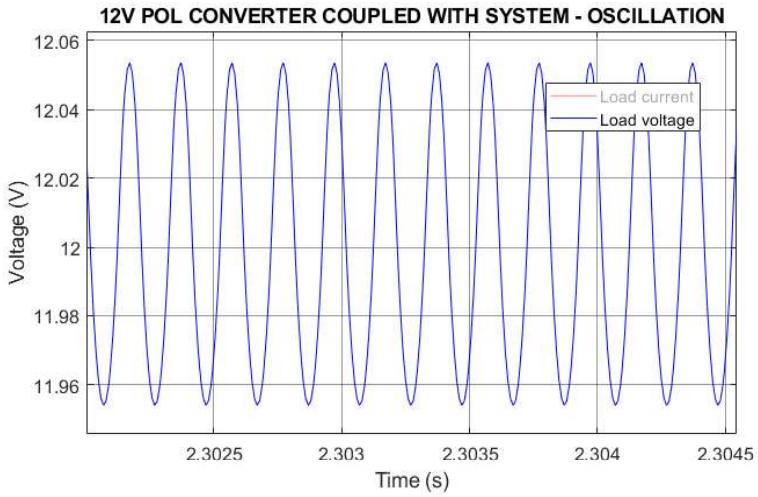

Figure 6-12: POL 12V converter coupled inside the whole EPS system voltage oscillation

6-5 Summary

In the present chapter, the main parameters design has been carried out. The oscillation of the different signals must be limited in order to achieve a good power quality. The main signals appearing in the oscillations are the harmonic content produced by the switches and the ripple of the signal. Both harmonics and ripple are limited by selecting appropriated converter parameters. Switching frequency is set at 5kHz due

to computing restrictions and switching losses limitation. The main points of interest are the load feeding points, the battery terminals and the generation terminals which depend on the POL converters, main converter and input filter, respectively.

For POL converters, a decoupling from the system is performed in order to save computation time. The different components of the POL converters for every voltage level are obtained by limiting the oscillation level up to 1% of the average values.

For the main converter, it is demonstrated that the current oscillation for maximum discharge current cannot be limited for the battery model employed. Thus a more precise design will be carried out during breadboarding phase. A significantly high value is obtained for the output capacitor in order to limit the voltage ripple in the battery.

Input filter is filtering out the harmonic content of the PV array generation terminals, with the input current being the most critical value. The worst case in input current generation is found for minimum generation and minimum load in the range of the EPS design. A large value for the input capacitor is obtained.

POL converters decoupling is demonstrated by integrating it with the general system and comparing the coupled and decoupled response. Necessity of paralleling in main converter and input filter is proposed as a possible solution for the reduction of capacitor size.

Chapter 7

Case study simulations

In this chapter, simulations for both MARIO and LUMIO case studies are performed taking into account the already described models, control and parameters. This chapter fulfils the necessity of obtaining approximated curves for the real operation of the CubeSat for each mission. By evaluating this possible operation curves, actions for future more detailed design can be planned.

For power electronics devices simulation, it is not desirable to simulate all aspects of the systems in detail. Instead, attention must be paid to the immediate objectives and the system must be simplified in order to meet the simulation goals. It is important to note that it may be desirable to verify simulations results by hardware prototype (breadboarding) in the laboratory, as simulations complement experiments and stand-alone do not achieve the accuracy and testing range a breadboarding test would offer [11].

Several case studies are defined taking into account the interesting points on operation where the EPS system will have to prove its proper performance. The case studies in this work are defined based on the critical operational points described by the authors of MARIO [5, 6] and LUMIO [4] missions.

The Simulink model employed for simulations will be the one explained in Figure 5-12. Number of Point of Load (POL) converters is one due to simulation time constraints. MARIO system will use a 24V converter and LUMIO will use a 12V converter. Most interesting curves are obtained from the battery State of Charge (SoC), PV array terminals and the power difference between consumed and produced power.

It would be computationally cumbersome and expensive to simulate long periods of operation (hours) for every simulation scenario. This is the reason why simulations of the main interesting parameters will be carried out by switching from steady-states of different operation conditions and analysing the main transient behaviour. For battery state analysis, the SoC is evaluated taking into account the slope of charge/discharge within a time window. This evaluation is enabled because of the constant operation during two consecutive states.

For EPS simulation, irradiation, temperature profile of PV arrays and power duty cycle are necessary. These characteristics are set for each operating phase in the missions. Irradiation and temperature profile are needed for Maximum Power Point (MPP) definition whilst the power duty cycle define the steady-state conditions inside the simulation scenarios.

Simulations are divided into the two main case studies which are LUMIO and MARIO missions.

7-1 LUMIO case study simulation

This section presents the developed EPS simulation results under the conditions imposed by LUMIO mission characteristics. Before showing simulation results, it is necessary to describe LUMIO mission stages and characteristics. Then, the selected scenarios are presented in order to set the boundary conditions of the simulation and finally, simulation results are described and commented.

7-1-1 LUMIO phase description and characteristic parameters

LUMIO CubeSat has mainly four operational phases:

- *Parking:* It starts when the auxiliary spacecraft which transports the CubeSat deploys LUMIO in the parking orbit. It finishes when LUMIO performs the Stable Manifold Injection Manoeuvre (SMIM). This phase lasts 14 days.
- *Transfer phase:* Starts with SMIM and lasts until the injection to the main operational orbit by performing the Halo Injection Manoeuvre (HIM). Last for other 14 days.
- *Operative phase:* Main phase of the mission where LUMIO has two main modes: Science Mode and Navigation and Engineering Mode (Nav & Eng), that alternate every 15 days. It ends after one year of operation.
- *End of Life (EOL):* De-commission of all subsystems is performed.

For the scenario definition, EOL phase is not taken into account. Only the first three phases are selected for EPS simulation. More information can be obtained in [4].

Irradiation and PV array surface temperatures are set for each operational phase. Also, power duty cycle is obtained for each phase, but it will be introduced in following sections.

The irradiation profile is first defined for each phase. Figure 7-1 depicts the evolution of irradiation along the different phases of LUMIO mission.

During Parking phase, it is possible to observe a small ripple in the irradiation profile. This effect is due to the Solar Array Drive Actuator (SADA) actuation which minimizes the angle between the normal of the PV surface and the Sun.

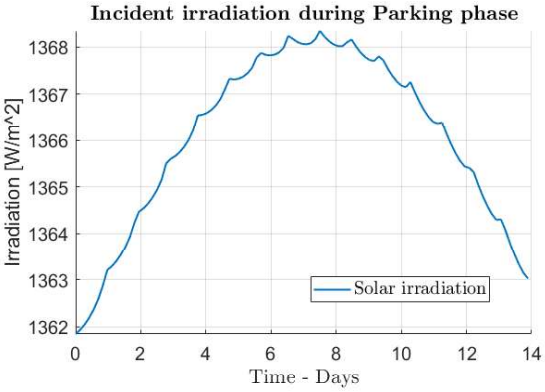

(a) Parking phase

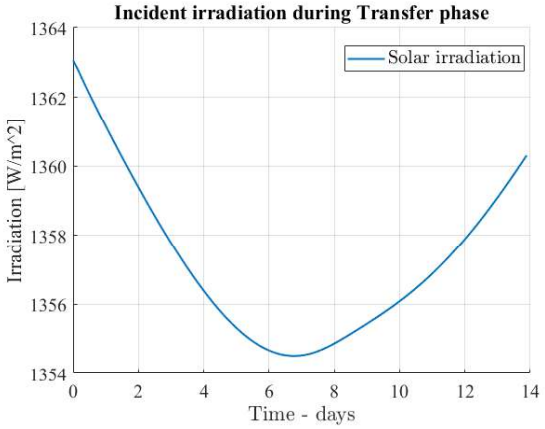

(b) Transfer phase

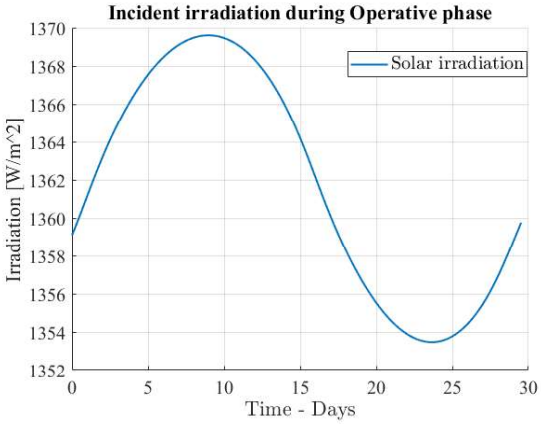

(c) Operative phase

Figure 7-1: Irradiation profile for the different LUMIO phases

For the temperature profile in the PV array, Parking and Transfer phase are represented together in a time window of 30 days. For operative phase only 30 days are represented since it is a repetitive phase which lasts for one year. The profile changes depending on the the performed thermal control tasks on the satellite. Control methods are not explained in detail due to the irrelevance of the thermal control in the present work. PV array temperature profiles for the different phases are represented in Figure 7-2.

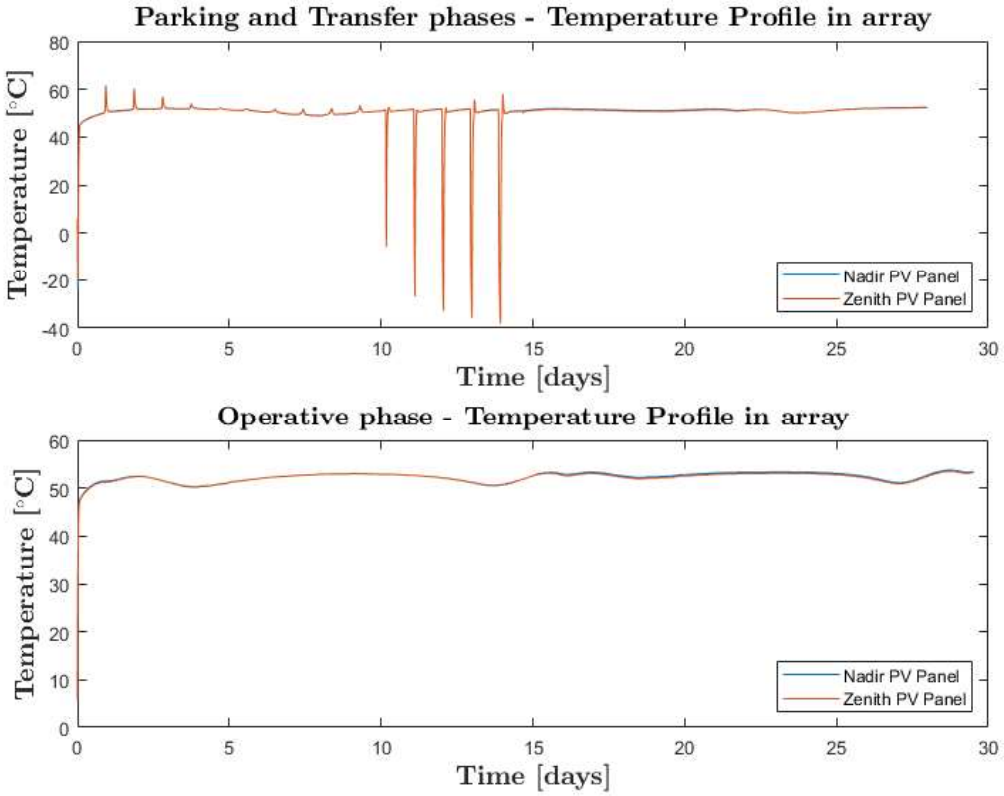

Figure 7-2: Temperature profile for the different LUMIO operational phases

The terms Nadir and Zenith in the legend of Figure 7-2 identify the two deployable solar arrays. Zenith indicates the vertical direction opposite to the apparent gravitational force at that that location. The opposite direction, in which the gravity pulls, is indicated as Nadir. The large magnitude peaks in the profile represents the eclipse periods experienced by the spacecraft, where the temperature drop is very high.

More information about the temperature profile and different parameters about thermal data and control in LUMIO mission can be consulted in [21].

7-1-2 LUMIO simulation scenarios definition

LUMIO mission involves multiple operations such as payload operation during meteoroid impact observation, communication data transmission, on-board orbit determination and navigation, propulsion system firing during transfer manoeuvres and station

keeping etc. This operational tasks have specific durations and the most interesting part to analyse is the transition between two steady-state operation conditions.

In previous stages of the mission design, generated power and power required for operations were estimated for all three phases of LUMIO lifespan. The strategy employed for calculating power generation was inexhaustive and an in-depth analysis is required. Moreover, that analysis has taken into account a general efficiency value of 90% for the converter based on systems engineering conventions [3]. In the current work, the estimated power generation during LUMIO mission study is used for comparison with the performance of the developed model and for PV array model verification.

Different simulations scenarios are described for every phase of LUMIO mission. Not all LUMIO operation are taken into account but only the most interesting ones to analyse the performance of the developed model.

Parking phase scenarios

During Parking phase two scenarios are primarily considered:

- **LUMIO - Scenario 1: Parking cruise to Station-Keeping (SK)**: During parking cruise, the spacecraft performs optical navigation, attitude determination and control, and housekeeping. In the parking orbit, the spacecraft requires orbit maintenance. Station-keeping is the operation in charge of maintaining the spacecraft orbit by using the chemical propulsion system. Thus, there is a transition between parking cruise mode and station-keeping mode.
- **LUMIO - Scenario 2: Parking cruise to Eclipse**: In the Parking orbit, the spacecraft experiences periods of eclipse where generation is zero and thermal control of the system must be performed.

Simulation scenarios are highlighted inside the plot in order to indicate the location of the desired simulation intervals. Figure 7-3 shows the Parking phase operations distribution.

Transfer phase scenarios

Transfer phase starts with the SMIM. The most interesting scenario will be the transition between SMIM and cruise mode during the transfer phase.

- **LUMIO - Scenario 3: SMIM to Transfer cruise**: After SMIM the spacecraft is injected into a transfer orbit towards Earth-Moon L2 halo orbit [4]. During the transfer orbit the spacecraft enters cruise mode where it performs navigation.

Transfer phase operations distribution plot is shown in Figure 7-4. The simulation scenario is again highlighted inside the plot.

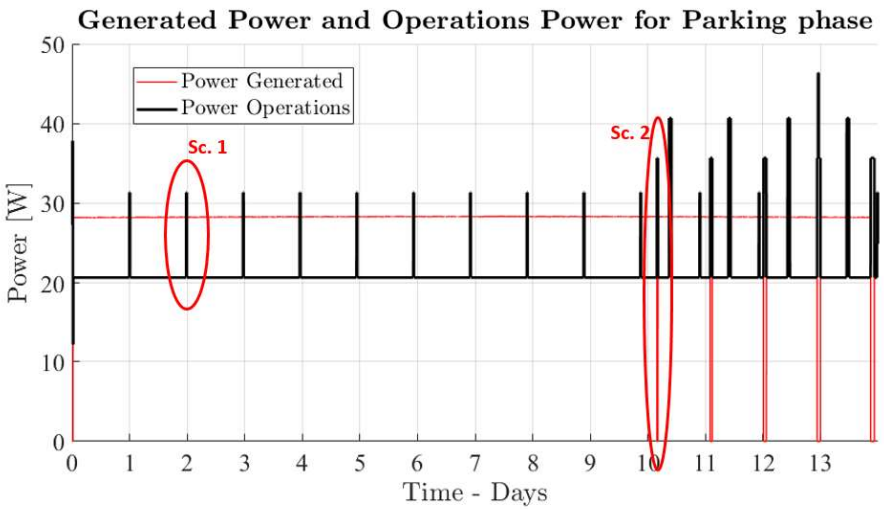

Figure 7-3: Parking phase operations distribution and selected simulation scenarios

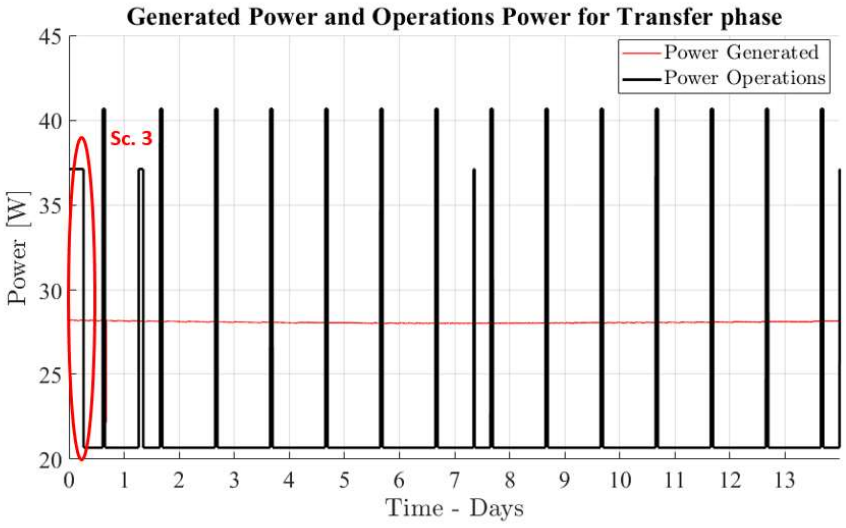

Figure 7-4: Transfer phase operations distribution and selected simulation scenarios

Operative phase scenarios

This phase is the main operational phase for LUMIO mission. Two scenarios are defined for the operative phase:

- **LUMIO - Scenario 4: Impacts Observation and Data Processing (IODP) to Data transmission operation**: IODP consists of continuous observation of meteoroid impacts and image processing. After a period of observation, the data must be transmitted to the lunar orbiter and some extra power will be required.
- **LUMIO - Scenario 5: Orbit Determination, Navigation and Acquisition (ODNAV) to Data transmission operation**: ODNAV is the necessary process for orbit determination and control. It is achieved by acquiring the lunar full-disk images by the payload camera. Communication with the lunar orbiter is performed in equal periods[a].

The Operative phase power duty cycle is depicted in Figure 7-5.

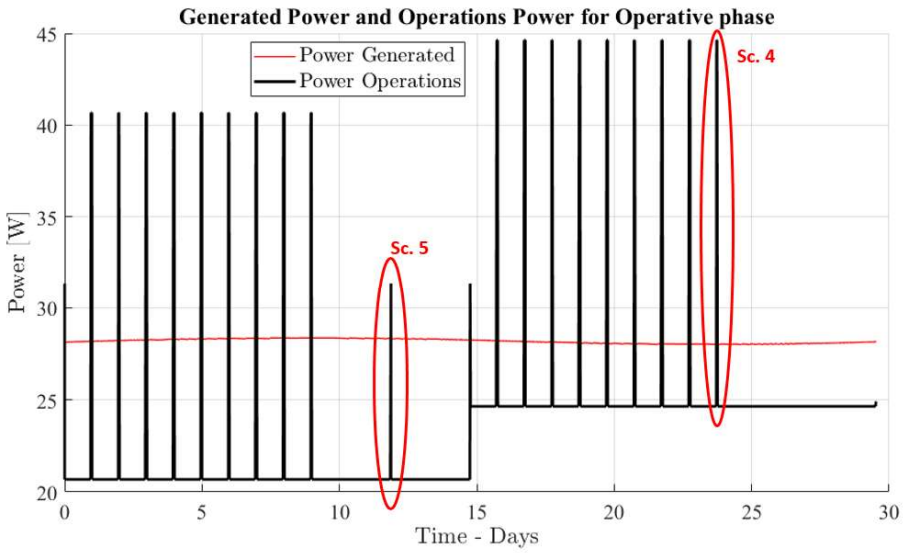

Figure 7-5: Operative phase power duty cycle and selected simulation scenarios

7-1-3 LUMIO simulation results

Once all the required data have been provided and the simulation scenarios have been defined, it is possible to carry out the simulations in order to obtain the behaviour between two different steady-state conditions.

[a]The spacecraft communicates in one hour per day with the lunar orbiter for the days in which the Spacecraft-Moon distance is less than 75000 km.

MPP parameters (MPP current and MPP voltage) are obtained from the temperature and irradiation values for each scenario by using the MPPT method explained in Section 4-2. Figures 7-2 and 7-1 provide the required values of temperature and irradiation for each time instant of the mission. Table 7-1 summarizes all the necessary data for LUMIO scenarios simulation.

The most interesting points of the system simulation are the generation terminals, battery SoC and the power difference between load consumption and power generation. Battery final SoC after the periods in which the battery supplies power to the load is also computed in order to assure the maximum allowed Depth of Discharge (DoD) characteristic.

Simulation time is set at two seconds. It is selected in order to have an appropriated time window to appreciate the transient behaviour of the different signals and to measure the SoC slope for final DoD computation.

Table 7-1: LUMIO simulation scenarios parameters

Scenarios	**Temp [°C]**	**Irradiance [W/m2]**	**Load I [W]**	**Load II [W]**	**MPP Current [A]**	**MPP Voltage [V]**
SCENARIO 1 - Cruise to SK transition	51.42	1363	20.679	32.324	3.9	8.3
SCENARIO 2 - Cruise to Eclipse transition	51.42	1367	20.679	35.680	3.9	8.3
SCENARIO 3 - SMIM to Cruise transition	51.2	1363	37.124	20.679	3.9	8.3
SCENARIO 4 - IODP to data transmission	53.05	1353	24.640	44.640	3.9	8.2
SSCENARIO 5 - ODNAV to data transmission	52.91	1370	21.679	40.680	4	8.2

Start time for simulation will be set at a point where the initial values of the first steady-state condition are stabilized and working in the desired point.

Scenario 1 : Parking cruise to SK transition

For Scenario 1, Figure 7-6 shows the obtained plots for voltage and current in the PV array terminals, power difference between consumed and generated power, and battery SoC.

At the beginning, load adjustment control is employed, supplying just the necessary power for load feeding. Once the second load period starts, generation starts operating at the MPP point which is slightly higher than the load level. Owing to converter

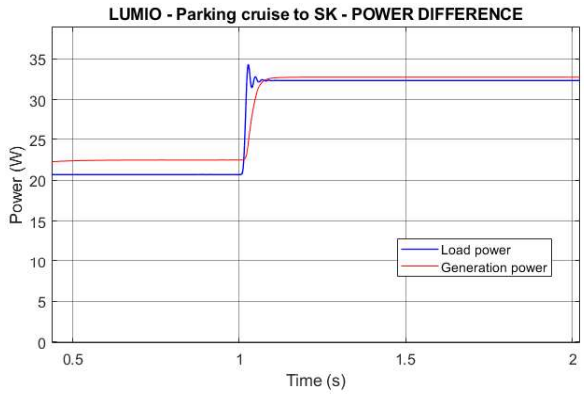

(a) Power difference

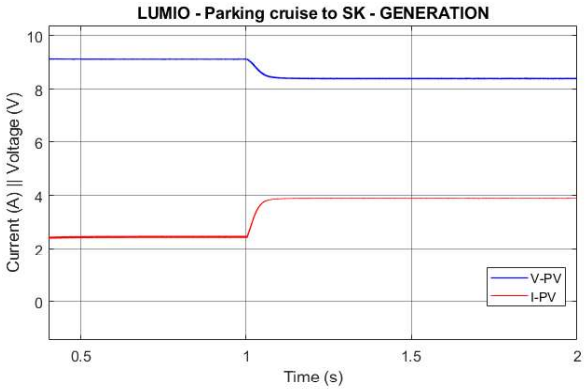

(b) Generation terminals

(c) SoC

Figure 7-6: LUMIO scenario 1 simulation results

efficiencies, generated power is not enough to supply the load and the battery must supply the remaining power. The battery damps the transient of power differences until the generation reaches its final value due to its slower dynamics.

Table 7-2 shows the computation of the final SoC in the present scenario. To calculate the final SoC, the slope of the curve is obtained from Figure7-6c and the duration of the whole SK operation is obtained from [4]. The final SoC is obtained by subtracting the product of the slope and the duration.

Table 7-2: LUMIO scenario 1 final SoC computation

Initial SoC [%]	SoC slope [%/s]	Duration (s)	Final SoC [%]	DoD [%]
80	1.80E-04	6156	78.89	1.11

Scenario 2 : Parking cruise to Eclipse transition

Under eclipse transitions, two different cases shall be analysed: Spacecraft going into eclipse and going out of eclipse conditions.

These simulations do not completely represent real world cases because the eclipse transitions last for several minutes in varying irradiation and temperature conditions. Two aspects of the simulation can not be achieved. The first one is the long simulation time this transition would require, which would imply very long simulation times. The second one is related to the MPPT algorithm which is not implemented in this work. In order to be able to work in the MPP of the PV array, the algorithm shall track the MPP point and not work with constant values as in the present work.

Owing to this constraints, sudden eclipse conditions are simulated. This kind of simulation is selected because if the system is able to stabilise for sudden conditions, it will be stable also for smoother ones. Thus, this simulations are justified.

Figure 7-7 shows the transition from Parking cruise to eclipse conditions under zero illumination. The irradiation is set at zero value when the time is equal to one second, making the current go towards zero. After reaching eclipse conditions, the controller reference feeding must be stopped and the main converter shall not work. This aspect will be ideally controlled by a higher control level coming from the On-Board Computer (OBC) of the system where the eclipse working conditions are detected.

Table 7-3 represents the final value of SoC after eclipse conditions.

Table 7-3: LUMIO scenario 2 final SoC computation

Initial SoC [%]	SoC slope [%/s]	Duration (s)	Final SoC [%]	DoD [%]
80	6.00E-03	6000	44.00	36.00

Once the final SoC at the end of Eclipse has been determined, it is possible to simulate the conditions of the exit form eclipse conditions. It was necessary to set the error of the Main controller to zero and at that instant the spacecraft goes into sunlight conditions, provides the MPP current reference by means of a soft-start device in order

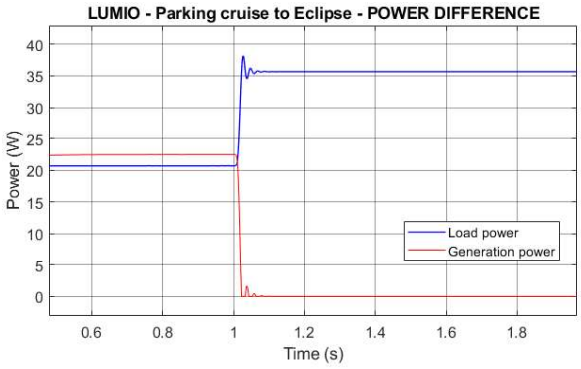

(a) Power difference

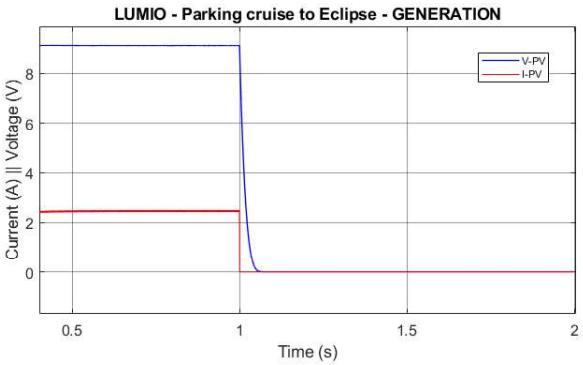

(b) Generation terminals

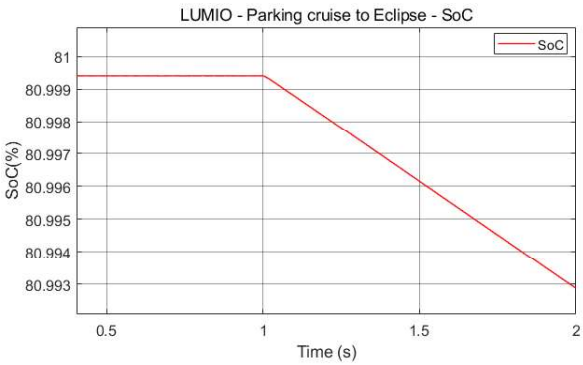

(c) SoC

Figure 7-7: LUMIO scenario 2 Sunlight to Eclipse simulation results

to keep the stability. Figure 7-8 shows the conditions of the spacecraft coming back to sunlight conditions. The EPS system will work in maximum generation mode in order to charge the battery after Eclipse. From one Eclipse to another, the battery will have more than enough time to get the maximum allowed SoC.

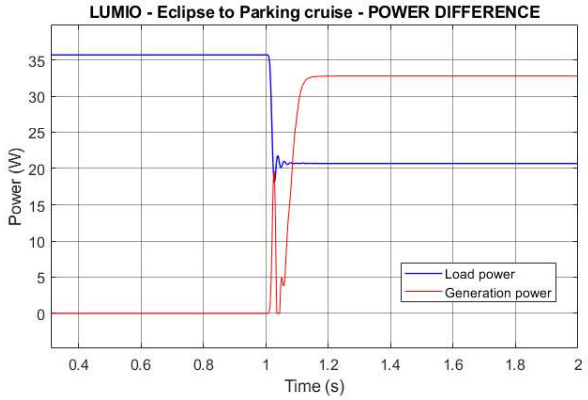

(a) Power difference

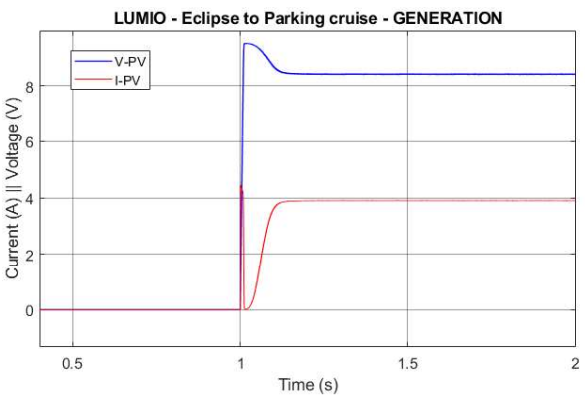

(b) Generation terminals

(c) SoC

Figure 7-8: LUMIO scenario 2 Eclipse to Sunlight simulation results

Scenario 3 : SMIM to Transfer cruise

This scenario occurs in the beginning of the Transfer phase. The steady-state power of the cruise is less than that of the SMIM. Battery SoC at the end of SMIM is calculated and is used as the initial condition for the transfer cruise. Battery initial charge level is assumed to be the maximum allowed one at the beginning of the SMIM. The slope of the SoC characteristic will be provided by the scenario SoC plot. Once the slope is obtained, SoC at the beginning of cruise is obtained and simulation is carried out. In Table 7-4 the SoC after SMIM and before cruise. Figure 7-9 shows the simulation results for scenario 3. The EPS will work at the MPP until the battery reach again the maximum allowable SoC. This is the reason why there is no change in the generation.

Table 7-4: LUMIO scenario 3 initial SoC computation

Initial SoC [%]	SoC slope [%/s]	Duration (s)	Final SoC [%]	DoD [%]
80	1.50E-03	22860	45.71	34.29

(a) Power difference

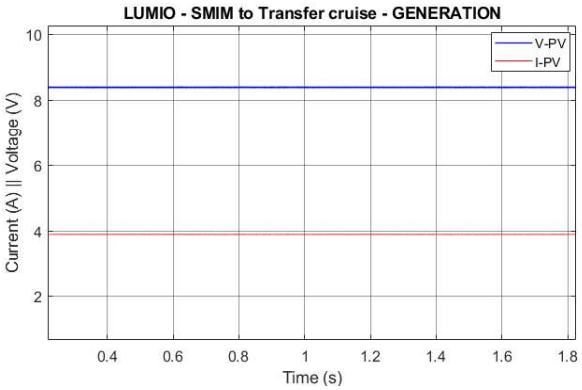

(b) Generation terminals

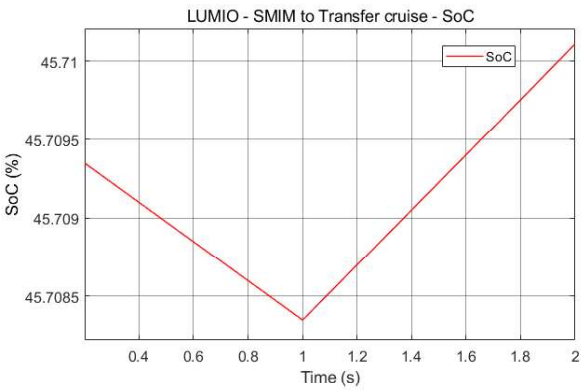

(c) SoC

Figure 7-9: LUMIO scenario 3 simulation results

Scenario 4 - IODP to Data transmission

Scenario 4 occurs in the operative phase of LUMIO mission. The operative phase lasts for one year with repetitive operations until the spacecraft reaches the EOL point. This scenario corresponds to the transition between nominal payload operations and data transmission. The simulation results are shown in Figure 7-10. The final SoC of the battery after one hour of data transmission is computed in Table 7-5.

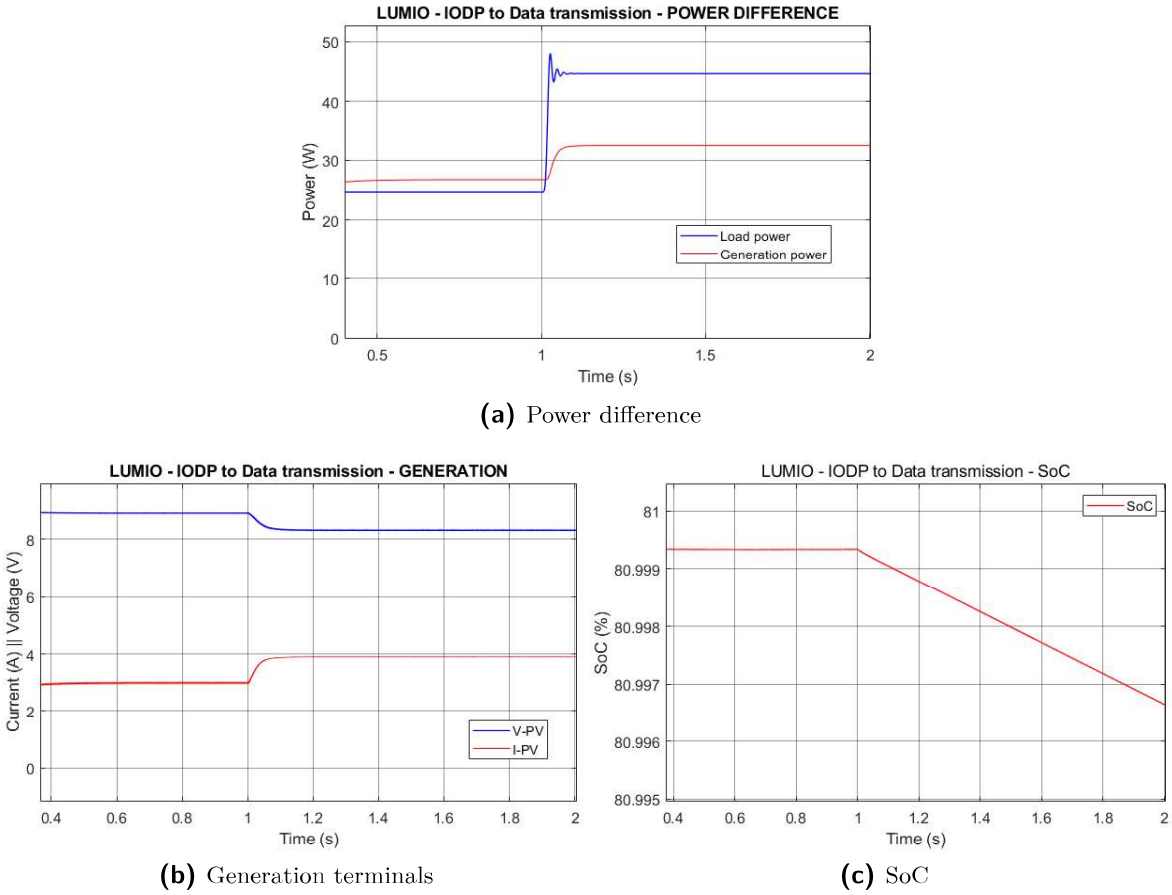

(a) Power difference

(b) Generation terminals

(c) SoC

Figure 7-10: LUMIO scenario 4 simulation results

Table 7-5: LUMIO scenario 4 final SoC computation

Initial SoC [%]	SoC slope [%/s]	Duration (s)	Final SoC [%]	DoD [%]
80	2.80E-03	3600	69.92	10.08

Scenario 5 - ODNAV to Data transmission

This scenario is similar to IODP to Data transmission transition. The only difference is that instead of science observation (IODP) the spacecraft performs orbit determination

through optical navigation. Figure 7-11 depicts the simulation results for scenario 5 and Table 7-6 shows the final SoC after a period of data transmission.

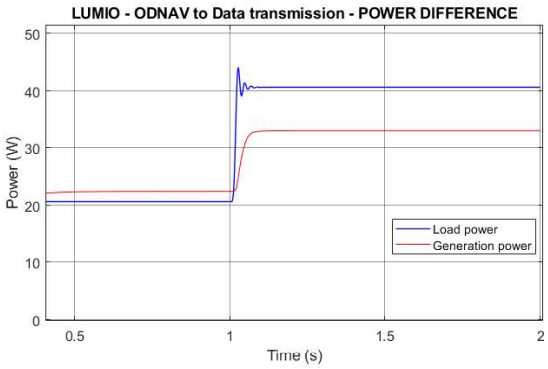

(a) Power difference

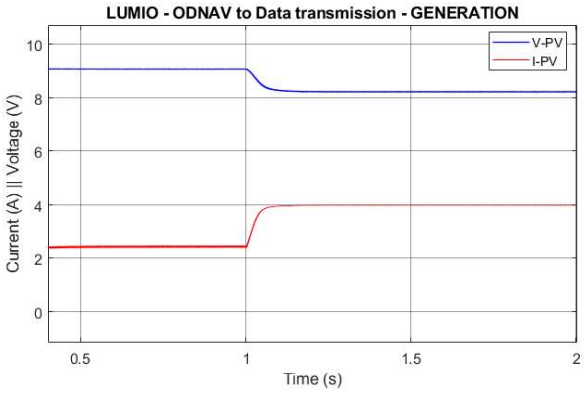

(b) Generation terminals

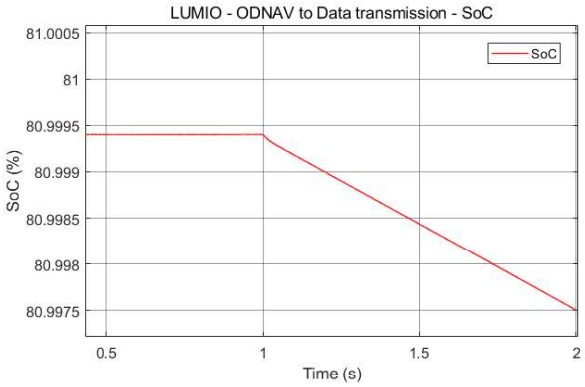

(c) SoC

Figure 7-11: LUMIO scenario 5 simulation results

Table 7-6: LUMIO scenario 5 final SoC computation

Initial SoC [%]	SoC slope [%/s]	Duration (s)	Final SoC [%]	DoD [%]
80	2.80E-03	3600	69.92	10.08

The final SoC value in the last two scenarios is the same because the battery energy consumption for data transmission during both scenarios is the same since data transmission requires the same amount of power.

To conclude LUMIO simulations, the battery DoD is checked to be correct because every scenario complies with the condition of maximum DoD of 60%. Maximum DoD is observed during Parking phase eclipse, where battery reaches a DoD level of 36%. Calculation of the battery SoC during SMIM considered considered full battery at the beginning of the manoeuvre. However there could be a scenario in which SMIM is executed immediately following a Parking orbit eclipse. This means that the overall DoD will reach up to 60% considering the cumulative operational scenarios of final parking orbit eclipse and SMIM. Avoidance of this situation is under study by the authors of LUMIO.

7-2 MARIO case study simulation

This section's aim is to present the EPS simulation under MARIO mission conditions. For this case study, there are not as much data as for the LUMIO case. Despite this fact, whatever data is available is employed during simulations and the rest of the missing values are assumed.

MARIO phases were already defined in Section 3-3 in order to set the operational phases the EPS was designed to deal with. Even though, MARIO phases will be redefined in order to put in context the simulation scenarios for EPS simulation.

7-2-1 MARIO phase definition and characteristic parameters

MARIO mission has five phases:

- *Launch and Early Operations Phase:* The CubeSat is launched and injected into a highly eccentric Geostationary Transfer Orbit. The solar arrays are deployed and the subsystems are commissioned.
- *Earth Orbiting Phase:* Spacecraft orbits around the Earth whilst experiencing eclipse periods and performs orbit raising manoeuvres using chemical propulsion system for swift Earth scape [6]. The most important operations inside this phase will be the chemical thruster firing and preparation for deep-space cruise.
- *Interplanetary Deep-Space Cruise:* During this phase, MARIO autonomously navigates and cruise towards Mars orbit by using electric propulsion system. The technique of electrical thruster firing is called *"Bang-Bang" method*, in which the fuel mass consumption is minimised and the thruster is switched on and switched off following an optimal control algorithm [22, 6].
- *Mars Orbit Ballistic Capture and Science:* The spacecraft performs ballistic capture [23] and then it is injected into the desired Mars orbit in which it will perform the science tasks. There will be eclipse periods and communication slots. For communication, special generation conditions are expected as it will be described in following sections.
- *End of Life and spacecraft disposal:* Once the spacecraft has finished its operations it will perform a final manoeuvre to enter in a safe orbit and then de-orbit.

The first and last phases in the life cycle of MARIO CubeSat are not taken into account for scenario definitions.

As for the first case study, some data is necessary in order to simulate the working conditions. For this mission, operation distributions and their corresponding powers for Earth orbiting phase and depp-space cruise phase are not defined precisely. The temperature profiles for Earth and Mars operation are represented in Figure 7-12 [5, 6].

Table 3-1 represents the different power consumption requirements along the mission. This table was already represented in Section 3-2 and provides the different power requirements during each phase of the mission.

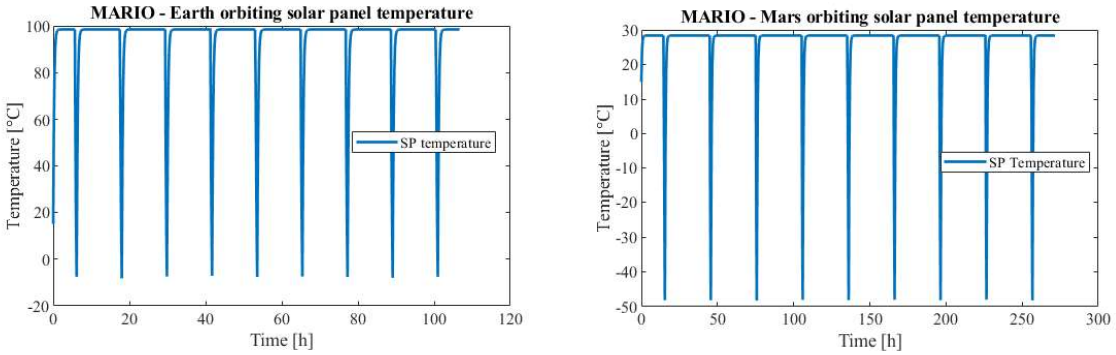

(a) Earth **(b)** Mars

Figure 7-12: Solar panel temperature profile during Earth and Mars orbiting

7-2-2 MARIO simulation scenarios definition

Earth orbiting phase

One scenario is mainly defined during Earth orbiting phase:

- **MARIO - Scenario 1: Earth orbiting cruise to Chemical propulsion firing**: Chemical propulsion is utilize for performing orbit raising and earth escape manoeuvres. This scenario pertains to the transition between cruise and propulsion system actuation. Steady-state powers go from 12.64W to 26.63W.

Interplanetary Deep-Space Cruise

During interplanetary transfer, an electrical thruster is employed. As the spacecraft moves away from the Earth, solar irradiation decreases proportional to the square of the distance and less power is generated compared to Beginning of Life (BOL) conditions.

The method employed for electrical thruster control is called *"Bang-Bang"* control method [22]. The thruster is switched on and switched off following an optimal control law to minimise fuel.

Three different *"Bang-Bang"* scenarios are defined in order to simulate different generation cases along the interplanetary trajectory.

- **MARIO - Scenario 2: Bang-Bang control 1.16 Astronomical Unit (AU)**: Generation scenario in the limit of the available power greater than the necessary one.
- **MARIO - Scenario 3: Bang-Bang control 1.33AU**: In this point, available power generation can be equal to the maximum in case the electrical thruster is fired using maximum available power.

- **MARIO - Scenario 4: Bang-Bang control 1.5AU**: Point close to the ballistic capture. The spacecraft will be under Martian conditions of irradiation and temperature.

Figure 7-13 depicts the different scenarios during interplanetary transfer.

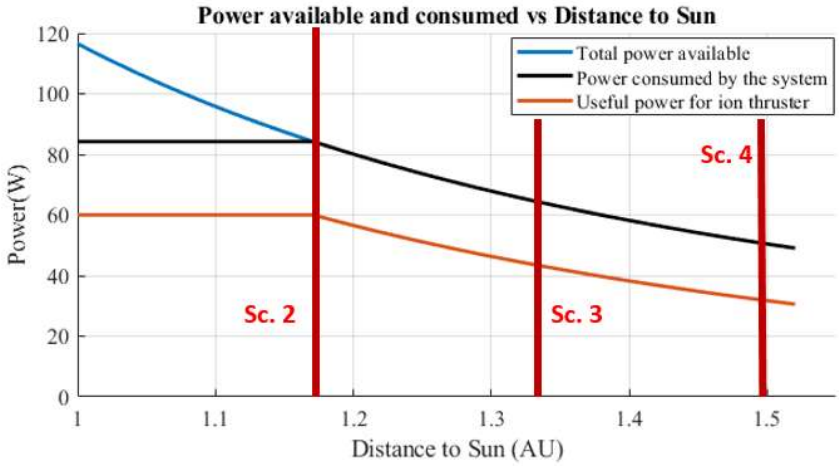

Figure 7-13: Interplanetary transfer power distribution and simulation scenarios

Mars Orbit Ballistic Capture and Science

Before defining the simulation scenarios, it is necessary to make some remarks on the communication operation characteristics during Mars orbiting.

A reflectarray for the High Gain Antenna (HGA) is used in the back side of one of the solar panels. This is necessary to transmit data to the Earth from Mars. Figure 7-14 shows the reflectarray in the back side of the PV panel.

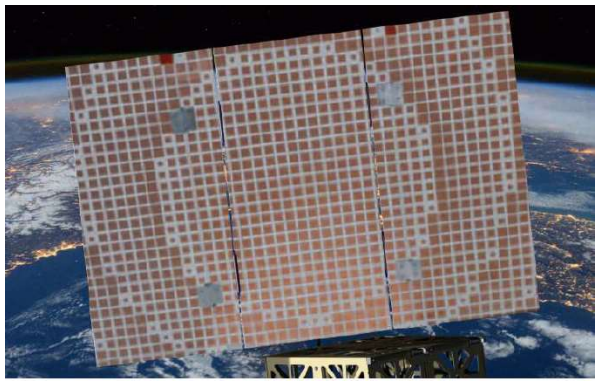

Figure 7-14: MARIO reflectarray [5, 6]

During communication operation, the spacecraft orients its body and one PV array towards the Earth. Meanwhile, the other PV array is oriented towards the Sun to

generate power. Thus, the generation capability is reduced to half of the maximum generation capability. In order to achieve this generation conditions, a special generation model is developed. Figure 7-15 describes the communication operation during Mars orbit.

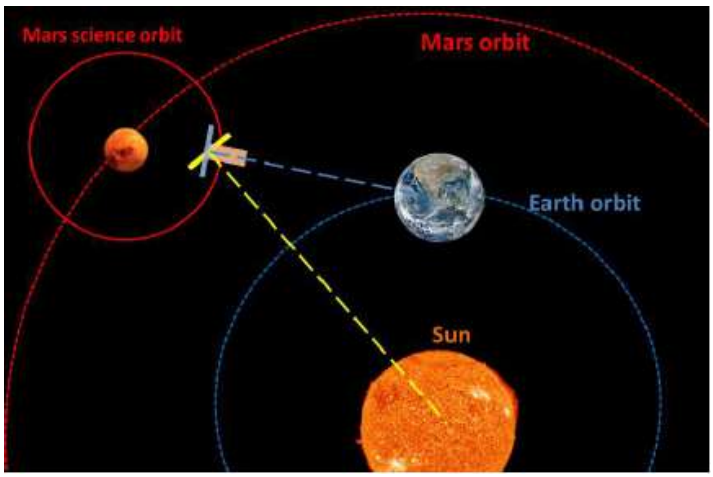

Figure 7-15: Communication from Mars explanation [5, 6]

Simulation scenarios during Mars orbiting phase are defined as follows:

- **Scenario 5 - Mars Altitude Determination and Control (ADCS) & Processing (PROC) to Communication operation**: This scenario encompasses the ADCS operation where both the solar arrays are oriented towards the Sun and the communication operation in which data transmission occurs and only one solar array is generating power.
- **Scenario 5 - Mars Science to Eclipse**: For every Martian orbit the spacecraft experiences an eclipse period. The transition is from payload operations to safe mode operations during eclipse.

Simulation scenarios for Mars orbiting phase are illustrated in the Figure 7-16. This operations distribution was developed by Sanz Casado et al [5, 6]

As it can be observed, the power available has a ripple representing the SADA actuator control. During communications battery will needed to provide the extra power.

7-2-3 MARIO simulation results

Every required data is obtained with the exception of the irradiation values. For irradiation, constant values are considered in Earth and Mars orbits with them being 1366 $\frac{W}{m^2}$ and 592 $\frac{W}{m^2}$ respectively. For interplanetary transfer, intermediate values between Mars and Earth orbits are chosen. This is due to the lack of data up to this research stage in MARIO mission. Table 7-7 shows an overview of MARIO simulation parameters.

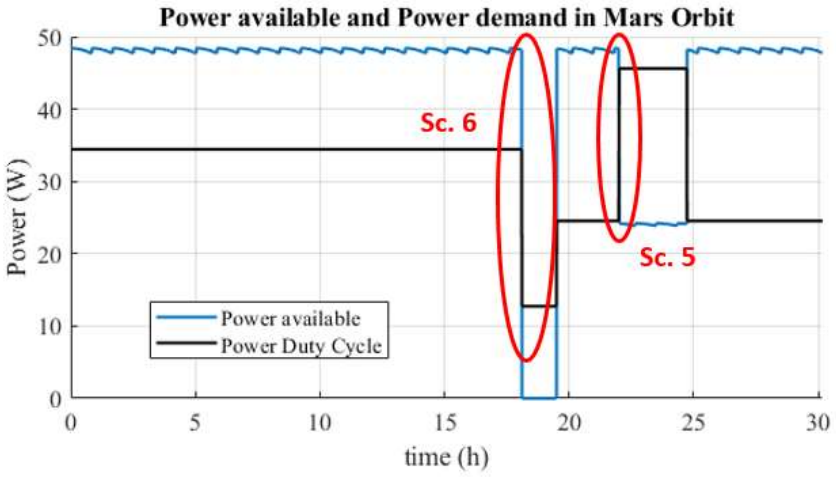

Figure 7-16: Operation power distribution in Mars orbit

Table 7-7: MARIO simulation scenarios parameters

Scenarios	**Temp [°C]**	**Irradiance [W/m2]**	**Load I [W]**	**Load II [W]**	**MPP Current [A]**	**MPP Voltage [V]**
SCENARIO 1: Earth orbiting cruise to Chemical prop.	98.47	1366	12.640	26.63	6.201	17.63
SCENARIO 2: Thruster Bang-Bang control 1.16 AU	75.10	1108	24.200	60	5.000	18.49
SCENARIO 3: Thruster Bang-Bang control 1.33 AU	51.73	850	24.200	45.24	3.780	19.700
SCENARIO 4: Thruster Bang-Bang control 1.5 AU	28.36	592	24.200	23	2.541	20.12
SCENARIO 5: Mars science to Eclipse	28.37	592	34.430	12.730	2.541	20.12
SCENARIO 6: MARS ADCS & PROC to Communications	28.37	592	24.530	43.54	1.268	20.17

Assumptions made for LUMIO simulations hold also for MARIO regarding simulation times and interesting points for simulation.

Scenario 1 - Earth orbiting cruise to Chemical propulsion

This operational condition is characterized by a very low load compared to the available generation. The system shall work under load adjusting control mode and feed the exact amount of energy the load will need without using the battery. Figure 7-17 shows the simulation results for Scenario 1.

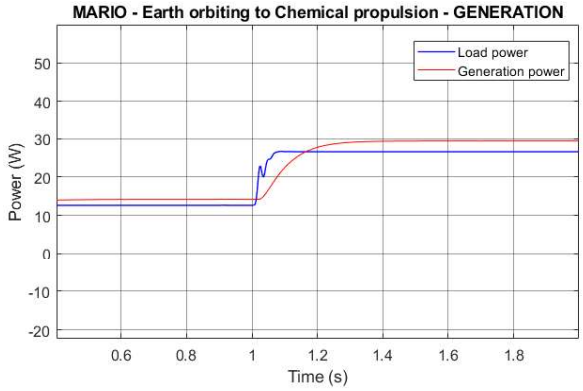

(a) Power difference

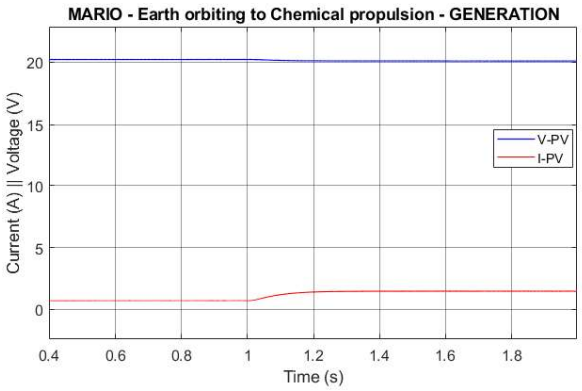

(b) Generation terminals

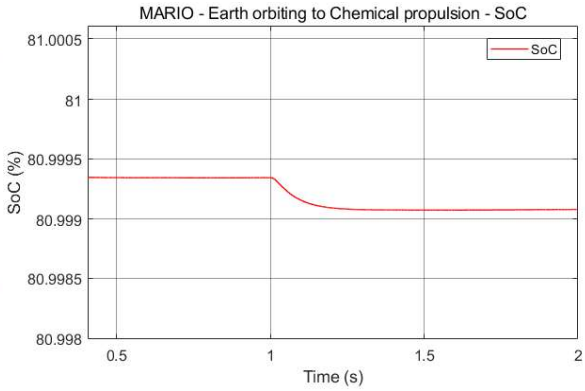

(c) SoC

Figure 7-17: MARIO scenario 1 simulation results

Battery SoC slightly decreases due to the transient damping. It is negligible since it is less than 0.0005 %. It is considered that the final SoC will be the same as the initial one after chemical propulsion firing.

Scenario 2 - Thruster Bang-Bang control 1.16 AU

In this scenario, the spacecraft is travelling from the Earth orbit to the Martian one. The available power is greater than the required so the thruster can be fired at maximum

power. For this scenario, the thruster shall start firing at 60 W and then, stop for one second before firing again. This simulation is achieved by controlling the load by a signal builder in Simulink. The load will follow the signal described in the builder, activating and deactivating it. Figure 7-18 shows how the Bang-Bang load is built. This method will also be employed for all the interplanetary transfer simulation scenarios. Figure 7-19 shows simulation results for MARIO mission scenario 2.

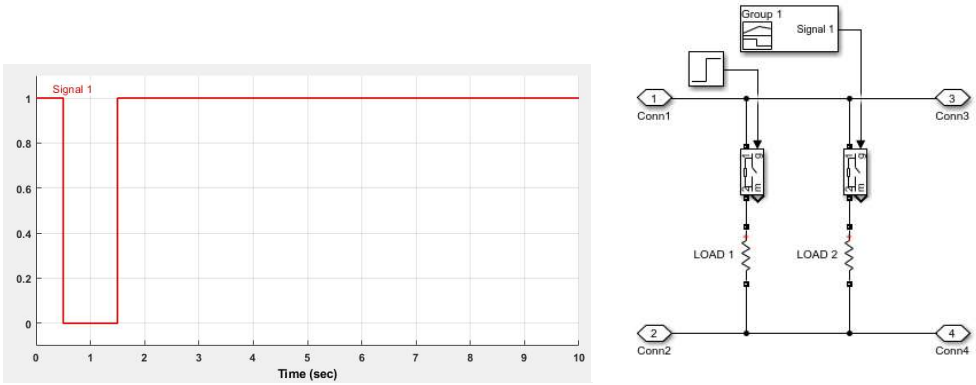

(a) Signal **(b)** Load model

Figure 7-18: Bang-Bang firing method simulation building

Once again, battery SoC fluctuates in order to damp the power transients but the final SoC after one Bang-Bang manoeuvre will be the same as in the beginning of the operation. The elongation in the transient comes from the PI controller employed to keep the voltage constant in the POL converter. For the following scenarios, the only change will be the magnitude of the different evaluated parameters and the transient behaviour will be very similar.

Scenario 3 - Thruster Bang-Bang control 1.33 AU

It is very similar to the last scenario with the only difference being that the available power will be equal to the employed one for thruster operation. The system will work under maximum generation mode. Figure 7-20 shows simulation results for MARIO mission scenario 3.

Scenario 4 - Thruster Bang-Bang control 1.5 AU

For this scenario, the spacecraft is located near Mars and is being prepared for the ballistic capture. Bang-Bang method simulation under Martian conditions is represented in Figure 7-21.

(a) Power difference

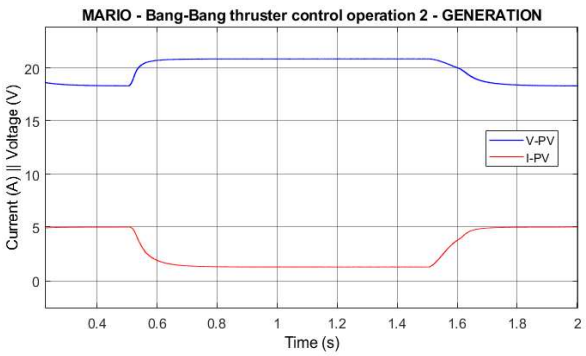

(b) Generation terminals

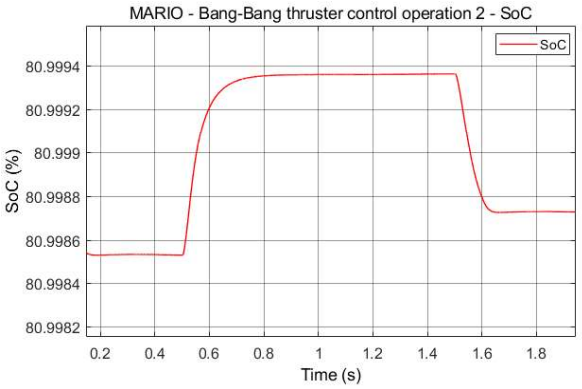

(c) SoC

Figure 7-19: MARIO scenario 2 simulation results

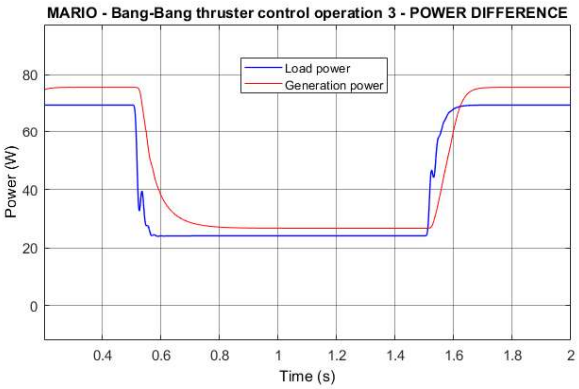

(a) Power difference

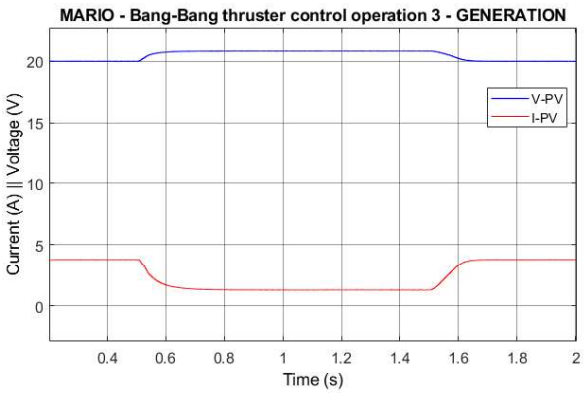

(b) Generation terminals

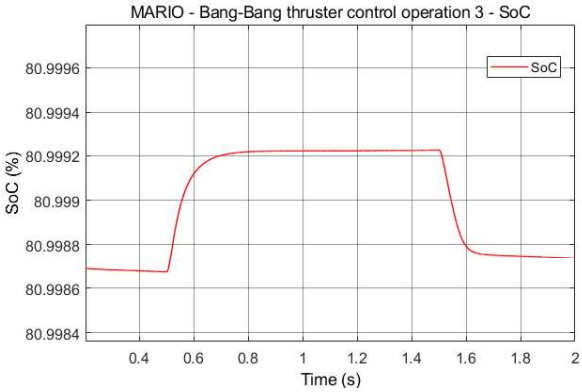

(c) SoC

Figure 7-20: MARIO scenario 3 simulation results

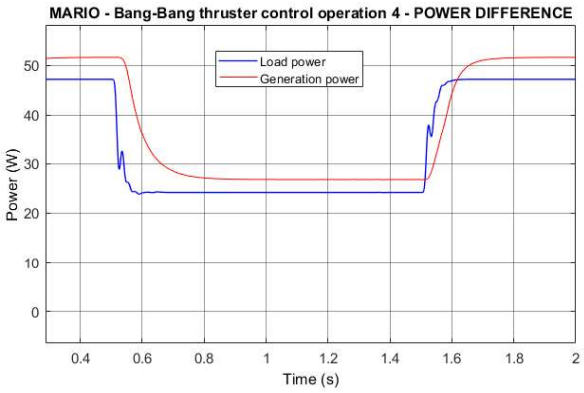

(a) Power difference

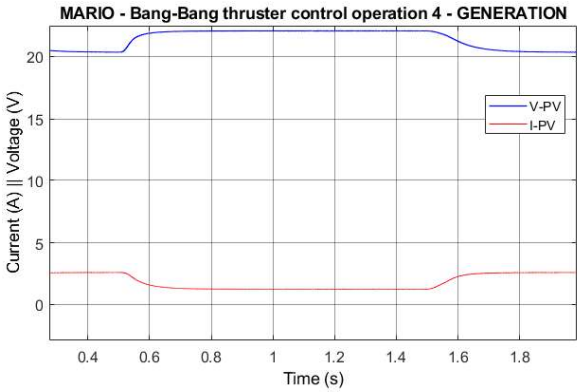

(b) Generation terminals

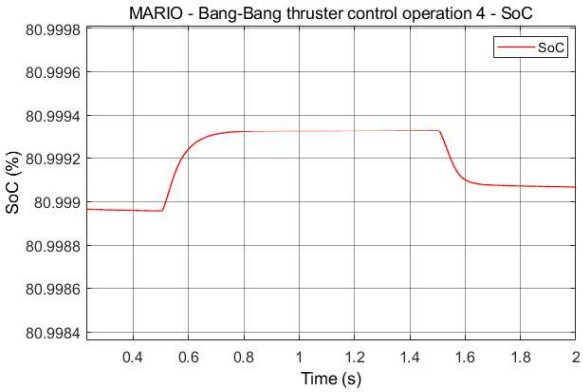

(c) SoC

Figure 7-21: MARIO scenario 4 simulation results

Scenario 5 - Mars ADCS & PROC to Communication operation

Communication from Mars to the Earth takes place under special conditions. It was necessary to simulate this scenario by changing the normal generation model. The arrays are now split in two halves in order to achieve half of maximum generation. Figure 7-22 depicts how the Simulink generation model has been developed.

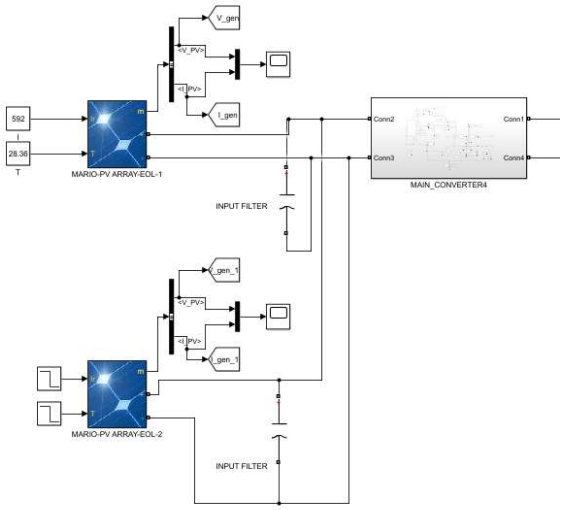

Figure 7-22: Simulink model for communication generation operation

Once the model has been modified, it is possible to present the simulation results. Figure 7-23 shows the simulation results for both PV array sides and the usual points of interest.

As it can be observed, panel number two is in charge of the reflection of the communication signal and its production will drop down to zero ideally. Panel number one, which is oriented in the optimal direction, will switch to the maximum generation control mode. The battery will experience a heavy discharge during communications and the final SoC after the operation is computed. Table 7-8 shows the battery SoC results.

Table 7-8: MARIO scenario 5 final SoC computation

Initial SoC [%]	SoC slope [%/s]	Duration (s)	Final SoC [%]	DoD [%]
80	5.00E-03	9720	31.40	48.60

Scenario 6 - Mars science to Eclipse

Spacecraft now operated in Martian orbit performing its science tasks. Then, an eclipse period happens where the solar irradiation drops to zero.

Simulation features for eclipse transition will be the same as the ones employed for LUMIO eclipse. These conditions were already described in section 7-1-3. Figure 7-24

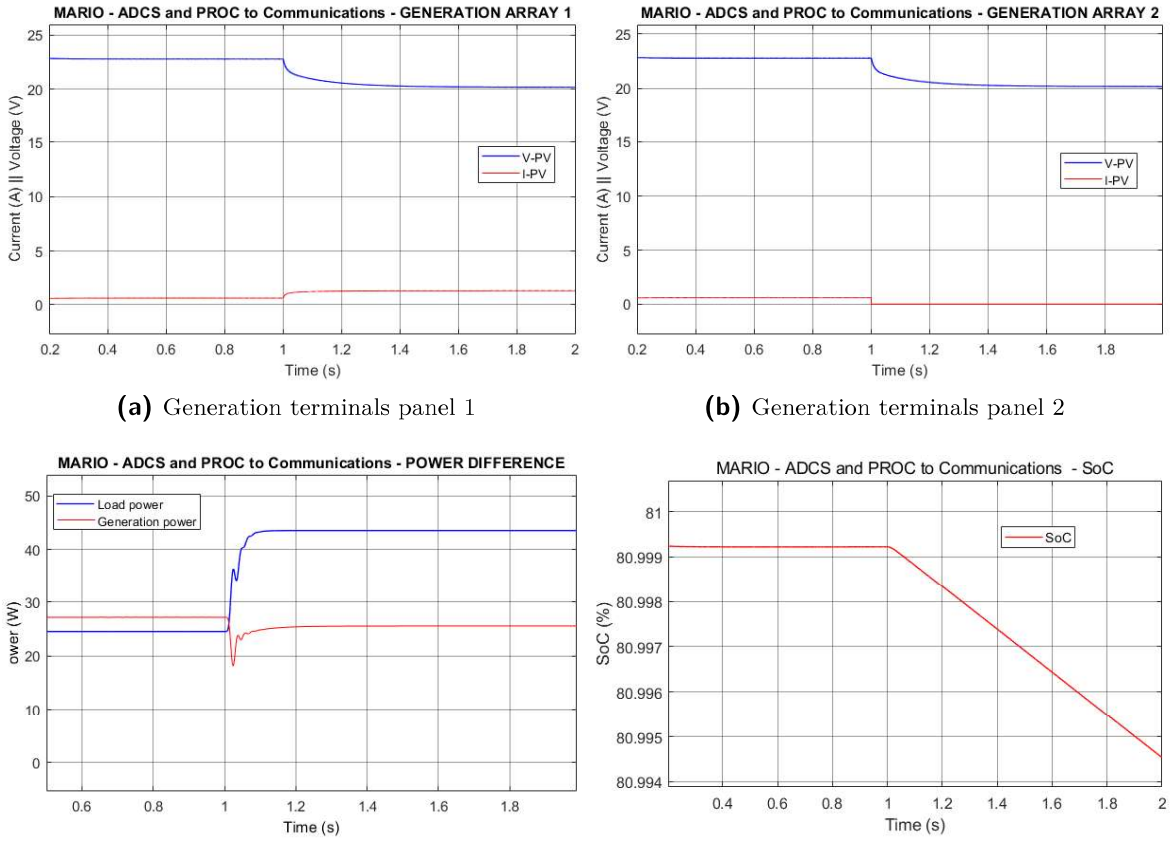

(a) Generation terminals panel 1

(b) Generation terminals panel 2

(c) Power difference

(d) SoC

Figure 7-23: MARIO scenario 5 simulation results

shows the simulation results for MARIO CubeSat operating towards Martian eclipse conditions.

In this case, for generation, it is possible to observe how generation curve has negative transient behaviour. This is due to a short negative value of generation current when irradiation drops to zero. These eclipse conditions are not adjusted to reality since the transition between sunlight and eclipse will last several minutes in real operation.

For this scenario, the SoC will vary after eclipse and the DoD is going is computed. Table 7-9 shows the SoC characteristics of MARIO battery for eclipse conditions.

Table 7-9: MARIO scenario 6 final SoC computation

Initial SoC [%]	SoC slope [%/s]	Duration (s)	Final SoC [%]	DoD [%]
80	2.80E-03	5040	65.89	14.11

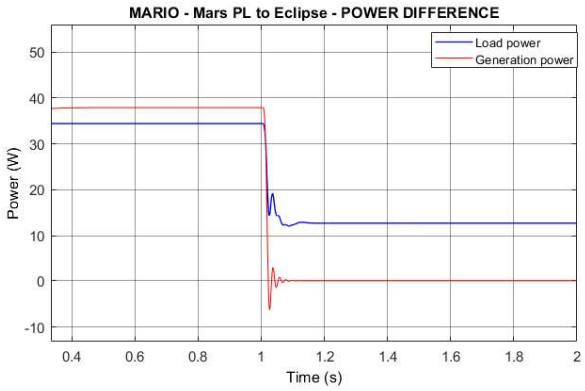

(a) Power difference

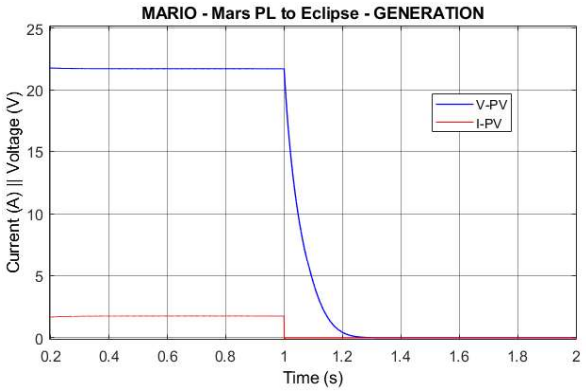

(b) Generation terminals

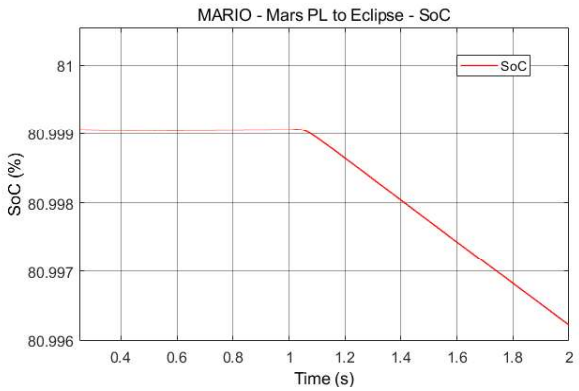

(c) SoC

Figure 7-24: MARIO scenario 6 Sunlight to Eclipse simulation results

After the eclipse the CubeSat will start operating under ADCS & PROC mode. Figure 7-25 shows the transition between eclipse conditions and nominal operations during illumination.

The communications phase will require battery power supply and there should be

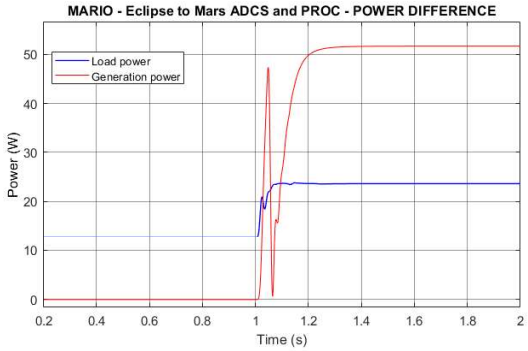

(a) Power difference

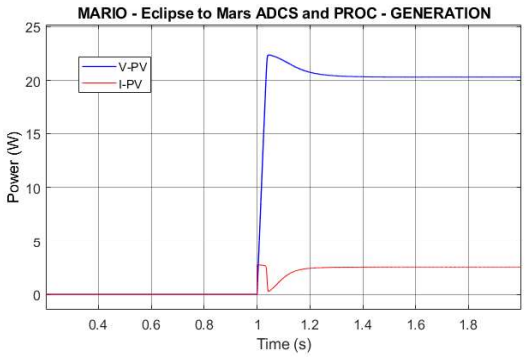

(b) Generation terminals

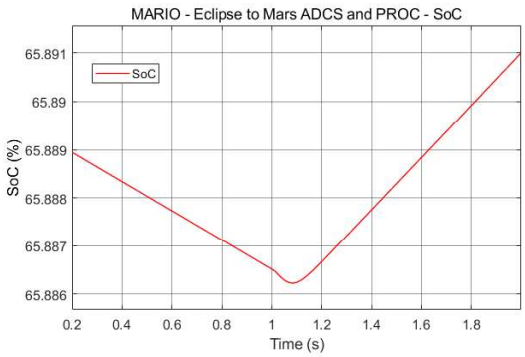

(c) SoC

Figure 7-25: MARIO scenario 6 Eclipse to Sunlight simulation results

enough time to recharge the battery before communications operation commences. Table 7-10 shows the necessary time for battery recharge, taking into account the slope of the charging characteristic after eclipse. The necessary time to recharge the battery is lower than the ADCS & PROC operation time, so there will be enough time to perform the recharge.

Table 7-10: MARIO charging time verification

Initial SoC [%]	SoC slope [%/s]	Duration (s)	Final SoC [%]	Duration of ADCS & PROC
65.89	6.00E-03	2351.67	80.00	28800

7-3 Battery charging check

In order to properly check the control method and assure that the battery does not overcome the maximum allowed SoC (around 80%), a case study is set in order to simulate the battery reaching 80 % SoC.

Figure 7-26 shows the simulation results for such a case study. Time is arbitrarily set in order to have enough time to appreciate the charging procedure.

It is possible to appreciate that when SoC rises above 80%, the control system starts decreasing the generation power, avoiding battery overcharge. The scenario was simulated using LUMIO PV array and a generic load. The generation PV array works mainly in the right part of its I-V characteristic (the one closer the the open-circuit voltage) after the MPP working conditions.

The control method is considered validated and working in a proper way. It was also checked that the charging current does not overcome the maximum allowed one as it was described in Section 5-3, so for the two case studies under analysis, this control method will not be employed.

7-4 Numerical integration remarks

This section deals with the numerical time integration issues which must be taken into account in order to properly simulate the designed system.

The integration problem comes from the employed technique to approximate the desired signals through numerical integration methods which will depend on the time variation of the different evaluated signals.

Depending upon the dynamics of the components, there exist two kinds of solvers that are suited for simulations: stiff and non-stiff. Description made in [24] regarding stiffness is:

"*Stiff systems describe problems that exhibit transients. Their solution is the sum of a rapidly decaying part, the transient, and a slowly varying part.*"

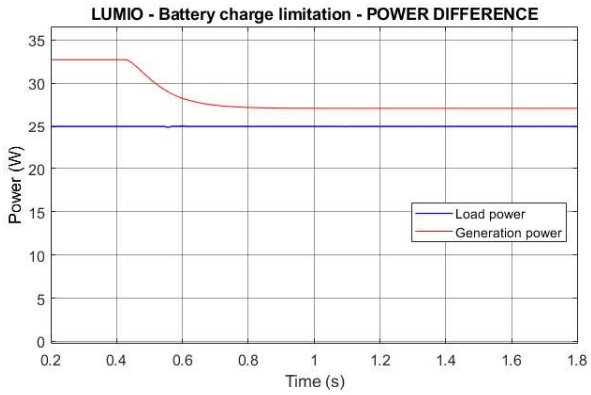

(a) Power difference

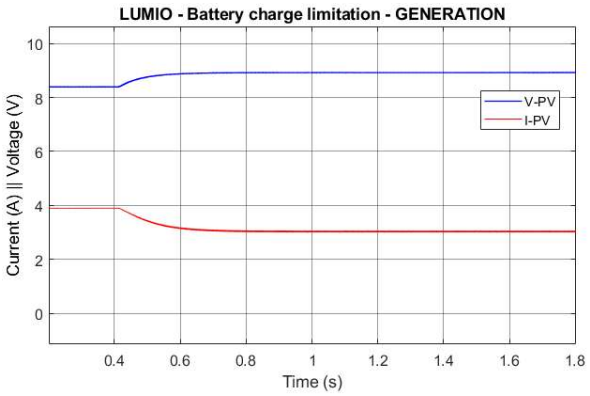

(b) Generation terminals

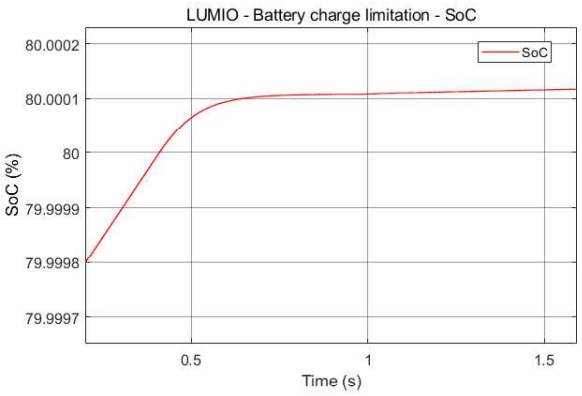

(c) SoC

Figure 7-26: Battery maximum SoC charge simulation results

A stiff method will employ a variable step sizes to capture the different time scales of the system dynamics. The traditional method to evaluate the system would be to get the system of differential equations. After that, it will be necessary to select an operation (equilibrium) point in which the system parameters will be set. The differential equation system will be linearised around that equilibrium point and the linearised system of equations would be obtained. Finally, the eigenvalues of such a system are obtained. These eigenvalues describe the behaviour of the system and allows us to evaluate stiffness depending on their positions in the complex space.

Owing to the highly non-linear and complex nature of the system under study, a comparison between different numerical integration methods is performed in order to evaluate stiffness, accuracy and stability since linearising such a set of differential equations is a very tedious task. Figure 7-27 shows the analysis of the different solvers for a simulation time of 0.2 seconds for the same model.

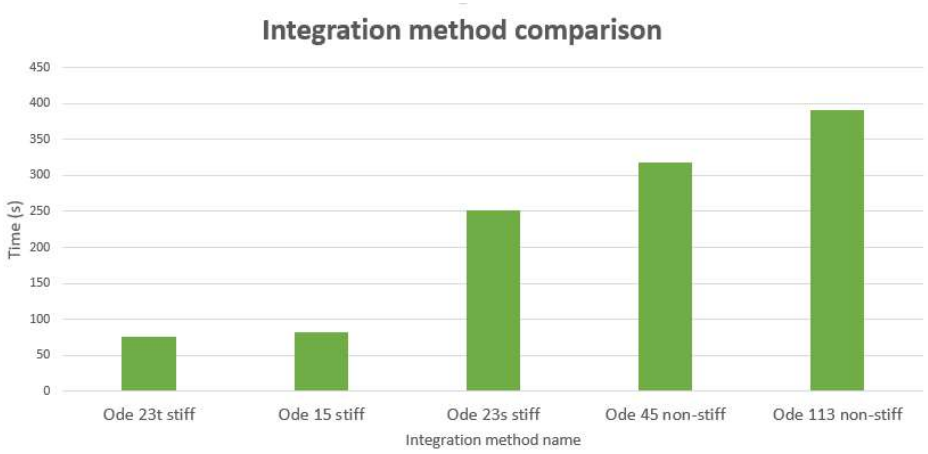

Figure 7-27: Numerical integration method comparison

It is clear that the system is stiff because this kind of method provides a quicker response. The system results are stable in every method under test.

A trapezoidal method provides the fastest simulation time and thus, this method will be the employed one. The system response will also depend on the step time of the sampling. It is necessary to evaluate the trapezoidal method working principle in order to define the step size.

This method uses linear interpolation between two values at times $t - \Delta t$ and t, assuming that $x(t)$ is known at time t. Figure 7-28 shows a graphical explanation for the method for a single variable $x(t)$, where A and b are scalars [11].

The trapezoidal area obtained by using linear interpolation between points $t - \Delta t$ and t approximates the value of the integral. By applying this method, the state variable vector $x(t)$ follows the expression described in Equation 7-1, where $g(t)$ represents a single input signal. It mainly represents the area inside the trapezium.

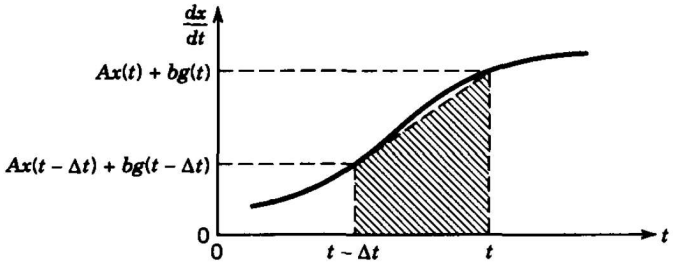

Figure 7-28: Trapezoidal method for numerical integration explanation [11]

$$x(t) = x(t-\Delta t) + \frac{1}{2}\Delta t[A(t-\Delta t)x(t-\Delta t) + A(t)x(t)] + \frac{1}{2}\Delta t[b((t-\Delta t)g(t-\Delta t) + bg)t)] \tag{7-1}$$

For non-linear equations, the last equation will become non-linear and the right part of the equation will depend on $x(t)$, becoming $f(x(t), t)$. Iterative methods are used in order to converge to the solution within a reasonable number of iterations [11].

One of the most important aspects is the maximum step time represented by $\max(\Delta t)$. It is necessary to choose a proper size for this step in order to achieve the accurate response of the system.

During the simulations performance, it was found that the default maximum step size was too big to get accurate responses. It was necessary to adjust this time interval size in order to get the desired signal without numerical problems. For 1e-5 s some of the signals were having inexplicable behaviour which was not comprehensible from an electrical point of view. The step-size of the method was reduced, incurring longer simulation times but providing an appropriate response. Figure 7-29 shows the signal comparison for two different maximum step sizes.

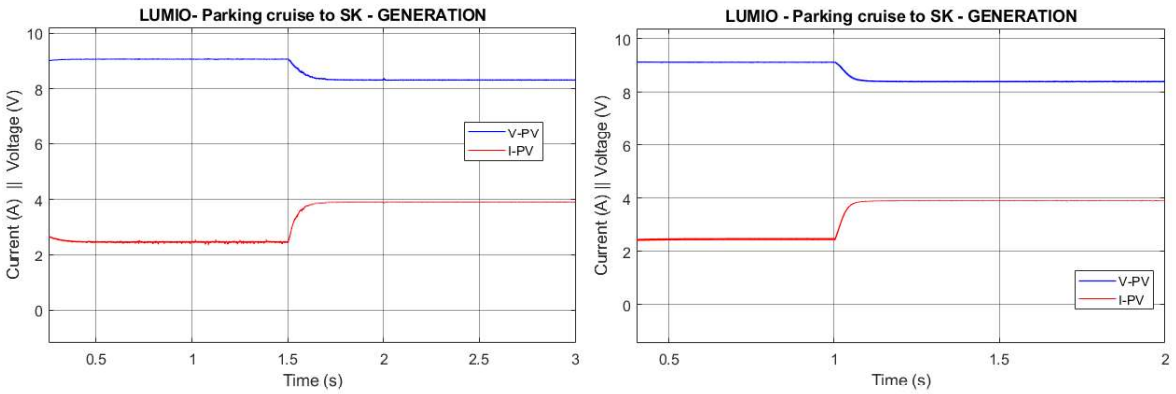

(a) Maximum step size: 1e-5 s **(b)** Maximum setep size: 1e-6 s

Figure 7-29: Difference in signal response for different maximum step sizes

As it can be observed in Figure 7-29, there exists a ripple deviation from the desired

signal. This was the effect of using incorrect maximum step size for the selected trapezoidal method.

7-5 Summary

In present chapter, simulation results were described. General remarks about the simulation procedure were made highlighting the most critical points during the process and the data that was needed for carrying out such simulations.

Then, LUMIO and MARIO case study simulations were shown. First step was setting the necessary data for simulation such as the irradiation and temperature profiles along the mission phases and life. After that, the different phases of each case study were explained and the scenarios for simulation in the desired points were explained. Finally, results were shown for each scenario by highlighting the main issues and particular characteristics for each simulation. Also the DoD of the battery for the different scenarios which needed extra energy supply from the battery, was computed in order to verify the battery design.

Battery charging check was also performed by simulating a particular scenario where the battery reaches its maximum allowable SoC, verifying the proper working of the control method for battery SoC limitation. Finally, the analysis of the numerical integration method employed for simulation was described.

Chapter 8

Closure

8-1 Summary

In the first chapter, the research topic under research was contextualised and motivations, research questions and main objectives were introduced:

- Design a flexible Electrical Power System (EPS) for 12U to 16U CubeSat pursuing lunar and interplanetary missions.
- Analyse the performance and the characteristics of flexible EPS during different mission scenarios.
- Transpose the knowledge of the design characteristics and performance to the system designers in order to enable technologies for affordable interplanetary missions.

MARIO and LUMIO CubeSat missions are the framework for the EPS design. They are described together with some of the critical points of this kind of interplanetary and lunar missions.

In the second chapter, a literature review is performed in order to set a starting point for the study. The different EPS system parts (generation, energy storage system, energy management, etc.) include different kind of technologies, requiring a research work in order to frame the type of components which are going to be employed. Different authors have developed different kinds of EPS systems, and they are described and defined. After analysing them, it is clear that a research gap exists for this type of mission under analysis.

Third chapter initiates the EPS design by setting the main boundaries in terms of generation, load consumption and functional features. Departing from this point, the EPS system requirements were defined in order to have a perfect overview for future

parameters design. The main architecture is described in order to achieve the defined requirements. Converters are the main elements of the EPS systems and their types and critical features are also described.

Chapter four explains how to model all the elements described in the general architecture in order to simulate the system and achieve the main objectives. The employed tool for system simulation is Matlab Simulink software. Main and Point of Load (POL) converters are described by highlighting their different working principles and the waveform of the different parameters. Their Simulink models are also described in order to perform simulation tasks. Photovoltaic (PV) arrays for LUMIO and MARIO are also modelled using a particular Simulink block. Working principles of the blocks are explained as well as the effects of the external changing conditions such as incident irradiation and temperature. The two missions under study have different number of connections and PV cells. The simulation block parameters are set and the two provided curves (I-V and P-V) are tuned in order to match the experimental curves provided by the manufacturer. The method for Maximum Power Point Tracking (MPPT) is explained, providing the Maximum Power Point (MPP) current and voltage for the different case study scenarios. Li-ion battery employed for EPS auxiliary energy supply is also modelled using a custom Simulink model. Main working principle of the battery block is explained and the different connections of the battery cells are depicted. The battery block is tuned using the required battery capacities for MARIO and LUMIO obtaining the discharging curves and characteristic parameters for each battery. The last elements to be modelled are the loads which are done by setting the connection interface of the EPS, their interaction with the different loads, and the power consumed by each load represented by their equivalent resistances.

Fifth chapter explains the basic control principles and architectures of the system. The converters are controlled in different ways depending on their function. Main converter is in charge of the main EPS regulation functions and it is controlled by two different methods which are selected depending mainly on the balance of consumed/produced power.

Chapter number six describes the different converters, modelling them by using parameters that are power quality oriented. The different lumped elements of the circuits are dimensioned taking into account the load, battery terminals and generation terminal parameters. The main dimensioned elements are the POL converters, Main converter and the input filter.

Finally, chapter seven presents the simulation results and fulfils the objective of the present work. Different phases of LUMIO and MARIO missions are described and simulation scenarios are defined. The main simulation points are the generation characteristics (current and voltage), the power difference between produced and consumed power, and the SoC of the battery. The final SoC values after the different scenarios requiring battery supply are also computed.

8-2 Conclusions

The research questions that were posed in the beginning are answered and the rationale behind them are expounded.

8-2-1 On the broad power generation and load power consumption handling

The EPS system is designed to deal with a broad range of powers both in generated and consumed power. This is achieved by adopting a Buck-Boost converter interfacing the PV generation source. In the load side, several converters are placed in order to achieve different voltage levels (3.3V, 5V, 12V and 24V) required by the different load specifications for the missions under analysis.

For high power demands, the battery provides the necessary extra power in addition to the PV generation.

The control system will assure stability and proper operation for the different phases of the mission by tuning the PI controllers.

Also, the converters shall assure a good power quality, which up to this point of the work is set at high standards by assuring a maximum oscillation (ripple plus harmonic content) of 1% in current and voltage at the load feeding points.

In the battery and generation terminals, the worst conditions are found. The main converter and the input filter are dimensioned in order to provide optimal conditions in these points, achieving around 5% of current in the generation and 1% of battery voltage oscillations. The capacitance values in the input and output of the main converter are really high. However, this feature can be improved by paralleling several converters and different input buses in the EPS, limiting the number of PV cells strings per input converter.

Reference power quality values for this kind of systems were not found in literature. A trade-off between component sizes, switching frequencies and power quality shall be performed in future breadboarding studies.

8-2-2 About the electrical interface in interplanetary and lunar CubeSats

The EPS system shall be as simple as possible in order to avoid element failure and electrical instability. In order to achieve this feature, electrical dissipation (shunt regulators) must be avoided and the system shall be able to provide the exact amount of power the system requires.

The electrical interface consists of a main converter facing a battery bus (operated at the battery voltage depending on its State of Charge (SoC)) and in order to centralise the system, several POL converters feed the loads depending upon the load requirements. The main converter is a Buck-Boost type in order to be able to step up and down the voltage. For the POL converters there exist Buck and Buck-Boost types. It was

demonstrated that for the MARIO case study, the 24V is required to be Buck-Boost. For the other POL, Buck type is employed.

The control method will work under two features, one operating at the MPP and other adjusting the generated power to the battery and load requirements. The main converter will be in charge of the main parameters control.

8-2-3 About the behaviour under the most critical conditions

Different simulation scenarios were chosen in order to test the system under the most critical load and generation variations.

Both for LUMIO and MARIO, the EPS under study has demonstrated its good performance in every scenario, always achieving stable points.

The control and performance of the POL converters were analysed for the maximum allowable load conditions while dimensioning the different converters. For generation and SoC of the battery, the test procedure was carried out for MARIO and LUMIO scenarios. Power differences do not provide a real transient behaviour because it does not affect the system components, which are mainly affected by voltage and current transients (even if the power is obtained from the multiplication of these two parameters). It is possible to appreciate how the battery damps the transient power difference, providing a better grade for safe operation of the system.

8-3 Problems found during EPS design

Several problems were found during the process:

- Complexity of the system and non-linearity of most of the involved equations hinder the optimal design of the controllers. Controller parameters are normally obtained from the closed-loop transfer function of the system which comes from the model under study. Instead, empirical PI tuning techniques coming from the control theory were employed.
- Lack of formal regulations on power quality in such EPS systems lead to the adoption of high power quality values in order to assure the design, which at the same time resulted in bigger component sizes. Some of the employed values were taken from manufacturers who provide smaller COTS EPS systems .
- Particular Simulink blocks insert some undesired elements such as the battery current ripple. In order to properly assess this problem, a real battery should be tested during the breadboarding stage.
- Computational time while simulating power electronics is crucial. This, limits the time horizon, making it impossible to simulate long times. In addition, switching frequencies can not be very high due to software issues.

8-4 Personal reflections of the author

At the beginning of this work it was difficult to define the scope of the project. There were so many points to work into since this EPS design for such spacecraft was a black box for people working in this field.

Interdisciplinarity of the thesis required long reading hours in order to understand the main root of the problem. It was difficult to find out the main points in which an electrical engineering student could work in.

After acquiring a base knowledge about CubeSat missions and the critical points inside the project, base objectives were set. As the project was going forward, some limitations were found in terms of computational hassles and complexity of some interesting issues such as the implementation of an MPPT algorithm. Discarding a continuous simulation, discrete simulation scenarios were defined and the EPS design was framed by them.

Future work points were also considered, but in terms of the thesis time they were not achievable. In next section, the future work proposal is described.

8-5 Future work

Once the EPS simulation stage has been completed, next step will be the breadboarding phase. It consists of assembling all the simulated components and achieve the desired response which has been obtained in the simulations or even improve them.

Some simulations should be also carried out by taking into account the parasitic components of switches, quality factor of inductances, Equivalent Series Resistance (ESR) of capacitors, etc. These elements will be present during breadboarding stage and will affect the frequency response of the system.

Also during breadboarding phase, the size of the different employed components shall be evaluated. It is probable that the final required power quality will be less strict than in the present work. Moreover, higher switching frequencies can be achieved and different kind of switches can be considered and tested.

For prototype testing, there exist some equipment available inside PoliMi for generation simulation. Project using this apparatus can be consulted in [25].

Bibliography

[1] S. Notani and S. Bhattacharya, "Flexible electrical power system controller design and battery integration for 1u to 12u cubesats," *Energy Conversion Congress and Exposition (ECCE) 2011 IEEE*, pp. 3633–3640, 2011.

[2] O. Shekoofa and E. Kosari, "Comparing the topologies of satellite electrical power subsystem based on system level specifications," *Recent Advances in Space Technologies (RAST), 2013 6th International Conference on*, pp. 671–675, 2013.

[3] J. R. Wertz, D. F. Everett, and J. J. Puschell, *Space mission engineering: the new SMAD*. Microcosm Press, 2015.

[4] F. Topputo, M. Massari, J. Biggs, and K. Mani, "Lumio - lunar meteoroid impacts observer," tech. rep., Politecnico di Milano, Italy, 2017.

[5] S. C. A., "Preliminary systems design of a stand-alone interplanetary cubesat to mars - msc thesis," tech. rep., Politecnico di Milano, Italy, 2017.

[6] K. V. Mani, F. Topputo, and A. Cervone, "Dual chemical-electric propulsion systems design for interplanetary cubesats," in *Space Propulsion Conference 2018*, pp. 1–12, 2018.

[7] A. E. Frost C., "Small spacecraft technology state of the art," tech. rep., National Aeronautics and Space Administration (NASA), 2005.

[8] L. M. Clark, "Power system challenges for small satellite missions," *Small Satellites Conference*, 2006.

[9] B. Johnston-Lemke and R. Grant Bonin, "Modular power system: Enabling scalable missions for the 1w to 1kw range," *27th annual AIAA/USU, Small Satellites Conference*, 2014.

[10] L. Peng, Z. Jun, Y. Xiaozhou, and C. Luping, "Design and validation of modular mppt electric power system for multi-u cubesat," *Control Science and Systems*

Engineering (ICCSSE), 2017 3rd IEEE International Conference on, pp. 374–377, 2017.

[11] Mohan, Undeland, and Robbins, *Power Electronics: Converters, Appllications and Design*. Wiley, 2015.

[12] B. Sahu and G. A. Rincón-Mora, "A low voltage, dynamic, noninverting, synchronous buck-boost converter for portable applications," *IEEE Transactions on power electronics*, vol. 19, no. 2, pp. 443–452, 2004.

[13] M. Brenna, "Lecture notes in electric power systems ii," September 2017.

[14] M. Swartwout, "The first one hundred cubesats: A statistical look," *Journal of Small Satellites*, vol. 2, no. 2, pp. 213–233, 2013.

[15] E. Gill, P. Sundaramoorthy, J. Bouwmeester, B. Zandbergen, and R. Reinhard, "Formation flying within a constellation of nano-satellites: The qb50 mission," *Acta Astronautica*, vol. 82, no. 1, pp. 110–117, 2013.

[16] S. Asmar and S. Matousek, "Mars cube one (marco): the first planetary cubesat mission," in *Proceedings of the Mars CubeSat/NanoSat Workshop, Pasadena, California, November*, vol. 20, p. 21, 2014.

[17] K. D. Kenny B., Cull R., "An analysis of space system masses," tech. rep., National Aeronautics and Space Administration. Lewis Research Center, Cleveland, 1990.

[18] V. Pooler, E. Priidel, and V. Sinivee, "Reliable smart electrical power supply for cubesat platforms," in *Electronics Conference (BEC), 2016 15th Biennial Baltic*, pp. 215–218, IEEE, 2016.

[19] M. Shah, A. Juneja, S. Bhattacharya, and A. G. Dean, "High frequency gan device-enabled cubesat eps with real-time scheduling," *Energy Conversion Congress and Exposition (ECCE), 2012 IEEE*, 2014.

[20] S. Singh, A. Shrivastav, and S. Bhattacharya, "Gan fet based cubesat electrical power system," *Applied Power Electronics Conference and Exposition (APEC), 2015 IEEE*, pp. 1388–1395, 2015.

[21] A. Lasagna, G. Merisio, and G. Zanotti, "Multi-physiscs assesment of sada installation on lumio," tech. rep., Politecnico di Milano, Italy, 2017.

[22] G. Cruz Chambel de Aguiar, "Earth–mars low-thrust transfers with ballistic capture and real-solar-system dynamics," 2017.

[23] F. Topputo and E. Belbruno, "Earth–mars transfers with ballistic capture," *Celestial Mechanics and Dynamical Astronomy*, vol. 121, no. 4, pp. 329–346, 2015.

[24] C. Vuik, P. van Beek, F. Vermolen, and J. van Kan, *Numerical Methods for Ordinary Differential Equations*. VSSD, 2007.

[25] F. Topputo and F. Bernelli-Zazzera, "Simulation of low-intensity, low-temperature solar arrays with software and hardware tools," *Aerotecnica Missili & Spazio*, vol. 92, no. 3-4, pp. 94–100, 2016.